DISSERTATION / DOCTORAL THESIS

Titel der Dissertation / Title of the Doctoral Thesis

Pharmacokinetic and bioimaging studies of platinum-based anticancer complexes by ICP-MS and LA-ICP-MS

verfasst von / submitted by

Mag. Sarah Theiner

angestrebter akademischer Grad / in partial fulfilment of the requirements for the degree of

Doktorin der Naturwissenschaften (Dr. rer. nat.)

Wien, 2015 / Vienna 2015

Studienkennzahl lt. Studienblatt / degree programme code as it appears on the student record sheet:	A 796 605 419
Dissertationsgebiet lt. Studienblatt / field of study as it appears on the student record sheet:	Chemie
Betreut von / Supervisor:	o. Univ.-Prof. Dr. Dr. Bernhard K. Keppler

Acknowledgements

A PhD thesis can not be conducted alone, there are lots of people behind the scene who contributed directly or indirectly with their constant support to this work.

I would like to acknowledge Prof. Bernhard Keppler for being my supervisor throughout the years of my PhD, for his constant backup and support. He enabled me to participate on international conferences, to perform scientific exchange and to work with the best ICP-MS on the market. I am especially thankful that he gave me the opportunity and also the freedom to perform my research independently and to try my own scientific ideas and projects, which helped me to develop as a scientist.

I am deeply thankful for my numerous 'daily' supervisors. On the first place there is Alexander Egger, who has supervised me from day zero of my PhD thesis. I want to thank him for listening my frustrations, helping me through times of desperations, for numerous scientfic and non-scientific discussions, sharing his endless knowledge with me, teaching me how to work scientifically, how to write scientific manuscripts, that comments and corrections are important to develop and to become better, to question results (especially the own ones), to give me advices for diplomacy,....the list is endless and I can not appreciate enough his support and contribution to my PhD thesis. I am also thankful for his patience and I think that we did not have the same opinion on many topics helped both of us.

In the second part of my PhD thesis I could count on the constant support of Gunda Köllensperger. I am especially thankful for her time for me, her advices how to deal in certain situations, for the analytical and scientific discussions, for trusting in me and trying to help me when needed and leaving me my scientific freedom when required.

I am really thankful to my colleagues in the Analytical lab (Lindi, Karla, Matthias, Christian and Sam) for the nice and warm working atmosphere and the support, when trying to cope with the same fate as PhD students. I also want to point out the help of Ricarda and Filip. We all had lots of fun together which helped in times when I was overloaded with work and close to desperation.

I am happy to know Luca and I really appreciate that he has been able to work with me for so long time already. I want to thank him for his daily assistance during my PhD, for listening me, sharing probelms and coffee with me. I appreciate him for being my friend and a person on which I can rely in every situation.

I would like to acknowledge all members of the Bioinorganic Chemistry research group, including the cell biologists and especially Anton for the great scientific discussions and good cooperation. I would also like to acknowledge former members of the group, Masha and Miljan who accompanied me at the beginning of my PhD thesis, helped me to feel welcome and to deal with everyday problems.

I would like to acknowledge my platinum cooperation partners Markus and Hristo for the discussions, their help with manuscripts and especially for sharing their knowledge on platinum compounds with me. They helped me to remain not only an analytical chemist by teaching me a lot for the platinum complexes I was working with and introducing me into this fascinating research field.

I would like to thank Wolfgang who was helping me a lot at the beginning despite being not an analytical chemist and who has always given me the feeling that I can come with every problem to him.

I would also like to acknowledge our collaboration partners Petra Heffeter and Walter Berger for their contribution to my PhD thesis, their assistance in writting manuscripts, the good cooperation with them and for giving me insights into the *in viv*o part of the drug development process.

I am also very thankful for Elfriede Limberger for assisting me to deal with the jungle of the University bureaucracy which is a nightmare for every scientist. I want to acknowledge Harald Fuchs for helping me every time when the ICP-MS computer crashed once again.

I want to acknowledge my colleagues and friends in Switzerland, especially Ronald, Tina, Cornel, Ismael, Lucy and Yousef which I had the pleasure to meet during my scientific stay at EPFL. I especially want to thank Prof. Paul Dyson for being able to knock on his door and talk to him any time I wanted, for welcoming me warmly in his group and enabling me to work at EPFL.

I also want to thank all my friends for their advices, numerous hiking activities to refresh my mind and their support in the last years.

Throughout the years I could always count on the backup and support of my family. I especially want to thank my parents Karin and Gerhard who have guided me through the different stages of my development, enabled me to study chemistry and who have given me constant support.

At the end I want to thank the person who has the biggest impact on my PhD thesis and on my personal development. I want to thank my best friend Hristo, who has accompanied me the last years, despite we are both not the easiest characters and who has given me more than he knows. His everyday support, listening to me in my times of desperation and giving me advices has guided me through my PhD. He was teaching me what it means to be a scientist, how to see things from different perspectives and not to take many things so serious.

Abstract

Platinum(II) complexes (cisplatin, carboplatin and oxaliplatin) are one of the most effectively and widely used classes of cytostatics in oncological treatment regimens. Platinum(IV) complexes as potential anticancer agents appear to be capable of overcoming the main limitations associated with classical platinum(II)-based chemotherapy including severe side effects due to low selectivity, acquired and/or intrinsic tumor resistance and inconvenience of intravenous administration. The modulation of the coordination sphere (especially of the axial ligands) offers a variety of opportunities for fine-tuning of pharmacologically relevant physicochemical properties, thus designing effective and safe prodrugs for oral administration.

In this PhD thesis, bioanalytical approaches based on inductively coupled plasma-mass spectrometry (ICP-MS) and laser ablation (LA) hyphenated to ICP-MS (LA-ICP-MS) were developed and applied for pharmacokinetic and bioimaging investigations of platinum-based complexes.

The pharmacokinetic behavior together with the anticancer activity of two experimental platinum(IV) complexes were evaluated in the murine CT-26 colon cancer model in comparison to satraplatin (the first orally active platinum compound in clinical trials). The two novel platinum(IV) anticancer complexes exhibited similar *in vivo* anticancer activity after oral treatment although the *in vitro* cytotoxicity and the platinum concentrations in tissues, tumor and serum differed significantly. Unexpectedly, the clinically-tested drug satraplatin proved to be inactive *in vivo* in the adopted model. Platinum accumulation in tissues of mice after p.o. and i.p. treatment with the drug candidates was determined using microwave-assisted acid digestion followed by platinum quantification with ICP-MS. All three compounds showed a similar pattern of accumulation for platinum with highest amounts in liver, followed by kidney and blood. Compound **1** ((OC-6-33)-dichloridobis((4-ethoxy)-4-oxobutanoato)-bis(ethylamine)platinum(IV)) features high drug absorption and tissue platinum levels after oral administration. Satraplatin exhibited lower platinum concentrations in tumor, whereas relatively low platinum amounts were detected in all tissue samples after treatment with compound **2** ((OC-6-33)-diammine(cyclobutane-1,1-dicarboxylato)-bis((4-cyclopentylamino)-4-oxobutanoato)platinum(IV)). In addition, the fate of the platinum(IV) complexes *in vivo* was studied in serum samples by size exclusion chromatography (SEC) hyphenated to ICP-MS, indicating extensive metabolisation and protein binding already after 2 h.

In a next step, we used a quantitative LA-ICP-MS approach, developed and validated in our group to get insights into the platinum distribution in histologically heterogeneous substructures of tissue sections after the treatment with the platinum complexes under investigation. Quantification with LA-ICP-MS is challenging due to elemental fractionation processes and certified reference materials are not at hand or unsuitable for many of the applications. Our quantification approach is based on matrix-matched calibration standards (prepared from homogenized liver) spiked with defined amounts of the respective metal (e.g. Pt and Ru) from standard solutions. The metal concentrations of the standards were verified by microwave-assisted acid digestion and consecutive quantification of the metal by ICP-MS.

Subsequently, the developed quantitative method of analysis by LA-ICP-MS was applied to assess the platinum distribution upon repetitive treatment with experimental platinum(IV)-based anticancer agents in comparison to satraplatin and oxaliplatin as reference compounds in tumor tissue of CT-26 bearing mice. We demonstrated that histologically confirmed tumor heterogeneity correlated well with the platinum accumulation pattern, determined by LA-ICP-MS. The highest levels of platinum were observed in loose, soft tissue compared to solid parts of the tumor tissue. Another focus of this study was to assess the potential of the platinum distribution in different compartments of kidney sections as indicator for nephrotoxicity. Similar to the nephrotoxic anticancer drug cisplatin, oxaliplatin and satraplatin exhibited elevated platinum levels in the cortex as compared to the medulla. However, treatment with the compounds in our study did not result in alteration of renal structures. This indicates that the nephrotoxic potential of platinum-based compounds cannot be predicted solely based on the metal distribution pattern determined by LA-ICP-MS.

Zusammenfassung

Platin(II)-Komplexe (Cisplatin, Carboplatin und Oxaliplatin) gehören zu den effektivsten und meist eingesetzten Substanzklassen in der Chemotherapie. Platin(IV)-Verbindungen als potenzielle Krebstherapeutika könnten die Hauptnachteile, die mit klassischer Platin(II)-basierender Chemotherapie verbunden sind, umgehen. Diese beinhalten schwerwiegende Nebenwirkungen wegen niedriger Selektivität, erworbene und/oder intrinsische Tumorresistenz und intravenöse Administration. Die Modulation der Koordinationssphäre (insbesondere der axialen Liganden) bietet eine Vielzahl von Möglichkeiten pharmakologisch relevante physikochemische Eigenschaften anzupassen und könnte das Design von effektiven und sicheren Prodrugs für orale Verabreichung ermöglichen.

In dieser Doktorarbeit wurden bioanalytische Methoden basierend auf induktiv gekoppelter Plasma-Massenspektrometrie (ICP-MS) und Laser Ablation (LA) gekoppelt mit ICP-MS entwickelt und verwendet, um pharmakokinetische Studien von Platinkomplexen durchzuführen.

Es wurden die pharmakokinetischen Eigenschaften und die Antitumoraktivität im Kolonkarzinoma Mausmodell CT-26 von zwei neu entwickelten Platin(IV)-Komplexen evaluiert und mit Satraplatin verglichen (der ersten oral aktiven Platinverbindung in klinischen Studien). Die zwei neuartigen Platin(IV)-Verbindungen zeigten ähnliche *in vivo* Aktivität nach oraler Verabreichung, obwohl die *in vitro* Zytotoxizität und die Platinkonzentrationen in Gewebe, Tumor und Serum signifikant unterschiedlich waren. Entgegen den Erwartungen war die klinisch getestete Platinverbindung Satraplatin inaktiv auf dem getesteten Maustumormodell. Die Platinakkumulation in Gewebeproben von Mäusen, die oral und intraperitoneal mit Platin(IV)-Komplexen behandelt wurden, wurde mittels Mikrowellenaufschluss und anschließender Platinquantifizierung mit ICP-MS bestimmt. Alle drei getesteten Platinverbindungen zeigten ein vergleichbares Platinakkumulationsmuster, wobei die höchsten Konzentrationen in Leber, Niere und Blut gefunden wurden. Komplex 1 zeichnete sich durch hohe Absorption und Platinkonzentrationen in Gewebeproben nach oraler Verabreichung aus. Satraplatin zeigte niedrigere Platinkonzentrationen in Tumor, während die niedrigsten Platinmengen in allen Gewebeproben nach Administration von Komplex 2 nachgewiesen wurden. Es wurde das Verhalten der Platin(IV)-Komplexe zusätzlich mittels Größenausschlusschromatographie gekoppelt mit ICP-MS *in vivo* in Mausserumproben untersucht. Die Resultate weisen auf eine Metabolisierung und Proteinanbindung der Platinverbindung bereits nach zwei Stunden hin.

Im nächsten Schritt wurde eine quantitative LA-ICP-MS Methode, die in unserer Gruppe entwickelt und validiert wurde, verwendet, um die Platinverteilung in histologisch heterogenen Gewebeproben zu untersuchen, die von Mäusen stammen, die mit Platinverbindungen behandelt wurden. Im Gegensatz zu Flüssigmessungen mit ICP-MS, stellt die Quantifizierung mit LA-ICP-MS eine Herausforderung dar, da Fraktionierungsprozesse der Elemente stattfinden können und oftmals geeignete zertifizierte Referenzmaterialien für bestimmte Anwendungen nicht verfügbar sind. Unsere Quantifizierungsstrategie basiert auf Kalibrationsstandards, die aus homogenisierter Leber hergestellt und mit definierten Konzentrationen von flüssigen Metallstandards (z.B. Platin oder Ruthenium) gespikt wurden. Die Konzentration der Standards wurde mit Mikrowellenaufschluss und anschließender Quantifizierung des Metalls mittels ICP-MS bestätigt.

In einer weiterführenden Studie wurde die LA-ICP-MS Methode verwendet, um die ortsaufgelöste Platinverteilung in Tumorgewebe des Kolonkarzinom CT-26 Mausmodells nach mehrmaliger Verabreichung von drei neuartigen Platin(IV)-Verbindungen im Vergleich zu Oxaliplatin und Satraplatin als Referenzverbindungen zu untersuchen. Wir konnten zeigen, dass die histologisch bestätigte Tumorheterogenität mit der Platinakkumulation, die mit LA-ICP-MS bestimmt wurde, korreliert. Es konnten höhere Platinkonzentrationen im weichen Bindegewebe als in dichteren Tumorgewebe nachgewiesen werden. Ein anderer Schwerpunkt der Studie lag darin, das Potential des Platinverteilungsmusters in verschiedenen Substrukturen von Nierengewebe als möglicher Indikator für Nephrotoxizität zu überprüfen. Oxaliplatin und Satraplatin weisen eine ähnliche Platinverteilung wie Cisplatin auf, mit höheren Platinkonzentrationen im Kortex der Niere, im Vergleich zur Medulla. Die Behandlung mit den Verbindungen unserer Studie resultierte jedoch im Gegensatz zum nephrotoxischen Cisplatin nicht in einer Veränderung der Nierenstrukturen. Dieses Ergebnis deutet darauf hin, dass es nicht möglich ist das nephrotoxische Potential von Platinverbindungen nur anhand der Metallverteilung, die mittels LA-ICP-MS bestimmt wurde, vorherzusagen.

Abbreviations

AAS – atomic absorption spectroscopy
CE – capillary electrophoresis
CRM – certified reference material
DLT – dose-limiting toxicity
ESI-MS – electrospray ionization-mass spectrometry
FDA – food and drug administration
GSH – glutathione
HSA – human serum albumin
ICP-MS – inductively coupled plasma – mass spectrometry
IP – ionization potential
LA – laser ablation
MALDI-MS – matrix-assisted laser desorption ionization-mass spectrometry
MEEKC – microemulsion electrokinetic capillary chromatography
NADH - nicotineamide adenine dinucleotide
NMR - nuclear magnetic resonance
SIMS – secondary ion mass spectrometry
QSAR – quantitative structure activity relationships
QSPR – quantitative structure-properties relationships
ROS – reactive oxygen species
RP-HPLC – reversed phase-high performance liquid chromatography
SCLC – small cell lung cancer
SEC – size exclusion chromatography
SRIXE – synchrotron radiation-induced X-ray emission
SXRF – synchrotron-based X-ray fluorescence microscopy
TOF-MS – time-of-flight-mass spectrometry
XANES – X-ray absorption near edge spectroscopy

Table of contents

I. INTRODUCTION

1. Cancer and treatment of cancer

Cancer is the name given to a collection of related diseases, characterized by abnormal cell behavior leading to uncontrolled growth of the tumorous tissue. Localized tumors, which do not spread to other parts of the body, are called benign, while these which are able to invade nearby tissues and to set up second type of tumors (forming metastasis), malignant.[1] There are more than 100 types of cancer (named for the organs or tissues where the cancer forms) and they can be classified in different categories: carcinoma (formed by epithelial cells), sarcoma (formed in bone and soft tissue), leukemia (origin in the blood-forming tissue of the bone marrow), lymphoma (origin in lymphocytes), multiple myeloma (begins in plasma cells), melanoma (origin in cells that become melanocytes) and brain and spinal cord tumors.[2]

Cancer is among the leading causes of death worldwide. In Europe, there were an estimated 3.45 million new cases of cancer with an average mortality of up to 50% reported for the year 2012. The most common cancer types reported included breast cancer (13.5%), colocteral cancer (13%), prostate cancer (12%) and lung cancer (12%). The most common causes of death from cancer were lung (20%), colocteral (12%), breast (7.5%) and stomach cancer (6%), which are among the most difficult to deal with together with malignant neoplasms with a generally poor prognosis (e.g. pancreas, liver or brain tumors).[3]

The classical treatment modalities for cancer include a combination of surgery, radiotherapy and chemotherapy. In the case of small-sized, localized tumors, the removal of the entire solid tumor by surgery can be performed. If surgery alone cannot cure the patient, an additional adjuvant or neoadjuvant radio- or chemotherapy is required. Radiation therapy employs high doses of radiation to kill cancer cells or slow their growth, to shrink the size of the tumor before surgery or to kill any cancer cells that might remain after other cancer treatments. For chemotherapy a full repertoire of antitumor agents is available, mainly organic compounds which are clinically applied.[4] They can be classified according to their chemical structure, mechanism of action, origin, cellular targets etc. Examples are alkylating and metallating anticancer drugs (platinum-based drugs), antitumor antibiotics (doxorubicin, bleomycin), antimetabolites (5-fluorouracil, gemcitabine, methotrexate), hormone receptor antagonists (tamoxifen), etc. They all share the disadvantage to affect also the cell growth of healthy cells and not being selective towards cancer cells which results in severe side effects for the patient.[5] In order to increase selectivity, reduce the toxicity to non-malignant cells and to deal with the occurrence of intrinsic and/or acquired tumor resistance to chemotherapy, personalized cancer treatment strategies have been developed. They include biological therapy (immunotherapy, targeted therapy, cancer vaccines and gene therapies), transplantation of bone marrow and peripheral blood stem cells, the use of angiogenic inhibitors and photodynamic therapy.[4]

2. Platinum(II)-based complexes in cancer therapy

The serendipitous discovery of the antiproliferative activity of cisplatin by Barnett Rosenberg in 1965 initiated the establishment of metal-based anticancer drugs in medicinal chemistry.[6-9] So far, three platinum(II) complexes cisplatin, carboplatin and oxaliplatin (Fig. 1) are employed in half of the oncological treatment regimens worldwide.[10] Cisplatin (SP-4-2)-diamminedichloridoplatinum(II) was approved in 1978 by the food and drug administration (FDA) and it is one of the most successful anticancer drugs. For example testicular cancer being almost incurable in the pre-cisplatin-era became curable to over 90%.[11] However, chemotherapy based on cisplatin is usually accompanied by severe side effects including nephrotoxicity (dose-limiting toxicity, DLT), neurotoxicity, ototoxicity, nausea and vomiting.[11,12] Another major challenge associated with cisplatin-based chemotherapy is to overcome tumor resistance which can be either intrinsic (as observed for patients with colocteral, prostate, lung or breast cancer) or acquired during cisplatin treatment cycles (e.g. for patients with ovarian cancer).[13] These drawbacks together with the aim to expand the therapeutic spectrum have initiated the synthesis of cisplatin analogues. The second generation drug carboplatin (SP-4-2)-diammine(1,1-cyclobutanedicarboxylato)platinum(II) (Fig. 1) exhibits considerably lower toxicity than cisplatin and therefore higher doses can be applied in treatment regimens; while myelosuppression is the DLT.[14] Carboplatin shows identical spectrum of activity as cisplatin and is mostly used in the treatment of ovarian and small cell lung cancers (SCLC).[15] Oxaliplatin (*SP*-4-2)-((1R,2R)-1,2-diaminocyclohexane)oxalato)platinum(II) (Fig. 1) gained worldwide approval in 2002 and is the first platinum drug that showed activity against cisplatin-resistant tumors.[10] It is used for the treatment of metastatic colocteral cancer in combination with 5-fluorouracil with neuropathy as DLT.[16] Apart from the worldwide clinically used platinum(II) complexes, another five are regionally approved in Asian countries (nedaplatin, lobaplatin, heptaplatin, miriplatin and dicycloplatin).[10]

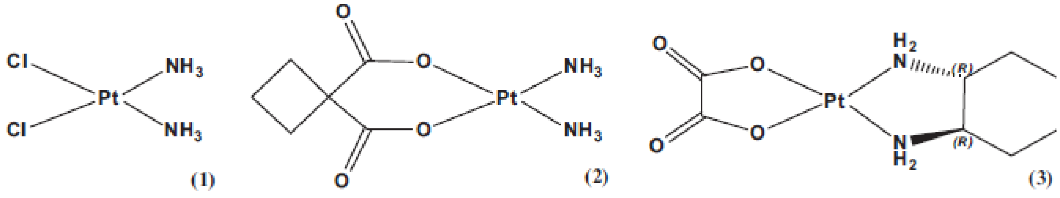

Figure 1. Platinum complexes with worldwide clinical approval: (1) cisplatin, (2) carboplatin and (3) oxaliplatin.

3. Platinum(IV) prodrugs

An attractive strategy to overcome the drawbacks associated with platinum(II)-based chemotherapy is the use of platinum(IV) prodrugs.[8,17] Platinum(IV) complexes are considered to be kinetically more inert and less prone to unspecific ligand interactions in biological systems than their platinum(II) congeners. Thus, less side effects and lower toxicological profile are expected.[18] In addition, the kinetic inertness allows oral administration, an advantage over the inconvenient way of parental administration of platinum(II)-based chemotherapeutics.[17]

The desired requirements of an optimal platinum(IV) complex for cancer treatment are as follows:

(1) stability in the gastrointestinal tract after oral administration (2) optimal lipophilicity to allow sufficient absorption from the intestinal lumen into the bloodstream (3) kinetic inertness towards metabolization processes in liver (especially towards the first-pass effect) (4) kinetic inertness towards reduction and ligand exchange reactions in the blood stream (5) arrival of the platinum(IV) complex at the

tumor site in its intact form (6) optimal lipophilicity to pass through the cell membrane showing sufficient, predominant accumulation in tumor cells (targeting approach) (7) specific reduction in the hypoxic tumor environment and in the tumor cells to the respective platinum(II) analogue (prodrug-concept).[17-19]

So far, three platinum(IV) complexes tetraplatin, iproplatin and satraplatin (Fig. 2) have entered clinical trials, but none of them has gained clinical approval yet.[10,20] Tetraplatin ((OC-6-22)-tetrachlorido(*trans*-1,2-cyclohexanediamine)platinum(IV)) was abandoned due to severe neurotoxicity as main side effect.[10] Iproplatin ((OC-6-33)-dichloridodihydroxidobis(isopropylamine)platinum(IV)) is the most studied platinum-based anticancer drug candidate, which entered clinical trials without clinical approval due to lower efficacy compared to cisplatin and carboplatin.[10] Satraplatin ((OC-6-43)-bis(acetato)amminedichlorido(cyclohexylamine)platinum(IV)) is the first orally administered platinum cytostatic evaluated in clinical trials.[10,20] It showed activity against several cisplatin sensitive and resistant cell lines and xenograft tumor models.[21] A large clinical phase III trial, the so-called SPARC trial (satraplatin and prednisone against refractory cancer *versus* placebo plus prednisone) was conducted with 950 patients with hormone refractory prostate cancer.[22,23] Despite the positive outcome, satraplatin was not approved by the FDA on the basis of non-convincing benefits in terms of overall survival.[20,22]

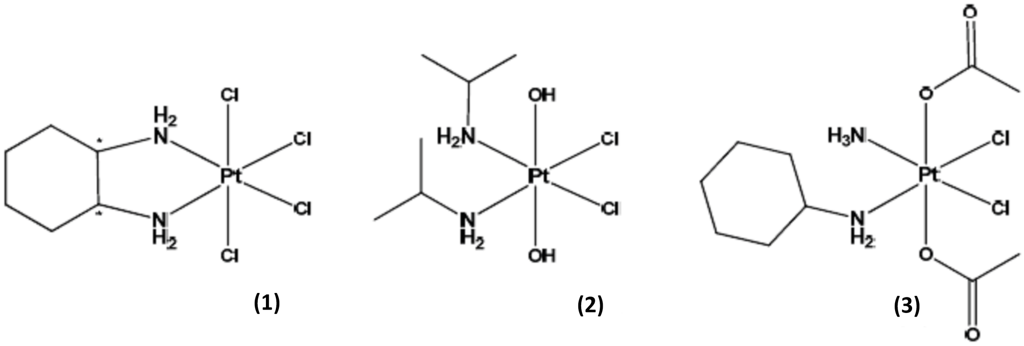

(1) (2) (3)

Figure 2. Platinum(IV) complexes evaluated in clinical trials: (1) tetraplatin, (2) iproplatin and (3) satraplatin.

3.1.Physicochemical properties and structure-activity relationships of platinum(IV) complexes

Platinum(II) complexes feature a square-planar, d^8 geometry, whereas platinum(IV) complexes exhibit a low-spin, d^6 octahedral geometry. There are two more (axial) ligands accessible for platinum(IV) complexes for structural modifications to improve the pharmacological profile.[17] In this context, the interplay between several parameters (lipophilicity, solubility, redox potential, rate of reduction, cellular accumulation, cytotoxicity etc.) has been addressed to develop structure-activity rules and to guide the rational design of platinum(IV) prodrugs.[17,24,25]

3.1.1. Lipophilicity of platinum(IV) complexes

Lipophilicity is an important physicochemical property determining a drug's ability to cross cell membranes and plays a crucial role to select the optimal route of administration and to adjust pharmacokinetic parameters such as the cellular uptake.[26,27] Tuning for an optimal lipophilicity window ensures that the complex will not be trapped within cell membranes and not become too insoluble in aqueous media.[28] For orally administered drugs a $\log P_{o/w}$ between 0.5 and 3.5 is considered as advantageous for good oral bioavailability.[27] In general, lipophilicity can be most conveniently altered by variation of the axial ligands of platinum(IV) complexes.

In order to estimate and compare the lipophilic character of metal-based drugs, the decadic logarithm of the partition coefficient between water and n-octanol ($\log P_{o/w} = \log c_{octanol}/c_{water}$) and the chromatographic retention parameter $\log k_w$ are widely used.[29,30] Several analytical methods, originally intended for organic drugs have been adapted to determine the lipophilicity of metal-based anticancer agents. Most commonly, the classical shake flask method is employed followed by quantification of the metal by atomic absorption spectroscopy (AAS) or inductively coupled plasma-mass spectrometry (ICP-MS),[31-34] whereas some studies also rely on $\log k_w$ determination by reversed phase (RP)-HPLC.[35,36] An alternative approach is the use of microemulsion electrokinetic chromatography (MEEKC) hyphenated to ICP-MS.[37] Based on experimental and literature data, quantitative structure-properties relationships (QSPR) models have been developed for the prediction of lipophilicity (log $P_{o/w}$ or log k_w) of platinum-based complexes.[38,39] In addition, a free access website for the log $P_{o/w}$ calculation of platinum-based compounds is available.[40,41]

3.1.2. Reduction of platinum(IV) complexes

Essential for the anticancer activity of platinum(IV) complexes is the *in vivo* activation by reduction preferably in the tumor cell to the corresponding platinum(II) analogues, followed by aquation.[18] The ligand sphere plays an important role in the reduction process of platinum(IV) complexes. For platinum(IV) complexes featuring two am(m)ine and two chlorido equatorial ligands, it was shown that the reduction potential and rate of reduction is primarily dependent on the nature of the axial ligands. Platinum(IV) complexes bearing axial trifluoracetato or chlorido ligands are most readily reduced, followed by carboxylato and hydroxido axial ligands.[42] Variation of the axial ligands while keeping the equatorial ligands constant revealed a direct correlation between the increase of reduction rates, electrochemical redox potentials and the electronegativity of the axial ligands. Interestingly, for platinum(IV) complexes, which are prodrugs of oxaliplatin, a correlation between the rates of reduction by ascorbate and the reduction potential were not observed.[43] An explanation could be the lower ability of the amine and carboxylate ligands to form a bridge with the reducing agents to facilitate electron transfer.[43]

3.1.3. Intracellular reduction of platinum(IV) complexes

The prevalent assumption is that ascorbate (two electron reducing agent) and glutathione (GSH) (one electron reducing agent) are mainly responsible for the reduction of platinum(IV) prodrugs.[18] Usually, model systems mimicking physiological conditions (37°C, pH=7.4) using single biological reducing agents or a mixture thereof (e.g. ascorbate, cysteine and glutathione) are employed to study the reduction of platinum(IV) complexes. Considering the complexity of biological systems such as the blood stream or the intracellular environment, model systems may not give an accurate picture of reduction processes of platinum(IV) complexes. Therefore, Gibson et al. incubated platinum(IV) compounds with aqueous extracts from different cancer cell lines and monitored the reduction process by 2D NMR spectroscopy.[44] It was shown that the intracellular environment that is specific for each cancer cell line has a significant impact on the rate of reduction of platinum(IV) complexes.[18] Recent studies demonstrated that high molecular weight biomolecules (>3000 Da) account for the majority of the reduction in cells.[44]

Hambley et al. have introduced X-ray absorption near edge spectroscopy (XANES) as analytical tool for the *in situ* monitoring of the oxidation state of platinum complexes in biological systems.[45] It was shown that platinum(II) and platinum(IV) complexes can be differentiated according to their peak heights in XANES spectra[45] and a method was developed to quantify the proportion of each oxidation state in a mixture.[46] By means of XANES the reduction of platinum(IV) prodrugs of cisplatin and transplatin was investigated in human ovarian cancer cells. The extent of intracellular reduction was found to correlate directly with the reduction potentials and cytotoxicity.[46] Another study, using the combination of synchrotron radiation-induced X-ray emission (SRIXE) and XANES measurements revealed the presence of both, platinum(II) and platinum(IV) species in human ovarian cancer cells.[47] These results indicate that platinum(IV) complexes can enter tumor cells in the platinum(IV) oxidation state, possibly in their intact form.[47,48]

3.1.4. Stability in the blood stream of platinum(IV) complexes

The reduction of platinum(IV) complexes has been extensively studied in the presence of ascorbate, GSH and in the cellular environment.[18] However, only a few studies investigated the stability of platinum(IV) complexes in blood plasma up to now. As mentioned previously, it is not favorable that platinum(IV) compounds undergo reduction followed by aquation already in the bloodstream. The metabolites formed (i.e. platinum(II) species) can undergo reactions with blood constituents. In this context, McKeage et al. showed that satraplatin can be reduced by hemoglobin and cytochrome c in the presence of NADH.[49] In addition, for satraplatin already 15 min after administration seven platinum-containing metabolites were found in patient's plasma ultrafiltrate, whereas the parent compound was no longer detectable.[20,50] For tetraplatin a $t_{1/2}$ of 3 s was determined by means of HPLC after incubation in plasma and the formation of platinum(II) species was observed.[51] *In vitro* studies of iproplatin in plasma by HPLC and NMR showed a stability of the parent compound over 48 h.[52] However, plasma data from patients indicated that all plasma platinum after 12 h corresponds to metabolites, whereas most of them are protein-bound.[53] Hambley et al. investigated the reactivity of platinum(IV) complexes with different ligand spheres towards selected plasma proteins (including HSA, cysteine) and correlated the results with the reduction potentials. They concluded that platinum(IV) complexes with axial acetato or hydroxido ligands should be relatively inert towards reactions in the blood plasma.[54]

4. Ruthenium-based anticancer compounds

Besides variation of the ligands and oxidation state of the metal, the exchange of the metal center is a third strategy to tune pharmacologically relevant physicochemical properties of metal-based complexes. Using this approach, compounds based on ruthenium, gallium, osmium, gold and titanium have been developed.[8] Ruthenium-based compounds exhibit a milder toxic profile and a different mode of action compared to platinum(II)-based anticancer agents.[7] The ruthenium compounds that have been evaluated in clinical trials so far are NAMI-A, KP1019 and NKP-1339 (Figure 3).

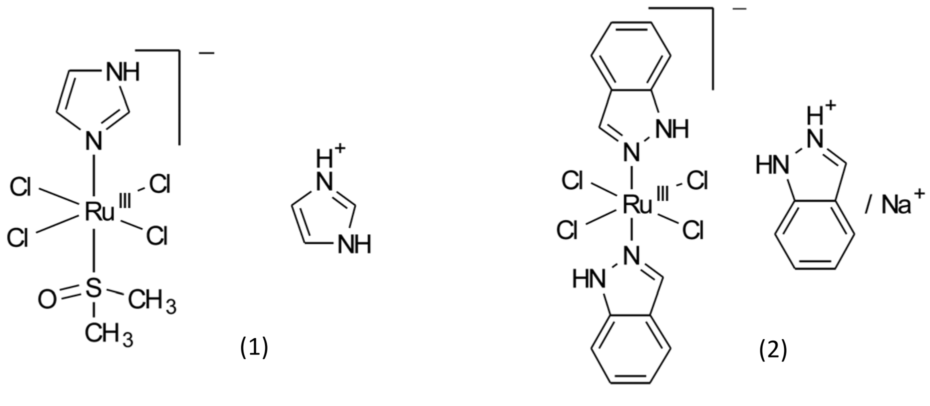

Figure 3. Ruthenium complexes evaluated in clinical trials (1) NAMI-A and (2) KP1019/NKP1339

NAMI-A [*trans*-tetrachlorido(dimethylsulfoxide)-imidazoleruthenate(III)] is the first ruthenium-based compound entering clinical trials in 1999.[55] Interestingly, NAMI-A (New Anti-tumor Metastasis Inhibitor) shows a selective effect on lung metastases of solid metastasizing tumors, with no direct effect on primary tumor growth.[56] The mechanism of metastasis control seems to be related to multiple interactions outside and inside the cell, i.e. enhanced cell adhesion, inhibition of the vascular endothelial growth factor as well as to the inhibition of angiogenesis in the tumor tissue.[57,58] Recently, NAMI-A completed a phase I/II study in combination with gemcitabine as a second line treatment for metastatic non-small cell lung cancer (NSCLC). It proved to be only moderately tolerated with renal toxicity, neutropenia, nausea and vomiting as side effects and was less active in NSCLS patients than gemcitabine alone. Thus, NAMI-A is not undergoing clinical trials at present and its future role remains uncertain due to the toxicity profile and the lack of convincing preliminary efficacy results.[59]

KP1019 (indazolium *trans*-[tetrachloridobis(*1H*-indazole)ruthenate(III)]) significantly reduced the tumor burden of chemically induced colocteral tumors in animal models.[60] Based on these promising results, a clinical phase I study in eight patients was conducted with intravenously administered dosages (between 25 and 600 mg) of KP1019 twice a week over three weeks. KP1019 was well tolerated with only mild toxicities up to the maximum dosage and a stabilization of the disease was found in five patients.[61] NKP-1339 (sodium *trans*-[tetrachloridobis(*1H*-indazole)ruthenate(III)], KP1339), the sodium salt analogue of KP1019 has originally been prepared as a precursor in the formulation of KP1019. Based on its higher water solubility, NKP-1339 has now been selected as lead candidate for further clinical development as it allows the administration of higher doses.[62] KP1019 and NKP1339 are administered intravenously and approximately 80-90% of the ruthenium-species are bound to albumin in the blood stream, whereas a small fraction is bound to transferrin (less than 2%), which is assumed to play an important role in the drug transport process.[63] Another hypothesis is based on the EPR (enhanced permeability and retention) effect, due to which albumin-bound KP1019 should accumulate in the tumor tissue, followed by drug release after albumin degradation. In general, Ru(III) complexes are more inert towards ligand exchange reactions than Ru(II) complexes. It is assumed that Ru(III) complexes are prodrugs that are selectively activated by reduction in the hypoxic tumor environment (activation-by-reduction concept). Different factors are considered to play a role in the activity of KP1019 including apoptosis via the mitochondrial pathway, also generating reactive oxygen species (ROS), as well as binding to target proteins in the endoplasmatic reticulum and DNA.[62] However, detailed investigations on the mode of action of KP1019/NKP1339 are still part of ongoing research.

5. Pharmacokinetics of metal-based anticancer drugs

'One can imagine the drug as chemical knight entering the body in order to make battle with an affliction. The drug is armed with a variety of weapons and armour, but it may not be obvious which weapons are important to the drug's activity, or which armour is essential for its surviving.'[27]

Pharmacokinetics describes the fate of a drug in the organism and is characterized by absorption, distribution, metabolisation and excretion (ADME). The understanding of pharmacokinetic processes is a main requirement for the choice of an appropriate drug formulation, for an appropriate route of administration and for the development of a dosage regimen for patients to ensure optimal efficacy and minimal toxicity.[26]

While intravenous administration of drugs typically results in well-defined plasma levels, the more convenient oral application underlies a large degree of variation: the acidic environment in the stomach, basic condition in the small intestine, varying presence of food/nutrients uptake from the intestine into blood and the first pass through liver tissue. Within liver, a broad spectrum of cytochrome enzymes may activate or deactivate drugs. Independent from the route of administration plasma protein binding, uptake in the target tissue and excretion via bile and/or kidney need to be considered carefully.[27]

The effectiveness of a drug is dependent on its concentration measured at the site of action. As this is not an easy task to accomplish, serum/plasma drug concentrations are measured as surrogates on a routine base.[64] Investigation of pharmacokinetic properties typically relies on separation techniques (such as

HPLC, CE, GC) hyphenated with mass spectrometry. In the case of metal-based complexes, element-specific detection techniques are applicable as well and will be introduced in the following chapter.

6. Analytical tools to study the pharmacokinetics of metal-based anticancer agents

6.1. Inductively coupled plasma-mass spectrometry (ICP-MS)

Inductively coupled plasma-mass spectrometry (ICP-MS) is a hard ionization mass spectrometry technique generating ions in a high temperature argon plasma. The low limits of detection (ppt to ppq range) for most metals and non-metals, combined with multielement capabilities, a large dynamic range over several orders of magnitude and the possibility of online coupling to different separation techniques (e.g. HPLC, CE) has brought ICP-MS to the method of choice for studying the fate of metallodrugs in different biological systems.[64-66]

If working with digested or aqueous samples, the sample is pumped into a nebulizer where an incoming argon flow provides the pneumatic force to dispersing the liquid into a fine aerosol. The liquid droplets then enter the spray chamber where they become subject to either centrifugal or gravitational forces in order to discard the largest droplets. The whole sample introduction is a critical step as only a small fraction of the sample will be brought into the argon plasma (< 1%).[67] Temperatures between 6000 and 10000 K dry, vaporize, atomize and ionize the sample.[68] Due to the high temperatures and the total decomposition of the sample, molecular information is lost during the process but enables the total quantification of elements regardless of their speciation.[64] Two cones (sampler and skimmer cone) represent the interface region where the transition from atmospheric pressure of the ICP to the MS high vacuum takes place.[69] In order to remove neutral species, photons and negatively charged ions, the ions emerging from the interface are subjected to several electrostatic lenses. The ions of interest are then focused into the MS where they are separated based on their mass-to-charge (m/z) ratios. Three different types of mass analyzers (quadrupole, sector field and TOF) have been employed in ICP-MS, whereas quadrupole is the most common one. By rapid switching of RF/DC voltages on the quadrupole rods (allowing only a stable trajectory for a certain m/z ratio through the mass analyzer), a 'quasi-simultaneous' determination of several analytes is possible.[70] In contrast to quadrupole, sector field (SF) and time of flight (TOF) are high mass resolution mass analyzers. Quadrupole offers a mass resolution of approximately 300, whereas SF and TOF can be operated at different mass resolving powers, where medium resolution is typically between 3000 and 4000 and high resolution between 8000 and 10000.[70] After getting past the mass analyzer, the ions are collected by an electron multiplier and the signal intensities are integrated with the provided software.[64]

6.1.1. Interferences in ICP-MS

When dealing with a specific chemical element, one major challenge in ICP-MS analysis is represented by the presence of interferences. Ions possessing the same m/z ratio as the analyte are called interferences, leading to an elevated background and false positives. Interferences comprise elemental isobaric interferences (e.g. $^{87}Rb^+$ on $^{87}Sr^+$), polyatomic ions (e.g. $^{40}Ar^{16}O^+$ interferes with $^{56}Fe^+$), or doubly charged ions (e.g. $^{140}Ce^{2+}$ interferes with $^{70}Ge^+$ and $^{70}Zn^+$). Polyatomic interferences and doubly charged species are caused by components of the argon plasma, atmospheric gases or matrix components; elemental interferences originate from the sample. In order to avoid an analytical bias caused by interferences, the measured isotope has to be carefully selected and/or mathematical corrections have to be applied.[71] Furthermore the use of sector field or TOF mass analyzer often overcomes interferences by providing a sufficiently high resolution;[71] however this strategy is limited by the cost of these ICP-MS instruments. Approximately 90% of commercially available ICP-MS devices are quadruple-featured instruments and in most cases they are additionally equipped with a collision/reaction cell (usually an octopole). In collision mode, an inert gas (e.g. He, Xe) can reduce the kinetic energy of the interfering species, thereby permitting only the analyte's detection.[71,72] In reaction mode, a reactive gas (e.g. O_2, H_2, NH_3) is introduced into the cell so that upon reaction the mass of either the analyte or the interfering species is shifted to another mass. In the case of sulfur, the most abundant isotope $^{32}S^+$ (interference $^{16}O_2^+$) reacts with O_2 forming the corresponding oxide ($^{32}S^{16}O^+$), which is detected at m/z 48 without interference. For $^{56}Fe^+$ the interfering species ($^{40}Ar^{16}O^+$) reacts with e.g. NH_3 whereas the analyte remains unaffected.[72] Recently, a tandem ICP-MS instrument was introduced on the market as a promise of better control over interference removal.[73,74] The Triple Quadrupole ICP-MS is equipped with an octopole (operated as collision or reaction cell), situated between two quadrupole mass filters enabling two separate mass selection steps. The first quadrupole transfers only ions with a defined mass-to-charge ratio into the octopole. Upon reaction or collision, the second quadrupole selects the ions of interest to be detected.[74] This approach has shown potential to overcome challenging spectral overlaps and to get a detailed insight into cell processes by the use of the precursor/product ion scan.[75,76]

6.1.2. (HPLC-) ICP-MS to study pharmacokinetics of metals and metallodrug-protein interactions

Tissue samples and biological fluids of mice treated with metal-based drugs are usually processed using microwave-assisted acid digestion followed by quantification of the total metal content by ICP-MS. The determination of platinum or ruthenium plasma levels provides information over important pharmacokinetic parameters such as the plasma half-life, volume of distribution, clearance etc.[77] Metal accumulation is determined in e.g. kidneys and nerve tissue as an indicator for possible side effects concerning nephrotoxicity and neurotoxicity, as well as in tumor tissue to study drug uptake.[32,36,78] This approach assumes that the metal is responsible for the efficacy of metal-based drugs and is used as first screening to determine the drug distribution in various tissues. In order to get a more detailed picture on metabolites or protein-adducts, elemental speciation analysis is performed, enabling the quantification of the intact drug and its reaction products on the basis of the metal signal.

The coupling of liquid chromatography systems to ICP-MS allows the studying of metallodrug-protein interactions in order to draw conclusions about the drug's fate in the blood (e.g. kinetics of binding, reversible/irreversible binding, percentage of protein-bound metal vs. non-protein bound, rate of protein binding etc.).[79] The hyphenation of LC to ICP-MS is straightforward because of the good compatibility for flow rates between the nebulization process in ICP-MS and the liquid elution in HPLC. Reversed Phase HPLC-ICP-MS allows studying of the hydrolysis of metallodrug products and metabolites however in most cases, gradient elution coming with organic mobile phases is required for high separation efficiency which can cause plasma instabilities.[80] Therefore, size exclusion chromatography (SEC) is usually used to separate intact proteins based on their molecular weight employing aqueous mobile phases. The column material consists of pores, whereas smaller molecules penetrate deep into the pores and larger molecules pass by and therefore elute before small-sized analytes. The principle of SEC is based on sorting the molecules by their size, making this method in combination with ICP-MS ideal to study the protein-bound fraction of metallodrugs.[66]

6.2. Elemental imaging techniques in metal-based anticancer drug development

Imaging enables the visualization of elemental and/or molecular distributions in biological tissue samples on microscopic and/or cellular level and yield important information when correlated with the corresponding histology. Thus, imaging techniques require high lateral resolution and sensitivity and can be divided in non-destructive (e.g. MALDI-MS, SXRF, SRIXE, μXRF, SIMS, etc.) and destructive methods (e.g. LA-ICP-MS).[81-84] A detailed review on these imaging techniques can be found elsewhere.[85] Matrix-assisted laser desorption ionization-MS (MALDI-MS) employs a laser to desorb and ionize analytes mixed with the matrix molecules that aids in the desorption/ionization process. Direct analysis is then performed by a raster of the sample by the laser beam. MALDI-MS is a soft ionization technique which allows analysis of molecules over a wide range of molecular weights.[86] Synchrotron-based X-ray fluorescence microscopy (SXRF) uses the fact, that each element possesses its unique fluorescence that is emitted upon X-ray excitation of electrons in the inner shell. The technique provides qualitative and quantitative information on the topography, concentration and oxidative state of metal cations.[83] Micro-

XRF provides lateral resolution of 10-0.1 µm with moderate sensitivity, but requires access to large synchrotrons and particle-accelerator facilities.[82] In the case of (Nano) secondary ion mass spectrometry (SIMS), the sample surface is rastered by a focused primary ion beam (either positively or negatively charged ions, e.g. Cs+, O_2^-), producing secondary ions that can be analyzed. This technique provides lateral resolution of 10-0.1 µm for standard SIMS and down to 50 nm for NanoSIMS.[83] Using LA-ICP-MS, the entire sample is ablated under atmospheric pressure, whereas in SIMS they are sputtered under high vacuum, requiring vacuum compatible sample preparation.[87] In comparison to X-ray methods, LA-ICP-MS offers lower detection limits, as well as access to isotopic information.[81]

LA-ICP-MS is the main analytical tool used during the work for this PhD thesis and will be therefore discussed in detail in the following chapters with regard to its application in metal-based anticancer drug development.

6.2.1. Laser ablation hyphenated to ICP-MS

6.2.1.1. Principles of laser

Laser is an acronym for light amplification by stimulated emission of radiation. In order to create light amplification in a laser it is necessary that the number of photons produced by stimulated emission exceeds the number of photons lost by absorption. This is only achieved when a population inversion from the normal distribution of energy state exists. This population inversion (activation of a laser material) is created by an external pumping source, so that a few photons of proper energy will trigger the formation of a cascade of photons of the same energy. As a consequence of its light-amplifying property, a laser produces spatially narrow and extremely intense beams of radiation, which are focused on the sample surface.[88] Interaction between the laser beam and the sample allows the conversion of photon energy into thermal energy, which is responsible for the vaporization of the exposed solid surface.

So far almost all available laser wavelengths (from visible and IR to UV wavelengths) have been tested in combination with ICP-MS for the ablation purpose. The laser ablation system used for the investigations in this PhD work operates with a solid state laser (Nd:YAG, yttrium aluminium garnet doped with neodymium). This type of laser emits in the infrared (1064 nm). However, shorter wavelengths (in the UV) proved to be advantageous in the ablation behavior. Thus nonlinear optics are used to obtain the fourth or fifth harmonic wavelength (266 or 213 nm, respectively).[89] An alternative type of laser to obtain a powerful laser beam in the UV are excimer lasers. Excited dimers of a noble gas and halogenides (eg. ArF, KrF) emit ultraviolet light, without the need of frequency duplication. Gas lasers such as CO_2 or N_2 as a third type of laser are typically not used for imaging experiments as these lasers media are limited to a much smaller number of laser shots compared to solid state or excimer lasers, which is not compatible with long lasting imaging experiments.[88]

6.2.1.2. Elemental bioimaging by means of LA-ICP-MS

LA-ICP-MS was initially introduced in the 1980s in the field of geology, before the pioneering work of Feldmann et al. in 2003 of a Cu and Zn profile map in sheep liver obtained by LA-ICP-TOF-MS[90] opened the way as elemental imaging tool in biological tissues. The entire workflow for bioimaging by LA-ICP-MS is shown in Figure 1.

Figure 1. Workflow of an LA-ICP-MS bioimaging experiment.

After sampling the biological tissue is immediately frozen and cryo-cut to preserve the biological material and the elemental distributions in its native physiological conditions. One major advantage of bioimaging by LA-ICP-MS is the simple and fast sample preparation (compared e.g. to MALDI-MS imaging). Most

LA-ICP-MS studies rely on cryo-sections, where the biological tissue is cut into cryo-microtome thin sections (typically between 5 and 30 µm) and is mounted on glass slides.[81,91] LA-ICP-MS is a destructive method as the whole biological sample material is ablated during the analysis. Thus, a consecutive section of the biological tissue is prepared for staining and histological evaluations. Some LA-ICP-MS studies also use paraffin-embedded samples where the sample undergoes several washing steps and formalin fixation which can result in alteration of elemental concentrations.[91]

In a next step, the whole sample is ablated with a focused laser beam (typically 10-100 µm in diameter) in parallel line scans at a scan speed of 10-100 µm/s. The ablated sample material is then transferred with an ablation/carrier gas (usually He, Ar or a mixture of them) to the ICP-MS system. After ionization in the ICP source, the ions are separated according to their mass-to-charge ratio in a mass analyzer (quadrupole, sector field or TOF). The ion intensities of each analyte are recorded as counts per second against time along the course of a laser scanning experiment and elemental distribution maps are generated.[91,92]

In general, LA-ICP-MS combines high spatial resolution (down to the cellular level) with the high sensitivity, wide concentration dynamic range and multielement analysis capabilities of the ICP-MS system.[81,93] Solvent- or air-based interferences by oxygen or nitrogen are absent in LA-ICP-MS improving the accuracy significantly, while short dwell times, required to account for the transient nature of the ablation signals, limit the precision. The major disadvantages of LA-ICP-MS are long acquisition times (several hours for high-resolution images) and challenging quantification.[94]

6.2.1.3. Quantification strategies for bioimaging by means of LA-ICP-MS

The development of unified, validated and reliable quantification strategies for bioimaging by LA-ICP-MS is still part of ongoing research.[95,96] Quantification is mainly hampered by elemental fractionation during ICP-MS analysis which is strongly matrix dependent and therefore, several different approaches have been proposed in literature to account for it.[95,96]

Single-point calibration using certified standard reference materials (CRMs) with defined elemental concentrations would be the method of choice. The quantification process can be traced back to a certified value and can be therefore validated. However, CRMs have to match the exact matrix composition of the sample subjected to LA-ICP-MS and their limited availability for bioimaging offers only few applications.[96] Therefore, most commonly, matrix-matched calibration standards are prepared individually for each analytical problem and sample material. Requirements for custom-prepared calibration standards include not only the well-defined chemical composition, but also the homogeneous distribution of the element in the tissue as well as controlled physical dimensions such as the sample thickness and the water content.[95,96] For this purpose, homogenates of tissue (resembling the composition of the sample) are spiked with known amounts of analytes. The elemental concentrations are verified by an independent method (e.g. microwave-assisted digestion followed by ICP-MS analysis) and the prepared standards are analyzed under the same experimental conditions as the sample.[95] Different matrices have been used in literature such as liver, chicken breast, brain tissue, whole human blood, etc. [97-100]

Another approach focused on thin polymeric films spiked with the elements of interest, which are spin coated on glass slides.[101] In this context also gelatin-based standards[102,103] as well as imprinted standards containing Cu[104] were proposed for quantification. The main disadvantage of this type of calibration standards is the possible difference in the ablation behavior as they do not possess the same features as biological tissues.

An on-line solution-based calibration method has been investigated for bioimaging by LA-ICP-MS. In this case, the laser-generated aerosol is combined with a second stream of aerosol (containing the calibration standard) generated by solution nebulization. The standard aerosol can either be introduced with the help of a micro-nebulizer placed in the laser ablation cell or directly into the injector tube of the ICP-MS torch.[105,106] Applying online addition of multi-element standard solutions can lead to more standardized plasma conditions, but can also cause more bias and polyatomic interferences.[105] In addition, it is independent from the ablation source and hence does not consider possible tissue inhomogeneity and different interaction between the laser beam and the tissue sample.[95]

All these techniques share the disadvantage that standards and samples are measured sequentially. Due to the long analysis-time, instrumental drift may occur and has to be evaluated and corrected (e.g. by normalization).

6.2.1.4. Signal normalization approaches

In order to monitor instrumental drift over the measurement time of LA-ICP-MS bioimaging experiments (which can last up to several hours), the use of an internal standard is recommended. An effective internal standard for LA-ICP-MS analysis should match the following criteria (1) it should account for differences in sample thickness (2) it should possess similar mass and first ionization potential compared to the analyte (3) it should behave similar to the analyte during the ablation process and the transport to the ICP-MS (4) it should compensate fluctuations of the plasma and drift in sensitivity over the measurement time.[95,96,107] The choice of the 'optimal' internal standard for LA-ICP-MS imaging is still the 'egg of Columbus' and usually a compromise between these criteria.

One class of internal standards for LA-ICP-MS imaging experiments comprises elements intrinsically present in the sample. In this context, the most commonly employed isotope is ^{13}C, which may account for differences in sample thickness (as indication for organic matter), but its signal can be affected by differing water contents of the ablated tissue.[107,108] In addition, ^{13}C is not always homogenously distributed within the different structures of soft tissue. Moreover, it has different mass and first ionization potential (11.3 eV) and is less sensitive to instrumental fluctuations compared to most analytes (e.g. IP of 9.0 and 7.4 for Pt and Ru, respectively).[95,107,108]

Alternatively, Austin et al. proposed the use of thin polymeric films spiked with internal standard elements (yttrium and ruthenium) that are spin coated on glass slides.[101] The sample section is then placed on the top of the film enabling simultaneous ablation of the tissue and internal standard layer. It was shown that the use of ^{13}C as internal standard improves precision, but that quantification is less accurate compared to the use of Y or Ru.[101] Similarly, also the use of gold layers sputtered on the sample surface has been proposed for signal normalization. It was demonstrated that gold standardization compensates for instrumental drifts and matrix-related differences in ablation.[104,109] Giesen et al. reported on iodination of cell nuclei of fibroblast cells and thin tissue slices as a concept for single cell imaging. In course of their study, they also concluded that iodine would be a suitable internal standard to correct for tissue inhomogeneity.[110]

6.2.1.5. LA-ICP-MS bioimaging in medicinal applications

One major focus of LA-ICP-MS research in life sciences is the study of neurodegenerative disorders (such as Alzheimer's, Parkinson's and Wilson's disease) which are closely related with metal-dysbalances in the brain.[92,111,112] The potential of LA-ICP-MS for elemental bioimaging of the morphological complex structure and fine branched, layered substructures of brain was first recognized by Jackson et al. by multielement mapping of an entire rodent brain hemisphere.[113] Subsequently, several LA-ICP-MS methodologies have been developed to reveal the physiological metalloarchitecture of the brain.[98,106,114-116] In this context, the essential elements Fe, Cu, Zn and Mn were quantified by LA-ICP-MS in a Parkinson mouse model.[100,117] In the field of cancer research, human and rat brain tumor resectates were characterized by LA-ICP-MS bioimaging.[118,119] A quantitative Cu, Zn, Pb and U profile was constructed whereas tumor mass regions and tumor invasion zones could be clearly distinguished from healthy surrounding tissue.[119] In a subsequent study, a depletion of P, S and Fe was observed in rat brain tumor tissue by LA-ICP-MS.[118] In addition, LA-ICP-MS was also applied to study tumor growth after injecting tumor cells into rat brain. A small size tumor was characterized by a deficit of carbon and zinc and a significant depletion of the $^{63}Cu/^{64}Zn$ ratio.[116] In a similar study, a decreased relative phosphorus concentration was found in lymph node metastases of myeloma patients.[120]

Recently, LA-ICP-MS has been introduced as promising tool for imaging of cancer biomarkers in tissue sections using elemental-tagged immunoassays.[121-123] The distribution of two breast cancer associated proteins (MUC-1 and HER2) was studied by employing gold nanoparticle labeled secondary antibodies and silver enhancement for signal amplification.[123] The use of lanthanide labeled antibodies was reported as detection for multiplexed immunohistochemistry of tissue sections by means of LA-ICP-MS. Optimization of sample preparation and laser parameters enabled to detect three tumor markers simultaneously in a single multiplex analysis of breast cancer tissue.[122] Another strategy employed direct labelling of antibodies with metal tags to selectively target metal and protein co-localizations.[124,125] In a recent study, Yb-tagged tyrosine hydroxylase antibodies were used to correlate dopamine localization in the brain with Fe by means of LA-ICP-MS throughout the entire mouse brain.[125] The same strategy was applied to a transgenic mouse model of Alzheimer's disease where the distribution of β-amyloid was visualized by LA-ICP-MS using Eu-tagged antibodies.[124]

LA-ICP-MS as tracking tool for metals in biological samples is very well suited to study the distribution of metal-based anticancer drugs in tissues at histological level. Only a few LA-ICP-MS bioimaging studies on metal-based antitumor agents have been conducted so far, focusing rather on analytical method development addressing the question of side effects of cisplatin-based chemotherapy (e.g. nephrotoxicity and ototoxicity). Therefore, most studies were dealing with platinum mapping in various biological tissues of cisplatin-treated animals or patients.[97,126-130] In this context, a LA-ICP-MS-based methodology was evaluated for bioimaging of Pt, Cu and Zn in whole kidney sections of rats upon treatment with pharmacological doses of cisplatin.[127] The observed platinum accumulation in the cortex and corticomedullary region suggested a correlation of renal damage with platinum distribution. In addition, lower Cu and Zn levels were detected in the presence of platinum, indicating possible displacement of these elements in renal cells. Moreover, nephroprotection induced by cilastatin-coadministration was monitored by biochemical parameters, as well as histological studies and was related to decreased platinum levels in the cortex region.[126,127] An investigation of the platinum distribution in therapy-affected organs (kidney, cochlea and testis) 1 h and 4 days after cisplatin infusion in mice, revealed a 95 % decrease of platinum levels.[128] In general, highest platinum levels were found in areas with high blood supply such as in the outer capsule of the testis and the bone areas in the cochlea. Regarding ototoxicity as one of the side effects of cisplatin-based chemotherapy, long-time exposure of the inner ear part to high platinum concentrations was observed which might result in degradation of sensory cells.[128] LA-ICP-MS was also employed for therapeutic monitoring of platinum in hair of patients undergoing cisplatin treatment.[131] In a recent study, the platinum distribution *Caenorhabditis elegans* (an established model organism for biomedical research) upon treatment with cisplatin was investigated with LA-ICP-MS with the aim to study cisplatin toxicity and pharmacokinetics.[132]

A promising preclinical application of LA-ICP-MS includes investigations on the drug uptake in the target (tumor) tissue.[103,133] In this context, a quantitative LA-ICP-MS approach was validated to study the penetration depth of oxaliplatin into rat tumor tissue of peritoneal carcinosis upon hyperthermic intraperitoneal chemotherapy. Platinum enrichment was observed mainly at the periphery of the tumor sections, which can be attributed to the direct contact with the drug perfusate.[103] In our study, the spatially-resolved platinum accumulation was analyzed by LA-ICP-MS in an *in vivo* preclinical murine tumor model upon treatment with platinum(II) and platinum(IV) complexes. Histologic features were reflected in the obtained platinum distribution maps. Interestingly, higher platinum accumulation was observed in soft tissue, sparsely infiltrated with tumor cells than in parts with densely packed tumor cells.[133] In addition, clinical samples from patients undergoing cisplatin or oxaliplatin chemotherapy against peritoneal carcinosis were subjected to MALDI-MS and LA-ICP-MS to obtain knowledge on the distributions of platinum-containing molecules and platinum, respectively within a single tissue section as a proof-of-principle.[134] Bonta et al. investigated a mesothelioma sample of a patient treated with cisplatin using LA-ICP-MS.[104] In addition, Egger et al. reported on the quantitative cisplatin and oxaliplatin extravasation in different tissue types (muscle, nerve tissue, connective tissue and fat tissue) and correlated the platinum burden with histologic structures and clinical outcome of the patients.[129]

6.2.1.6. Recent developments and future trends in LA-ICP-MS bioimaging

In most LA-ICP-MS imaging studies scanning mass analyzers (quadrupole) are employed, usually recording few isotopes and using ablation parameters that yield spatial resolution in the tens of µm scale.[81] Recent developments aimed to improve lateral resolution without compromising sensitivity and scan time, as well as to achieve parallel detection of trace and major elements.[91,135] In this context, small inner volume laser ablation cells were developed to reduce wash out times, increase signal intensity and to employ smaller spot sizes and apply laser impulses more frequently. The lowest dispersion cells for elemental imaging developed so far, deliver signal-pulse-signal duration of 30 ms[136] and 6 ms[137] (full width at 1 % maximum). The advances in fast aerosol transport from the laser also require a fast mass analyzer for analyte detection. However, scanning frequencies of most of the sequential instruments (ICP-Q-MS or ICP-SF-MS) are usually not sufficient for detecting the signal of more analytes in short transient signals, leading to the introduction of a laser ablation system hyphenated to ICP-MS with a TOF mass analyzer.[138] The simultaneous multielement capability of high mass resolution ICP-TOF-MS has already proven its applicability in the field of single particle analysis.[139,140] Recently, its combination with a high-washout laser ablation cell provided sensitivities for trace and major elements down to a spot size of 1.5 µm.[141] The resulting improvement in lateral resolution was in parallel with fast analysis times, making this technology superior to conventional LA-ICP-MS systems. These developments in laser and ICP-MS technology enabled to scale down the analysis from tissue level to single cells.[142] In this context, biomarkers were detected upon antibody labeling in breast cancer tissue with a spatial resolution of around 1 µm.[136] With the aim to perform single cell analysis, a quantitative bioimaging method for gold and silver nanoparticle distribution in individual fibroblast cells was developed, using the high spatial resolution power of LA-ICP-SF-MS.[143]

References

1 D. Hanahan and R. A. Weinberg, *Cell*, 2000, **100**, 57-70.

2 http://www.cancer.gov/types, Accessed 16.10.2015.

3 J. Ferlay, E. Steliarova-Foucher, J. Lortet-Tieulent, S. Rosso, J. W. W. Coebergh, H. Comber, D. Forman and F. Bray, *Eur J Cancer*, 2013, **49**, 1374-1403.

4 http://www.cancer.gov/about-cancer/treatment, Accessed 16.10.2015.

5 http://www.cancer.gov/about-cancer/treatment/drugs, Accessed 16.10.2015.

6 B. Rosenberg, L. VanCamp and T. Krigas, *Nature*, 1965, **205**, 698-699.

7 M. A. Jakupec, M. Galanski, V. B. Arion, C. G. Hartinger and B. K. Keppler, *Dalton Trans.*, 2008, 183-194.

8 M. Galanski, V. B. Arion, M. A. Jakupec and B. K. Keppler, *Curr. Pharm. Des.*, 2003, **9**, 2078-2089.

9 S. H. van Rijt and P. J. Sadler, *Drug Discov. Today*, 2009, **14**, 1089-1097.

10 N. J. Wheate, S. Walker, G. E. Craig and R. Oun, *Dalton Trans.*, 2010, **39**, 8113-8127.

11 B. Lippert, *Cisplatin. Chemistry and Biochemistry of a Leading Drug*, 1999, **Wiley-VCH**.

12 X. Yao, K. Panichpisal, N. Kurtzman and N. Kenneth, *Am. J. Med. Sci.*, 2007, **334**, 115-124.

13 L. R. Kelland, *Nat. Rev. Cancer*, 2007, **7**, 573-584.

14 E. Wong and C. M. Giandomenico, *Chem. Rev.*, 1999, **99**, 2451-2466.

15 A. J. Di Pasqua, J. Goodisman and J. C. Dabrowiak, *Inorg. Chim. Acta*, 2012, **389**, 29-35.

16 G. Yothers, M. J. O'Connell, C. J. Allegra, J. P. Kuebler, L. H. Colangelo, N. J. Petrelli and N. Wolmark, *J. Clin. Oncol.*, 2011, **29**, 3768-3774.

17 M. D. Hall and T. W. Hambley, *Coord. Chem. Rev.*, 2002, **232**, 49-67.

18 E. Wexselblatt and D. Gibson, *J. Inorg. Biochem.*, 2012, **117**, 220-229.

19 D. Gibson, *Dalton Trans.*, 2009, 10681-10689.

20 H. Choy, C. Park and M. Yao, *Clin. Cancer Res.*, 2008, **14**, 1633-1638.

21 K. Wosikowski, L. Lamphere, G. Unteregger, V. Jung, F. Kaplan, J. Xu, B. Rattel and M. Caligiuri, *Cancer Chemother Pharmacol*, 2007, **60**, 589-600.

22 C. N. Sternberg, D. P. Petrylak, O. Sartor, J. A. Witjes, T. Demkow, J. M. Ferrero, J. C. Eymard, S. Falcon, F. Calabro, N. James, I. Bodrogi, P. Harper, M. Wirth, W. Berrry, M. E. Petrone, T. J. McKearn, M. Noursalehi, M. George and M. Rozencweig, *J. Clin. Oncol.*, 2009, **27**, 5431-5438.

23 A. J. Armstrong and D. J. George, *Ther Clin Risk Manag.*, 2007, **3**, 877-883.

24 M. D. Hall, H. R. Mellor, R. Callaghan and T. W. Hambley, *J. Med. Chem.*, 2007, **50**, 3403-3411.

25 H. P. Varbanov, M. A. Jakupec, A. Roller, F. Jensen, M. Galanski and B. K. Keppler, *J. Med. Chem.*, 2013, **56**, 330-344.

26 M. V. S. Varma, Z. A. Radi, C. J. Rotter, J. Litchfield, A. F. El-Kattan and A. V. Lyubimov, in *Encyclopedia of Drug Metabolism and Interactions*, John Wiley & Sons, Inc., 2011.

27 G. L. Patrick, *An Introduction to Medicinal Chemistry*, Fourth Edition edn., Oxford University Press, 2008.

28 N. Graf and S. J. Lippard, *Adv. Drug Deliver. Rev.*, 2012, **64**, 993-1004.

29 *OECD Guideline for Testing of Chemicals, 107 OECD, Paris (1995)*.

30 A. Nasal, D. Siluk and R. Kaliszan, *Curr. Med. Chem.*, 2003, **10**, 381-426.

31 M. R. Reithofer, A. K. Bytzek, S. M. Valiahdi, C. R. Kowol, M. Groessl, C. G. Hartinger, M. A. Jakupec, M. Galanski and B. K. Keppler, *J. Inorg. Biochem.*, 2011, **105**, 46-51.

32 D. Screnci, M. J. McKeage, P. Galettis, T. W. Hambley, B. D. Palmer and B. C. Baguley, *Br J Cancer*, 2000, **82**, 966-972.

33 M. S. Robillard, M. Galanski, W. Zimmermann, B. K. Keppler and J. Reedijk, *J. Inorg. Biochem.*, 2002, **88**, 254-259.

34 M. D. Hall, S. Amjadi, M. Zhang, P. J. Beale and T. W. Hambley, *J. Inorg. Biochem.*, 2004, **98**, 1614-1624.

35 H. P. Varbanov, S. M. Valiahdi, C. R. Kowol, M. A. Jakupec, M. Galanski and B. K. Keppler, *Dalton Trans.*, 2012, **41**, 14404-14415.

36 H. P. Varbanov, S. Göschl, P. Heffeter, S. Theiner, A. Roller, F. Jensen, M. A. Jakupec, W. Berger, M. Galanski and B. K. Keppler, *J.Med.Chem.*, 2014, **57**, 6751-6764.

37 A. K. Bytzek, M. R. Reithofer, M. Galanski, M. Groessl, B. K. Keppler and C. G. Hartinger, *Electrophoresis*, 2010, **31**, 1144-1150.

38 J. Platts, G. Ermondi, G. Caron, M. Ravera, E. Gabano, L. Gaviglio, G. Pelosi and D. Osella, *J Biol Inorg Chem*, 2011, **16**, 361-372.

39 J. A. Platts, S. P. Oldfield, M. M. Reif, A. Palmucci, E. Gabano and D. Osella, *J. Inorg. Biochem.*, 2006, **100**, 1199-1207.

40 www.ochem.eu, Accessed 08.09.2015.

41 I. V. Tetko, I. Jaroszewicz, J. A. Platts and J. Kuduk-Jaworska, *J. Inorg. Biochem.*, 2008, **102**, 1424-1437.

42 S. Choi, C. Filotto, M. Bisanzo, S. Delaney, D. Lagasee, J. L. Whitworth, A. Jusko, C. Li, N. A. Wood, J. Willingham, A. Schwenker and K. Spaulding, *Inorg. Chem.*, 1998, **37**, 2500-2504.

43 J. Z. Zhang, E. Wexselblatt, T. W. Hambley and D. Gibson, *Chemical Communications*, 2012, **48**, 847-849.

44 A. Nemirovski, Y. Kasherman, Y. Tzaraf and D. Gibson, *J. Med. Chem.*, 2007, **50**, 5554-5556.

45 M. D. Hall, G. J. Foran, M. Zhang, P. J. Beale and T. W. Hambley, *J Am Chem Soc*, 2003, **125**, 7524-7525.

46 M. D. Hall, H. L. Daly, J. Z. Zhang, M. Zhang, R. A. Alderden, D. Pursche, G. J. Foran and T. W. Hambley, *Metallomics*, 2012, **4**, 568-575.

47 M. Hall, C. Dillon, M. Zhang, P. Beale, Z. Cai, B. Lai, A. J. Stampfl and T. Hambley, *J Biol Inorg Chem*, 2003, **8**, 726-732.

48 M. D. Hall, R. A. Alderden, M. Zhang, P. J. Beale, Z. Cai, B. Lai, A. P. J. Stampfl and T. W. Hambley, *J Struct Biol*, 2006, **155**, 38-44.

49 J. Carr, M. Tingle and M. McKeage, *Cancer Chemother Pharmacol*, 2006, **57**, 483-490.

50 D. N. Bell, J. J. Liu, M. D. Tingle, B. Rattel, T. U. Meyer and M. J. McKeage, *Clin Exp Pharmacol Physiol.*, 2008, **35**, 1440-1446.

51 S. G. Chaney, S. Wyrick and G. K. Till, *Cancer Res.*, 1990, **50**, 4539.

52 L. Pendyala, B. S. Krishnan, J. R. Walsh, A. V. Arakali, J. W. Cowens and P. J. Creaven, *Cancer Chemother Pharmacol*, 1989, **25**, 10-14.

53 L. Pendyala, W. Greco, J. W. Cowens, S. Madajewicz and P. J. Creaven, *Cancer Chemother Pharmacol*, 1983, **11**, 23-28.

54 R. C. Dolman, G. B. Deacon and T. W. Hambley, *J. Inorg. Biochem.*, 2002, **88**, 260-267.

55 G. Sava, R. Gagliardi, A. Bergamo, E. Alessio and G. Mestroni, *Anticancer Res.*, 1999, **19**, 969-972.

56 A. Bergamo, C. Gaiddon, J. H. M. Schellens, J. H. Beijnen and G. Sava, *J. Inorg. Biochem.*, 2012, **106**, 90-99.

57 E. Alessio, G. Mestroni, A. Bergamo and G. Sava, *Curr Top Med Chem*, 2004, **4**, 1525-1535.

58 P. J. Dyson and G. Sava, *Dalton Trans.*, 2006, 1929-1933.

59 S. Leijen, S. Burgers, P. Baas, D. Pluim, M. Tibben, E. van Werkhoven, E. Alessio, G. Sava, J. Beijnen and J. M. Schellens, *Invest New Drugs*, 2015, **33**, 201-214.

60 M. R. Berger, F. T. Garzon, B. K. Keppler and D. Schmahl, *Anticanc. Res.*, 1989, **9**, 761-765.

61 C. G. Hartinger, M. A. Jakupec, S. Zorbas-Seifried, M. Groessl, A. Egger, W. Berger, H. Zorbas, P. J. Dyson and B. K. Keppler, *Chem. Biodivers.*, 2008, **5**, 2140-2155.

62 R. Trondl, P. Heffeter, C. R. Kowol, M. A. Jakupec, W. Berger and B. K. Keppler, *Chem. Sci.*, 2014, **5**, 2925-2932.

63 C. G. Hartinger, S. Zorbas-Seifried, M. A. Jakupec, B. Kynast, H. Zorbas and B. K. Keppler, *J. Inorg. Biochem.*, 2006, **100**, 891-904.

64 B. Gammelgaard, S. Stürup, C. Møller and A. V. Lyubimov, in *Encyclopedia of Drug Metabolism and Interactions*, John Wiley & Sons, Inc., 2011.

65 B. Gammelgaard, H. R. Hansen, S. Stürup and C. Møller, *Expert Opinion on Drug Metabolism and Toxicology*, 2008, **4**, 1187-1207.

66 E. E. M. Brouwers, M. Tibben, H. Rosing, J. H. M. Schellen and J. H. Beijnen, *Mass Spectrom. Rev.*, 2008, **27**, 67-100.

67 R. Thomas, *Spectroscopy*, 2001, **16**, 56-60.

68 R. Thomas, *Spectroscopy*, 2001, **16**, 26-30.

69 R. Thomas, *Spectroscopy*, 2001, **16**, 26-34.

70 R. Thomas, *Spectroscopy*, 2001, **16**, 44-48.

71 R. Thomas, *Spectroscopy*, 2002, **17**, 24-31.

72 S. D. Tanner, V. I. Baranov and D. R. Bandura, *Spectrochim. Acta B*, 2002, **57**, 1361-1452.

73 A. Technologies, *Agilent 8800 Application Handbook*, 2013.

74 L. Balcaen, E. Bolea-Fernandez, M. Resano and F. Vanhaecke, *Anal Chim Acta*, 2015, **894**, 7-19.

75 L. Balcaen, G. Woods, M. Resano and F. Vanhaecke, *J. Anal. At. Spectrom.*, 2013, **28**, 33-39.

76 E. Bolea-Fernandez, L. Balcaen, M. Resano and F. Vanhaecke, *Anal. Chem.*, 2014, **86**, 7969-7977.

77 P. Sova, A. Mistr, A. Kroutil, M. Semerád, H. Chlubnová, V. Hrusková, J. Chládková and J. Chládek, *Cancer Chemother Pharmacol.*, 2011, **67**, 1247-1256.

78 S. Theiner, H. Varbanov, M. Galanksi, A. Egger, W. Berger, P. Heffeter and B. K. Keppler, *J. Biol. Inorg. Chem.*, 2015, **20**, 89-99.

79 B. Meermann and M. Sperling, *Anal Bioanal Chem*, 2012, **403**, 1501-1522.

80 M. Groessl and C. Hartinger, *Anal Bioanal Chem*, 2013, **405**, 1791-1808.

81 J. S. Becker, M. Zoriy, A. Matusch, B. Wu, D. Salber, C. Palm and J. S. Becker, *Mass Spectrom Rev*, 2010, **29**, 156-175.

82 C. J. Fahrni, *Curr Opin Chem Biol*, 2007, **11**, 121-127.

83 L. Wedlock and S. J. Berners-Price, *Austral J Chem*, 2011, **64**, 692-704.

84 Z. Qin, J. A. Caruso, B. Lai, A. Matusch and J. S. Becker, *Metallomics*, 2011, **3**, 28-37.

85 S. Theiner, L. Galvez-Montano, G. Koellensperger and B. K. Keppler, in *Analytical Techniques and Speciation Methods*, ed. B. Michalke, Wiley-VCH, Weinheim, Germany, 2015.

86 J. L. Norris and R. M. Caprioli, *Chemical Reviews*, 2013.

87 C. R. M. Grovenor, K. E. Smart, M. Kilburn, J. R. Dilworth, B. Martin, C. Hawes and R. E. M. Rickaby, *Appl Surf Sci*, 2006, **252**, 6917-6924.

88 D. A. Skoog and J. J. Leary, *Instrumentelle Analytik*, Springer Verlag, Berlin Heidelberg, 1996.

89 D. Günther and B. Hattendorf, *TrAC Trends in Analytical Chemistry*, 2005, **24**, 255-265.

90 A. Kindness, C. N. Sekaran and J. Feldmann, *Clin Chem*, 2003, **49**, 1916-1923.

91 J. S. Becker, A. Matusch and B. Wu, *Anal Chim Acta*, 2014, **835**, 1-18.

92 J. S. Becker, *Int. J. Mass Spectrom.*, 2010, **289**, 65-75.

93 J. Sabine Becker, *J Mass Spectrom*, 2013, **48**, 255-268.

94 J. S. Becker and N. Jakubowski, *Chem. Soc. Rev.*, 2009, **38**, 1969-1983.

95 I. Konz, B. Fernández, M. Fernández, R. Pereiro and A. Sanz-Medel, *Anal. Bioanal. Chem.*, 2012, **403**, 2113-2125.

96 D. Hare, C. Austin and P. Doble, *Analyst*, 2012, **137**, 1527-1537.

97 A. E. Egger, S. Theiner, C. Kornauth, P. Heffeter, W. Berger, B. K. Keppler and C. Hartinger, *Metallomics*, 2014, **6**, 1616-1625.

98 A. Matusch, C. Depboylu, C. Palm, B. Wu, G. U. Höglinger, M. K. H. Schäfer and J. S. Becker, *J. Am. Mass Spectrom.*, 2010, **21**, 161-171.

99 J. A. T. Pugh, A. G. Cox, C. W. McLeod, J. Bunch, B. Whitby, B. Gordon, T. Kalber and E. White, *J. Anal. At. Spectrom.*, 2011, **26**, 1667-1673.

100 D. Hare, B. Reedy, R. Grimm, S. Wilkins, I. Volitakis, J. L. George, R. A. Cherny, A. I. Bush, D. I. Finkelstein and P. Doble, *Metallomics*, 2009, **1**, 53-58.

101 C. Austin, D. Hare, T. Rawling, A. M. McDonagh and P. Doble, *J Anal At Spectrom*, 2010, **25**, 722-725.

102 A. Izmer, D. Gholap, K. De Houwer, F. Cuyckens and F. Vanhaecke, *J Anal At Spectrom*, 2012, **27**, 413-418.

103 D. Gholap, J. Verhulst, W. Ceelen and F. Vanhaecke, *Anal. Bioanal. Chem.*, 2012, **402**, 2121-2129.

104 M. Bonta, H. Lohninger, M. Marchetti-Deschmann and A. Limbeck, *Analyst*, 2014, **139**, 1521-1531.

105 D. Pozebon, V. L. Dressler, M. F. Mesko, A. Matusch and J. S. Becker, *J. Anal. At. Spectrom.*, 2010, **25**, 1739-1744.

106 J. S. Becker, M. V. Zoriy, C. Pickhardt, N. Palomero-Gallagher and K. Zilles, *Anal Chem*, 2005, **77**, 3208-3216.

107 C. Austin, F. Fryer, J. Lear, D. Bishop, D. Hare, T. Rawling, L. Kirkup, A. McDonagh and P. Doble, *J Anal At Spectrom*, 2011, **26**, 1494-1501.

108 D. A. Frick and D. Gunther, *J. Anal. At. Spectrom.*, 2012, **27**, 1294-1303.

109 I. Konz, B. Fernández, M. L. Fernández, R. Pereiro, H. González, L. Álvarez, M. Coca-Prados and A. Sanz-Medel, *Anal Bioanal Chem*, 2013, **405**, 3091-3096.

110 C. Giesen, L. Waentig, T. Mairinger, D. Drescher, J. Kneipp, P. H. Roos, U. Panne and N. Jakubowski, *J Anal At Spectrom*, 2011, **26**, 2160-2165.

111 J. Sabine Becker, A. Matusch, C. Palm, D. Salber, K. A. Morton and J. Susanne Becker, *Metallomics*, 2010, **2**, 104-111.

112 J. S. Becker and D. Salber, *TrAC Trends in Analytical Chemistry*, 2010, **29**, 966-979.

113 B. Jackson, S. Harper, L. Smith and J. Flinn, *Anal. Bioanal. Chem.*, 2006, **384**, 951-957.

114 M. V. Zoriy and J. S. Becker, *Int. J. Mass Spectrom.*, 2007, **264**, 175-180.

115 J. Dobrowolska, M. Dehnhardt, A. Matusch, M. Zoriy, N. Palomero-Gallagher, P. Koscielniak, K. Zilles and J. S. Becker, *Talanta*, 2008, **74**, 717-723.

116 J. S. Becker, M. V. Zoriy, M. Dehnhardt, C. Pickhardt and K. Zilles, *J. Anal. At. Spectrom.*, 2005, **20**, 912-917.

117 D. J. Hare, J. L. George, R. Grimm, S. Wilkins, P. A. Adlard, R. A. Cherny, A. I. Bush, D. I. Finkelstein and P. Doble, *Metallomics*, 2010, **2**, 745-753.

118 M. V. Zoriy, M. Dehnhardt, A. Matusch and J. S. Becker, *Spectrochim. Acta B*, 2008, **63**, 375-382.

119 M. V. Zoriy, M. Dehnhardt, G. Reifenberger, K. Zilles and J. S. Becker, *Int. J. Mass Spectrom.*, 2006, **257**, 27-33.

120 D. Hare, F. Burger, C. Austin, F. Fryer, R. Grimm, B. Reedy, R. A. Scolyer, J. F. Thompson and P. Doble, *Analyst*, 2009, **134**, 450-453.

121 C. Giesen, L. Waentig, U. Panne and N. Jakubowski, *Spectrochim. Acta B*, 2012.

122 C. Giesen, T. Mairinger, L. Khoury, L. Waentig, N. Jakubowski and U. Panne, *Anal. Chem.*, 2011, **83**, 8177-8183.

123 J. Seuma, J. Bunch, A. Cox, C. McLeod, J. Bell and C. Murray, *Proteomics*, 2008, **8**, 3775-3784.

124 R. W. Hutchinson, A. G. Cox, C. W. McLeod, P. S. Marshall, A. Harper, E. L. Dawson and D. R. Howlett, *Anal. Biochem.*, 2005, **346**, 225-233.

125 B. Paul, D. J. Hare, D. P. Bishop, C. Paton, V. T. Nguyen, N. Cole, M. M. Niedwiecki, E. Andreozzi, A. Vais, J. L. Billings, L. Bray, A. I. Bush, G. McColl, B. R. Roberts, P. A. Adlard, D. I. Finkelstein, J. Hellstrom, J. M. Hergt, J. D. Woodhead and P. A. Doble, *Chem. Sci.*, 2015, **6**, 5383-5393.

126 M. Zoriy, A. Matusch, T. Spruss and J. S. Becker, *Int. J. Mass Spectrom.*, 2007, **260**, 102-106.

127 E. Moreno-Gordaliza, C. Giesen, A. Lázaro, D. Esteban-Fernández, B. Humanes, B. Cañas, U. Panne, A. Tejedor, N. Jakubowski and M. M. Gómez-Gómez, *Anal Chem*, 2011, **83**, 7933-7940.

128 O. Reifschneider, C. A. Wehe, I. Raj, j. Ehmcke, G. Ciarimboli, M. Sperling and U. Karst, *Metallomics*, 2013, **5**, 1440-1447.

129 A. E. Egger, C. Kornauth, W. Haslik, S. Hann, S. Theiner, G. Bayer, C. G. Hartinger, B. K. Keppler, U. Pluschnig and R. M. Mader, *Metallomics*, 2015, **7**, 508-515.

130 C. Koppen, O. Reifschneider, I. Castanheira, M. Sperling, U. Karst and G. Ciarimboli, *Metallomics*, 2015.

131 D. Pozebon, V. L. Dressler, A. Matusch and J. S. Becker, *Int. J. Mass Spectrom.*, 2008, **272**, 57-62.

132 B. Crone, M. Aschner, T. Schwerdtle, U. Karst and J. Bornhorst, *Metallomics*, 2015, **7**, 1189-1195.

133 S. Theiner, C. Kornauth, H. P. Varbanov, M. Galanski, S. Van Schoonhoven, P. Heffeter, W. Berger, A. E. Egger and B. K. Keppler, *Metallomics*, 2015, **7**, 1256-1264.

134 J. Bianga, A. Bouslimani, N. Bec, F. Quenet, S. Mounicou, J. Szpunar, B. Bouyssiere, R. Lobinski and C. Larroque, *Metallomics*, 2014, **6**, 1382-1386.

135 M. Tanner and D. Günther, *Anal Chim Acta*, 2009, **633**, 19-28.

136 H. A. O. Wang, D. Grolimund, C. Giesen, C. N. Borca, J. R. H. Shaw-Stewart, B. Bodenmiller and D. Günther, *Anal Chem*, 2013, **85**, 10107-10116.

137 S. J. M. Van Malderen, J. T. van Elteren and F. Vanhaecke, *J Anal At Spectrom*, 2015, **30**, 119-125.

138 M. Tanner and D. Günther, *Anal Bioanal Chem*, 2008, **391**, 1211-1220.

139 O. Borovinskaya, S. Gschwind, B. Hattendorf, M. Tanner and D. Günther, *Anal Chem*, 2014, **86**, 8142-8148.

140 O. Borovinskaya, B. Hattendorf, M. Tanner, S. Gschwind and D. Gunther, *J Anal At Spectrom*, 2013, **28**, 226-233.

141 A. Gundlach-Graham, M. Burger, S. Allner, G. Schwarz, H. A. O. Wang, L. Gyr, D. Grolimund, B. Hattendorf and D. Günther, *Anal Chem*, 2015.

142 L. Mueller, H. Traub, N. Jakubowski, D. Drescher, V. Baranov and J. Kneipp, *Anal Bioanal Chem*, 2014, **406**, 6963-6977.

143 D. Drescher, C. Giesen, H. Traub, U. Panne, J. Kneipp and N. Jakubowski, *Anal. Chem.*, 2012, **84**, 9684-9688.

II. RESULTS

This cumulative PhD thesis is based on the following publications and on one contribution to a book chapter, dealing with elemental imaging by LA-ICP-MS and the investigation of the pharmacokinetics and anticancer activity of platinum-based complexes. The publications are presented in the original format:

Comparative *in vitro* and *in vivo* pharmacological investigation of platinum(IV) complexes as novel anticancer drug candidates for oral application

Sarah Theiner, Hristo P. Varbanov, Markus Galanski, Alexander E. Egger, Walter Berger, Petra Heffeter, Bernhard K. Keppler

J. Biol. Inorg. Chem., **2015**, 20(1): 89-99

Two novel platinum(IV) anticancer drug candidates were evaluated in comparison to satraplatin with regard to their *in vitro* cytotoxicity, *in vivo* activity in the murine colon cancer CT-26 model (after p.o. and i.p. administration) and platinum distribution in tissues, serum and tumor (determined by ICP-MS).
As the first author I contributed to every part of the project and coordinated the collaboration with the co-authors. I performed the ICP-MS studies to determine the average platinum concentration in different tissues, serum and tumor of CT-26 bearing mice upon treatment with platinum-based compounds and I conducted SEC-ICP-MS experiments to study metabolisation. I made a major contribution to all chapters of the manuscript.

Tumor microenvironment in focus: LA-ICP-MS bioimaging of a preclinical tumor model upon treatment with platinum(IV)-based anticancer agents

Sarah Theiner, Christoph Kornauth, Hristo P. Varbanov, Markus Galanski, Sushilla Van Schoonhoven, Petra Heffeter, Walter Berger, Alexander E. Egger, Bernhard K. Keppler

Metallomics, **2015**, 7, 1256-1264

Bioimaging by LA-ICP-MS was performed to study the quantitative platinum uptake in tumor tissue of CT-26 tumor-bearing mice after treatment with platinum-based compounds and correlated with the anticancer activity. In addition, the platinum distribution was assessed in heterogeneous renal structures as possible indicator for nephrotoxicity as side effect of platinum-based chemotherapy.

As the first author I designed the project, contributed to every part of it and coordinated the collaboration with the co-authors. I performed the LA-ICP-MS as well as the ICP-MS studies on mice organs and tumor sections. I made a major contribution to all chapters of the manuscript.

Quantitative bioimaging by LA-ICP-MS: a methodological study on the distribution of Pt and Ru in viscera originating from cisplatin- and KP1339-treated mice

Alexander E. Egger, Sarah Theiner, Christoph Kornauth, Petra Heffeter, Walter Berger, Bernhard K. Keppler, Christian G. Hartinger

Metallomics, **2014**, 6(9): 1616-1625

A quantitative LA-ICP-MS method based on matrix-matched calibration standards was developed and applied to analyze the spatially-resolved platinum and ruthenium distribution in different tissues of mice treated with cisplatin and the investigational drug KP1339, respectively.

I contributed as second author to the LA-ICP-MS as well as to the ICP-MS experiments and data evaluation. I also participated in the discussion and preparation of all chapters of the manuscript.

'Analysis of Pt- and Ru-based anticancer drugs – new developments' in Metallomics: Analytical Techniques and Speciation Methods, Wiley-VCH (Weinheim, Germany), 2015

Sarah Theiner, Luis Galvez-Montano, Gunda Köllensperger, Bernhard K. Keppler, submitted

I contributed to the book chapter with an overview of the state of the art of imaging in metal-based anticancer drug development with emphasis on LA-ICP-MS.

J Biol Inorg Chem (2015) 20:89–99
DOI 10.1007/s00775-014-1214-6

ORIGINAL PAPER

Comparative in vitro and in vivo pharmacological investigation of platinum(IV) complexes as novel anticancer drug candidates for oral application

Sarah Theiner · Hristo P. Varbanov · Markus Galanski · Alexander E. Egger · Walter Berger · Petra Heffeter · Bernhard K. Keppler

Received: 16 September 2014 / Accepted: 2 November 2014 / Published online: 21 November 2014

Abstract Platinum(IV) complexes are promising candidates as prodrugs for oral application in anticancer chemotherapy. However, only a few Pt(IV) compounds entered (pre)clinical trials, e.g. satraplatin, while most of the others were only tested in vitro. Aim of the study was investigation of the in vivo pharmacological behavior as well as the anticancer activity of two novel platinum(IV) complexes vs. satraplatin. The drugs were selected due to significantly different in vitro cytotoxicity while sharing some physicochemical properties (e.g. lipophilicity). Initial experiments indicated that the highly in vitro cytotoxic compound **1** ((OC-6-33)-dichloridobis((4-ethoxy)-4-oxobutanoato)-bis(ethylamine)platinum(IV)) was also characterized by high drug absorption and tissue platinum levels after oral application. Interestingly, analysis of serum samples using SEC-ICP-MS revealed that the administered drugs have completely been metabolized and/or bound to proteins in serum within 2 h after treatment. With regard to the activity in vivo, the outcomes were rather unexpected: although potent anticancer effect of **1** was observed in cell culture, the effects in vivo were rather minor. Nevertheless, **1** was superior to **2** ((OC-6-33)-diammine(cyclobutane-1,1-dicarboxylato)-bis((4-cyclopentylamino)-4-oxobutanoato)platinum(IV)) after i.p. administration, which was, at least to some extent, in accordance to the cell culture experiments. After oral gavage, both compounds exhibited comparable activity. This is remarkable considering the distinctly lower activity of **2** in cell culture as well as the low platinum levels detected both in serum and tissues after oral application. Consequently, our data indicate that the prediction of in vivo anticancer activity by cell culture experiments is not trivial, especially for orally applied drugs.

Keywords Platinum(IV) complexes · Anticancer activity · ICP-MS · Oral administration

Introduction

Platinum-based complexes are established drugs as part of standard therapy in cancer treatment with usage in 50 % of chemotherapeutic regimens in clinics [1]. However, application of the three worldwide approved platinum(II)-based cytostatics (cisplatin, carboplatin and oxaliplatin) are limited by their severe side effects (e.g. nephrotoxicity, neurotoxicity, ototoxicity, myelosuppression, emesis and alopecia), intrinsic and/or acquired therapy resistance and the inconvenient way of intravenous administration [1–5]. These limitations together with the goal of

---

Electronic supplementary material The online version of this article (doi:10.1007/s00775-014-1214-6) contains supplementary material, which is available to authorized users.

S. Theiner · H. P. Varbanov · M. Galanski · B. K. Keppler
Institute of Inorganic Chemistry, University of Vienna,
Waehringer Strasse 42, 1090 Vienna, Austria

S. Theiner · W. Berger · P. Heffeter · B. K. Keppler
Research Platform 'Translational Cancer Therapy Research',
University of Vienna, Waehringer Strasse 42, 1090 Vienna,
Austria

A. E. Egger
ADSI-Austrian Drug Screening Institute GmbH, Innrain 66a,
6020 Innsbruck, Austria

W. Berger · P. Heffeter (✉)
Department of Medicine I, Comprehensive Cancer Center of the
Medical University, Institute of Cancer Research, Medical
University of Vienna, Borschkegasse 8a, 1090 Vienna, Austria
e-mail: petra.heffeter@meduniwien.ac.at

expanding the therapeutic spectrum have led to an intense search for improved metal-based anticancer agents over the past decades [6–8]. One promising approach has focused on the development of platinum(IV) complexes featuring an octahedral geometry and consequently two additional ligand sites [9, 10]. Essential for the anticancer activity of Pt(IV) compounds is their in vivo activation by reduction (preferentially in the tumor cell) to the corresponding platinum(II) analogs, followed by aquation and induction of apoptotic cell death (prodrug-concept). In particular, the increased possibilities for tuning of pharmacological properties via modification of axial ligands combined with the high kinetic inertness to substitution reactions have turned platinum(IV) complexes into promising anticancer drug candidates [11, 12]. So far, three Pt(IV) compounds (tetraplatin, iproplatin and satraplatin) underwent clinical trials, but none of them has gained clinical approval yet. Tetraplatin ((OC-6-22)-tetrachlorido(*trans*-1,2-cyclohexanediamine)platinum(IV)) was abandoned due to severe neurotoxicity, while iproplatin ((OC-6-33)-dichloridodihydroxidobis(isopropylamine)platinum(IV)) demonstrated lower activity compared with carboplatin and cisplatin [1]. Satraplatin ((OC-6-43)-bis(acetato)amminedichlorido(cyclohexylamine)platinum(IV)) was the first orally administered platinum complex with documented efficacy and acceptable safety in patients with hormone-refractory prostate cancer and small-cell lung cancer [13]. Despite the positive outcome after completion of the satraplatin and prednisone against refractory cancer (SPARC) phase III clinical trials, satraplatin was not approved by the FDA as it did not show a convincing benefit in terms of overall survival. However, clinical studies with satraplatin are still ongoing [1].

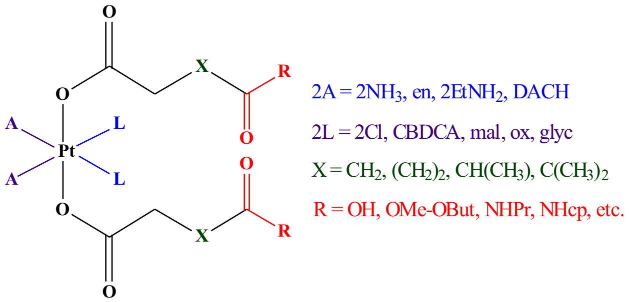

$2A = 2NH_3$, en, $2EtNH_2$, DACH
$2L = 2Cl$, CBDCA, mal, ox, glyc
$X = CH_2$, $(CH_2)_2$, $CH(CH_3)$, $C(CH_3)_2$
R = OH, OMe-OBut, NHPr, NHcp, etc.

Fig. 1 General formula of diam(m)inebis-, tris- and tetrakis(carboxylato)platinum(IV) complexes developed, in our group (*DACH* 1R,2R-diaminocyclohexane, *CBDCA* 1,1-cyclobutanedicarboxylate, *mal* malonate, *ox* oxalate, *glyc* glycolate)

Recently, our group has reported a convenient synthetic procedure for preparation of novel bis(carboxylato)platinum(IV) complexes and modulation of their physicochemical properties of interest (e.g. solubility, lipophilicity and redox behavior) [14]. Consequently, a plethora of diam(m)inebis-, tris- and tetrakis(carboxylato) platinum(IV) complexes featuring prodrugs of cisplatin, its bis(ethylamine) and ethylenediamine analogs, carboplatin, and its malonato analog, oxaliplatin, and nedaplatin, has been developed utilizing this approach (Fig. 1) [14–20]. The set of compounds covers a broad range of in vitro cytotoxicity (IC_{50} values from 0.009 to >500 μM) in the cancer cell lines tested.

The analytical and biochemical, as well as theoretical and QSAR studies performed in the series [20] allowed us to select the most interesting compounds for further in vivo investigations (i.e. pharmacokinetic behavior and anticancer activity). (OC-6-33)-dichloridobis((4-ethoxy)-4-oxobutanoato)bis(ethylamine)platinum(IV) (Fig. 2, **(1)**) is one of the most active compounds in our set of over 60 investigated complexes, with higher or comparable potency to cisplatin in all the tested cell lines and adequate solubility and lipophilicity for further in vivo experiments [17, 20]. (OC-6-33)-diammine(cyclobutane-1,1-dicarboxylato)bis((4-cyclopentylamino)-4-oxobutanoato)platinum(IV) (Fig. 2, **(2)**) is a carboplatin prodrug representative, characterized with high kinetic stability towards biological reducing agents (e.g. ascorbate). This compound was chosen with respect to its solubility, lipophilicity and in vitro cytotoxicity in the subseries [18].

Herein, we have investigated the anticancer activity in murine cancer cell models as well as the platinum

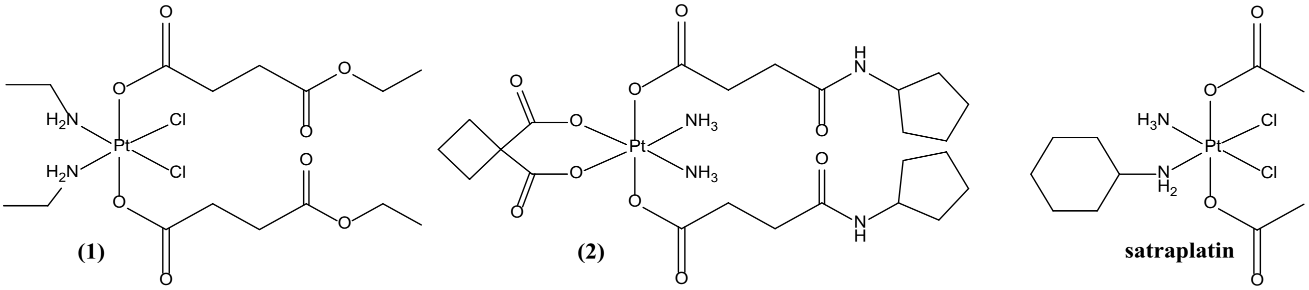

Fig. 2 Structural formulas of the platinum(IV) complexes under investigation

distribution in tissues by means of ICP-MS of the selected drug candidates in comparison to satraplatin (Fig. 2). The predictability of (1) cell culture experiments, (2) platinum accumulation in mice tissue samples and (3) serum platinum levels for the in vivo anticancer activity of Pt(IV) complexes has been assessed.

Experimental

Chemicals

Milli-Q water (18.2 MΩ cm, Milli-Q Advantage, Darmstadt, Germany) was used for RP-HPLC and SEC-ICP-MS experiments as well as for all dilutions for ICP-MS measurements. Nitric acid (≥65 %, p.a., Fluka, Buchs, Switzerland) was further purified in a quartz sub-boiling point distillation unit (Milestone-MLS GmbH, Leutkirch, Germany). Platinum and rhenium standards for ICP-MS measurements were derived from CPI International (Amsterdam, The Netherlands). All other reagents and solvents were obtained from commercial sources and were used without further purification. Synthesis and characterization of the novel Pt(IV)-based drug candidates (**1** and **2**) were described previously [17, 18] Satraplatin was prepared according to Ref. [21].

ICP-MS measurements

Quantification of platinum in liquid samples (including on-line sample introduction via SEC) was carried out with an ICP-quadrupole MS instrument Agilent 7500ce (Agilent Technologies, Waldbronn, Germany) equipped with a CETAC ASX-520 autosampler (Nebraska, USA) and a MicroMist nebulizer at a sample uptake rate of approx. 0.25 ml/min. The instrument was tuned on a daily base to achieve maximum sensitivity. Rhenium served as internal standard for platinum to account for instrumental fluctuations and matrix effects. The Agilent MassHunter software package (Workstation Software, version B.01.01, 2012) was used for data processing. The experimental parameters for ICP-MS are summarized in Table 1.

Digestion of tissue samples (approx. 10–30 mg) was performed with 2 ml of 32.5 % subboiled nitric acid using a microwave system Discover SP-D (CEM Microwave Technology, Germany). The following microwave parameters were used: temperature, 200 °C; ramp time, 4 min; hold time, 6 min; maximal power, 300 W. Digested samples were diluted with Milli-Q water resulting in nitric acid concentrations lower than 3 % and platinum concentrations lower than 15 µg/g. In the case of serum and whole blood, approx. 50 µl were weighed and digestion was done under the same conditions as the organs. The total platinum content was determined with ICP-MS using the experimental parameters given in Table 1.

Table 1 Instrumental parameters for quantification of platinum with ICP-MS

	ICP-MS
RF power (W)	1500
Cone material	Nickel
Carrier gas (l/min)	0.92–0.96
Make up gas (l/min)	0.16–0.19
Plasma gas (l/min)	15
Monitored isotopes	^{185}Re, ^{194}Pt, ^{195}Pt
Dwell time (s)	0.1
Number of replicates	10

Determination of solubility

Solubility was determined using the conditions described in the OECD guidelines [22] with slight modifications. Saturated solutions of the investigated compounds were prepared in Milli-Q water at room temperature. Undissolved particles, remaining after repeated steps of ultrasonication, were removed using a 0.45 µm filter. Solubility of the complexes was calculated after dilution of the samples with 1 % HNO_3 and determination of the platinum concentration by means of ICP-MS (using the instrumental parameters given in Table 1).

Determination of lipophilicity and stability

Lipophilicity was determined as the partition coefficient between *n*-octanol and water (log $P_{o/w}$) and as the chromatographic retention factor (log k_w). The log $P_{o/w}$ determination was carried out according to the OECD guidelines for the classical shake flask method [23] with slight modifications. The complexes were dissolved in Milli-Q water (pre-saturated with 1-octanol) and the platinum concentration was determined by ICP-MS. The remaining stock solution was mixed with an equal volume of 1-octanol (pre-saturated with Milli-Q water) and shaken for 1 h. After phase separation, the platinum concentration was again determined in the aqueous phase by ICP-MS and the partition coefficients were calculated assuming the missing quantity (compared to the stock solution) in the organic phase. ICP-MS measurements were carried out after dilution of the samples with 1 % HNO_3 using the instrumental parameters given in Table 1.

The chromatographic retention factor (log k_w) was assessed by means of RP-HPLC as described previously [17]. The analysis was carried out on a Dionex Summit system (Dionex, Germering, Germany) controlled by the

Dionex Chromeleon 6.80 software. The following chromatographic conditions were used: Agilent ZORBAX SB aq C18 column (4.6 mm × 250 mm, 5 µm); injection volume: 20 µl; flow rate: 1 ml/min; isocratic elution; temperature of the column: 25 °C; UV–Vis detection set up at 210 nm; uracil was used as an internal reference to determine the column dead time (t_0); 0.1 % TFA aqueous solution/MeOH-based mobile phases were employed. The chromatograms for each complex were run in triplicates with at least three different mobile phase compositions and the respective capacity factors ($k = (t_R - t_0)/t_0$) were calculated. The extrapolated retention factor to 0 % MeOH ($\log k_w$) was determined, using the linear relationship between $\log k$ and the concentration of MeOH in the mobile phase. The same chromatographic conditions were used to determine the stability of the compounds in water solution. The complexes proved to be stable within 24 h of incubation at 37 °C.

SEC-ICP-MS experiments

Serum obtained from mice 2 h after single dose oral administration of compound **1**, **2** and satraplatin was diluted in phosphate-buffered saline (PBS) and subjected to SEC-ICP-MS. For comparison reasons, the compounds were dissolved in PBS, incubated for 1 and 24 h at 37 °C and also analysed by SEC-ICP-MS. A size exclusion column (10 mm × 300 mm, 13 µm) (Superdex^{TM} 200, 10/300 GL, GE Healthcare) with an approximate bed volume of 24 ml and a linear separation range of 10–600 kDa was used. Analysis was carried out on a Dionex Ultimate 3000 RS system (Dionex, Germering, Germany) controlled by the Dionex Chromeleon 6.80 software. Injection volume was 20 µl and elution was performed in isocratic mode with an aqueous solution of ammonium acetate (100 mmol/l, pH = 7.4) as mobile phase at a flow rate of 0.7 ml/min. The column was calibrated with a mixture of ferritin (440 kDa), aldolase (158 kDa), conalbumin (75 kDa), ovalbumin (43 kDa), carbonic anhydrase (29 kDa), ribonuclease (13.7 kDa) and aprotinin (6.5 kDa) using UV–Vis detection at 280 nm. The retention times (t) were plotted against the logarithm of the molecular mass (y) and showed linear correlation ($y = -0.150t + 7.849$, $R^2 = 0.993$). The column was coupled via a PEEK tubing directly to a MiraMist nebulizer of the ICP-MS. The platinum trace was recorded using the Agilent MassHunter Chromatography software package (Workstation Software, version B.01.01, 2012). The instrumental parameters of ICP-MS are given in Table 1.

Cell cultures

The following cell lines were used in this study: the murine leukemia model L1210 (generously provided by Dr. Ganapathi, Cleaveland Clinic Foundation, Ohio, USA) and the murine colon cancer cell model CT-26 (from American Type Culture Collection, Manassas, VA, USA). All cells were grown in a humidified atmosphere with 5 % CO_2 at 37 °C in medium supplemented with 10 % fetal bovine serum (FCS). L1210 cells were grown in RPMI 1640 and CT-26 cells in DMEM/F12 medium. Cultures were regularly checked for Mycoplasma contamination.

Cytotoxicity assay

The above described cells were seeded (2×10^3 cells/well) in 100 µl per well in 96 well plates. After a recovery period of 24 h, stock solutions (10 mM) of the drugs (freshly prepared in DMSO) were serially diluted with growth medium and added to the samples in volumes of 100 µl per well. Final DMSO concentrations never exceeded 0.5 %. At this concentration, DMSO neither impacted cell viability nor drug stability (confirmed by ^{1}H NMR) of the test compounds, which is in accordance to the work of Hall et al. [24]. After exposure for 72 h, the cell viability was determined by MTT (3-(4,5-dimethyl-2-thiazolyl)-2,5-diphenyl-2*H*-tetrazolium bromide) assay following the manufacturer's recommendations (EZ4U, Biomedica, Vienna, Austria).

Animal experiments

All animal experiments were approved by the local ethics commission and carried out according to the Austrian and FELASA guidelines for animal care and protection. 6- to 8-week-old Balb/c or DBA/2J mice (weighing 25–30 g) were purchased from Harlan Laboratories, San Pietro al Natisone, Italy. The animals were kept in a pathogen-free environment and every procedure was done in a laminar airflow cabinet.

Kinetic experiments with Balb/c mice

Mice which received the drugs as an oral single dose (40 mg/kg, solutions freshly prepared in water with 1 % DMSO), were anesthetized after 2 h and blood was collected by heart punctuation. Serum was isolated by centrifugation of the blood samples at 3000 rpm for 10 min for two times and stored at −20 °C for SEC-ICP-MS experiments. In addition, samples of organs (kidney, liver, lung) were collected and stored at −20 °C for quantitative determination of platinum by means of ICP-MS after microwave-assisted digestion. For kinetic experiments, the compounds were administered orally at single dose of 0.05 mmol/kg (i.e. 34.1, 40, and 25.8 mg/kg for compound **1**, **2**, and satraplatin, respectively; solutions freshly prepared in water with 1 % DMSO; Table S1) and total blood was collected after 2, 4 and 6 h by tail vain puncture. Mice were sacrificed after 24 h and blood as well as organs was collected for platinum determination without prior perfusion of the animal.

Table 2 In vitro cytotoxicity in three human cancer cell lines and pharmacologically relevant physicochemical properties of compound **1**, **2** and satraplatin

Compound	**1**	**2**	Satraplatin
Formula	$C_{16}H_{32}N_2O_8PtCl_2$	$C_{24}H_{40}N_4O_{10}Pt{\bullet}H_2O$	$C_{10}H_{22}N_2O_4PtCl_2$
MW (g/mol)	646.4	757.7	500.3
Aqueous solubility (mg/ml)	1.94 ± 0.02	10.2 ± 0.04	0.10 ± 0.01
Lipophilicity (log k_w)	2.87 ± 0.01	2.99 ± 0.06	1.49 ± 0.03
Lipophilicity (log $P_{o/w}$)	0.72 ± 0.03	0.77 ± 0.06	0.23 ± 0.01
IC_{50} (CH1), μM[a]	0.061 ± 0.015[b]	15 ± 5[c]	0.10 ± 0.02[d]
IC_{50} (SW480), μM[a]	0.30 ± 0.05[b]	>500[c]	1.5 ± 0.1[d]
IC_{50} (A549), μM[a]	1.0 ± 0.4[b]	>500[c]	6.4 ± 0.4[d]

[a] 50 % inhibitory concentrations (means ± standard deviations from at least three independent experiments) as obtained by the MTT assay, 96 h exposure

[b] Data taken from Ref. [17]

[c] Data taken from Ref. [18]

[d] Data taken from Ref. [28]

Anticancer activity against CT-26 cells in vivo

Murine CT-26 cells (5×10^5) were injected subcutaneously into the right flank of female Balb/c mice. Animals were treated with the drug either intraperitoneally (solutions freshly prepared in water) or orally (solutions freshly prepared in water with 1 % DMSO) at indicated drug concentrations on days 4, 7, 11, and 14 (Table S1). Animals were controlled for distress development every day and tumor size was assessed regularly by caliper measurement. Tumor volume was calculated using the formula: length × width^2/2. At day 15, tissue and blood samples from anesthetized animals were collected for quantitative determination of platinum as described above.

Antileukemic activity in vivo

L1210 murine leukemia cells (1×10^5) were injected intraperitoneally in a volume of 0.2 ml into male DBA/2 J mice on day 0. The test compounds (dissolved in water) were administered intraperitoneally at indicated drug concentrations on day 1, 5 and 9 (Table S1). Toxicity was monitored by daily observation of animals and registration of their body weight. Therapeutic efficacy of the investigated compounds was monitored by recording the lengths of survival of experimental mice compared to untreated control animals.

Results and discussion

Overview of in vitro cytotoxicity and pharmacologically relevant physicochemical properties

Physicochemical properties, relevant for the pharmacological behavior of the novel platinum(IV) anticancer drug candidates and satraplatin, together with their in vitro cytotoxicity in three human tumor cell lines, are summarized in Table 2. The new compounds have a lipophilicity being in an optimal range (log $P_{o/w}$ 0.5–3.5) for oral application which should in both cases allow a sufficient absorption from the intestinal lumen into the bloodstream [25]. Our approach for modification of the axial ligands of platinum(IV) complexes [18, 26] allows adjusting the lipophilicity to optimal values without compromising the solubility. As a consequence, compound **1** and **2** possess advantageous (20- to 100-fold higher) water solubility compared to satraplatin. This is also of importance as aqueous solubility is often a limiting factor for drugs when administered intraperitoneally (i.p.). Although being less critical for p.o. administration, it also impacts on the drug absorption efficiency via this route, as only the dissolved fraction can be absorbed in the digestive tract [25]. Regarding the Lipinski's rule of five criteria for evaluation of drug likeness [27], all tested compounds satisfy the criteria for lipophilicity (log $P_{o/w} < 5$), but not for a maximum molecular weight (MW < 500 Da). Compound **1** and **2** (646.4 and 757.7 Da, respectively) have a higher molecular weight, while satraplatin is exactly on the border of the limit (MW = 500.3 Da). The above-mentioned approach for tuning the lipophilicity via modification of the axial ligands also results in a higher number of hydrogen bond acceptors for compound **1** and **2**, compared to satraplatin. However, complex **1** and satraplatin still satisfy Lipinski's requirement for the maximal number of hydrogen bond donors and acceptors. Nevertheless, it should be mentioned that Lipinski's rules of five were postulated for organic molecules and should be considered for metal-based drugs more carefully. For example, the heavy metal platinum (with a molecular weight of 195 Da) already contributes to approximately 40 % of the molecular weight limit.

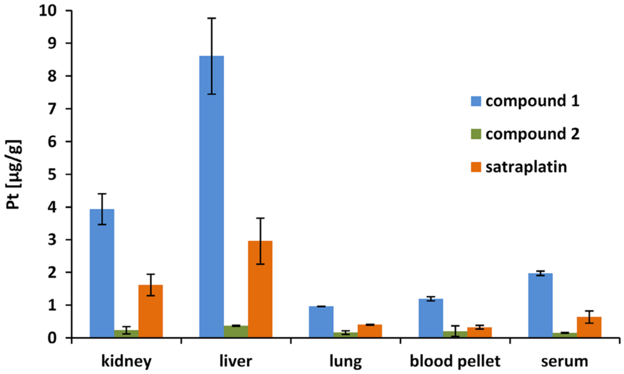

Fig. 3 Total platinum levels of compound **1**, **2** and satraplatin in mice organs, blood pellet and serum 2 h after single dose oral application (40 mg/kg), corresponding to Pt doses of 12.1, 10.32 and 15.63 mg/kg, respectively

With regard to the anticancer activity, compound **1** demonstrated pronounced in vitro cytotoxicity, slightly higher than satraplatin in the cell lines tested. Despite featuring similar lipophilicity, compound **2** proved to be far less potent than complex **1**, most probably due to its slower rate of activation (reduction and subsequent aquation) [18].

Tissue distribution of platinum in mice after single dose oral administration of the investigational drugs

As a first approach to test the bioavailability of the novel platinum(IV) drugs, healthy mice were treated orally with the test compounds (Table S1). After 2 h, blood and organs were collected and the total platinum concentrations were determined by ICP-MS measurements. In these preliminary experiments, a dose of 40 mg/kg was chosen as this represents a frequently used oral dose for satraplatin [29]. Overall, a similar platinum distribution pattern could be observed for all three compounds with highest platinum levels in liver, followed by kidney and lung tissue (Fig. 3). The mice were not perfused after sacrificing, thus the high platinum concentrations in liver and kidney can be explained by their high blood supply as well as their biological functions. Liver is responsible for drug metabolism and especially for orally administered drugs the first-pass metabolism can be extensive [25]. In renal tissues frequently high drug levels occur due to the high blood flow to the kidneys (~25 % of cardiac output) together with the enormous concentrating ability of the organ [30]. This often results in high concentrations of parent compounds as well as their metabolites. Lung tissue showed platinum concentrations similar to serum and blood clot, containing the total cellular fraction of the blood samples (blood pellet), which can be also explained by the high blood perfusion of the organ [31].

Notably, although the relative platinum distribution patterns of the three drugs were very similar, the total platinum concentrations differed distinctly (Fig. 3, Table S2). Thus, 2 h after drug application highest platinum levels were observed in mice treated with compound **1** (~9 µg/g in liver > ~4 µg/g in kidneys > ~2 µg/ml in serum > ~1 µg/g in blood pellet = ~1 µg/g in lungs). Satraplatin exhibited 2–3 times lower platinum concentrations in the investigated tissues. In contrast, complex **2** showed the lowest platinum accumulation with less than 0.5 µg/g in all organ samples. This might be based on the comparably low platinum levels in the blood serum (~0.15 µg/ml), indicating lower oral bioavailability and/or faster excretion of **2** than of compound **1** and satraplatin. Ranking the complexes according to the percentage of platinum amount found in serum after 2 h relative to the administered platinum dose, was as follows: ~16 % Pt for compound **1** > ~4 % Pt for satraplatin > ~1.5 % Pt for compound **2**.

SEC-ICP-MS study in mice serum after single dose oral administration of the investigational drugs

In addition to the absolute quantification of platinum in tissues, the interaction with protein binding partners in serum in vivo can provide further information on the fate of the drug in the organism. For this purpose, size-exclusion chromatography (SEC) was hyphenated to ICP-MS, allowing the separation and detection of metal-containing species in serum according to their molecular weight. Overall, all three compounds demonstrated high affinity to serum proteins and appeared to have binding partners with similar size as the general pattern of chromatograms was comparable (Figure S1). The main peak observed at ~20 min (corresponding to approx. 66 kDa) represents most likely platinum bound to serum albumin (molecular weight 66.5 kDa), the most abundant serum protein which has been identified as the main binding partner in serum for several metal-based drugs (e.g. cisplatin, oxaliplatin and KP1019) [32–35]. Thus, all three drugs seem to be predominately bound to albumin and to lesser extent to serum proteins and protein complexes corresponding to fractions eluting after ~17 min (approx. 170 kDa) and ~12 min (> 600 kDa). In addition, a peak at 42 min corresponding to the void volume of the column was found in all samples investigated. Thus, small platinum-containing molecules, which do not interact with the column material, are present in the serum samples.

To assign these peaks to metabolites or parent drug molecules, the compounds were dissolved in phosphate-buffered saline (PBS) and injected into the SEC column, either freshly prepared or after 1 and 24 h of incubation at 37 °C. The different species of the metal-based drugs are separated due to unspecific interactions with the stationary phase, since these molecules are too small to be separated based on their molecular weights [36]. Subsequently, the obtained serum-free chromatograms were compared with those of the serum samples to identify unbound platinum-containing species (Figure S1, arrows indicate metabolites and the parent drug). For all spectra, the above-mentioned peak at 42 min was assigned to metabolites of the respective drugs. Satraplatin exhibits two more metabolites at ~29 and ~32 min, while compound **2** was the only one showing the presence of a small amount (~5 %) of the free intact platinum(IV) complex. The absence of intact satraplatin in serum samples is in accordance with literature reports for satraplatin [37, 38]. Thus, it was demonstrated in clinical trials that already 15 min after oral application of satraplatin, six new species were found in patients' plasma ultrafiltrate whereas no parent drug was detected [38].

Kinetics of whole blood platinum following single p.o. administration

Platinum levels in whole blood (collected after vein puncture using a capillary) upon single oral administration of novel drug candidates and satraplatin were determined by means of ICP-MS at 2, 4, 6 and 24 h. For all three compounds, highest levels of platinum were found at the first time point investigated (2 h) with subsequent decreasing amounts of platinum in blood (up to 24 h) (Figure S2). According to literature reports on the pharmacokinetics of satraplatin in rats, the maximum concentration of platinum in plasma after p.o. application of satraplatin is found between 1.5 and 4 h [39]. Similar results were observed in clinical trials where patients were treated with satraplatin [40]. Based on these reports and the platinum concentration–time curves obtained in our experiments, it can be assumed that the highest platinum levels in blood are reached ≤2 h upon oral administration of the investigated complexes. Main pharmacokinetic parameters for compound **1**, **2** and satraplatin are summarized in Table 3. The calculated AUC_{2-24} indicate that the total systemic platinum exposure (between the 2nd and 24th hour) after single oral administration of compound **1** and satraplatin is rather similar and more than two times higher than that for complex **2**. The lower C_{2h} and AUC_{2-24}, observed for complex **2** are probably connected with its lower oral bioavailability and/or fast excretion before the 2nd hour after oral administration.

Table 3 Preliminary pharmacokinetic parameters of blood platinum, following a single oral dose of 0.05 mmol/kg of **1**, **2** or satraplatin, corresponding to approx. 0.2 mg of administered platinum

Compound	C_{2h} (μg/ml)[a]	K_{el} (1/h)[b]	$t_{1/2}$ (h)[b]	AUC_{2-24} (μg h/ml)[c]
1	1.89	0.058	12	17.36
2	0.82	0.065	11	8.66
Satraplatin	1.36	0.037	19	19.40

Values were calculated using the trapezoidal rule

[a] Platinum concentration after 2 h is set to be close to C_{max}

[b] Elimination rate constants (K_{el}) and half-lives ($t_{1/2}$) were determined using the ln *C*/*t* plot

[c] Area under the curve between the 2nd and 24th hour after administration (AUC_{2-24})

Evaluation of in vivo anticancer activity of novel platinum(IV) compounds in comparison to satraplatin

As a first step, the cytotoxic potential of the compounds was assessed against the murine leukemia L1210 and the colon carcinoma model CT-26 in cell culture experiments. As shown in Table 4, compound **1** and satraplatin displayed potent activity in the low μM range in both cell lines tested. Comparable to the experiments on human cell models (see Table 2), complex **1** showed slightly higher cytotoxicity than satraplatin in L1210 cells, while in CT-26 cells satraplatin was ~2-fold more active than **1**. In contrast, compound **2** was inactive in both cell lines, with no signs of cytotoxicity up to the highest tested concentration of 50 μM.

Table 4 In vitro cytotoxicity of complex **1**, **2** and satraplatin in two murine cancer cell lines

Compound	IC_{50} (μM)[a] mean ± SD	
	L1210	CT-26
1	1.5 ± 0.4	5.7 ± 0.2
2	>50	>50
Satraplatin	2.5 ± 0.2	2.9 ± 0.3

[a] 50 % inhibitory concentrations (means ± standard deviations from at least three independent experiments), as obtained by the MTT assay, 72 h exposure

Subsequently, the in vivo anticancer activity of the novel platinum(IV)-based drug candidates was evaluated in CT-26-bearing mice in comparison to satraplatin. For these experiments, the drugs were applied four times (on days 4, 7, 11, and 14) and mice were sacrificed 24 h after the last application (Table S1). For oral application, a dosage of 40 mg/kg was used for satraplatin and compound **2**. In case of compound **1**, two dosages were tested orally: 51.7 mg/kg (equimolar to 40 mg/kg satraplatin) and 34.1 mg/kg (equimolar to 40 mg/kg of complex **2**). In addition, complex **1** and **2** were tested intraperitoneally at equimolar concentration (8.5 mg/kg for **1** and 10 mg/kg for **2**). In all experiments, the compounds were well tolerated with no signs of toxicity such as fatigue or weight loss.

The anticancer activity of the three platinum(IV) compounds, expressed as tumor volume (mm^3), is shown in Fig. 4a. Upon oral administration, treatment with complex

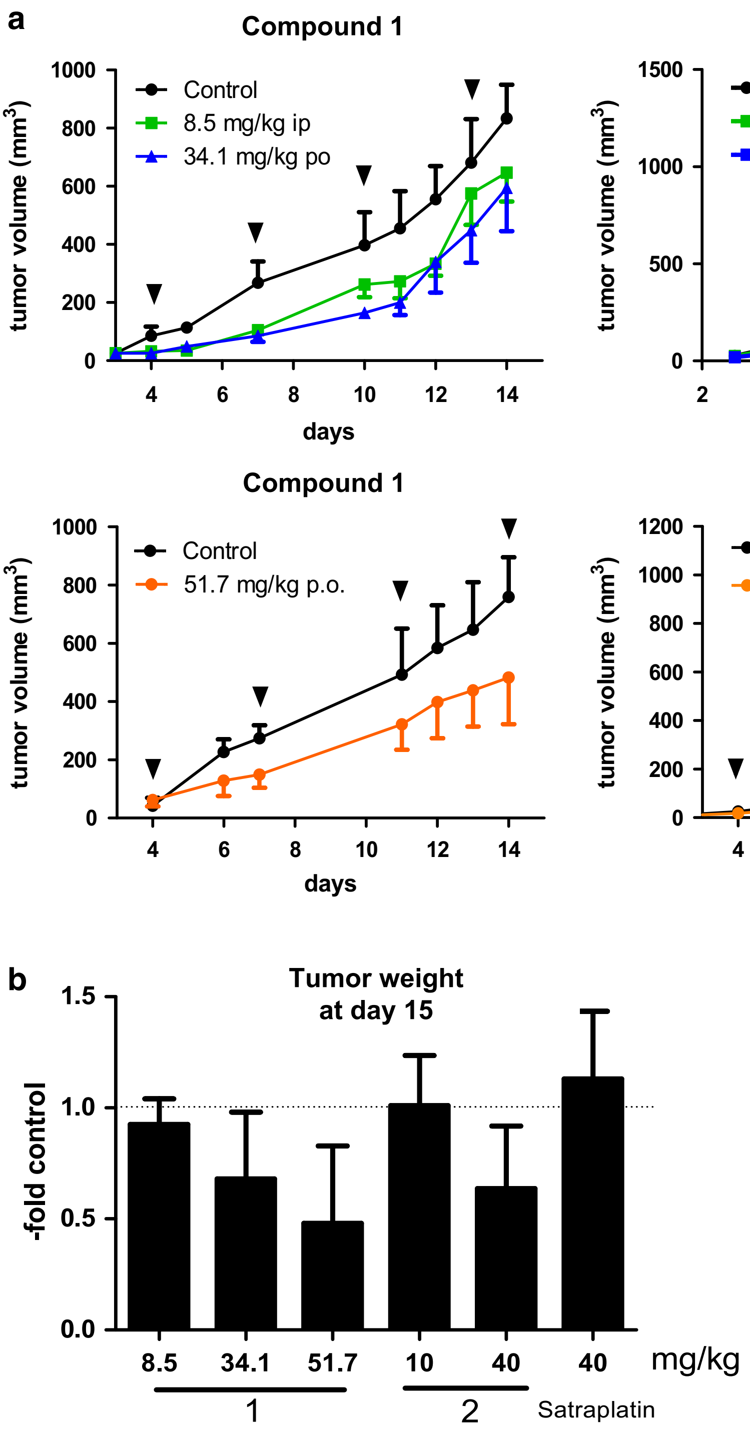

Fig. 4 In vivo anticancer activity of compound **1**, **2** and satraplatin. CT-26 cells were injected subcutaneously into the right flank of BALB/c mice. Mice were treated on day 4, 7, 11, and 14 (indicated by *black triangles*) with either compound **1** at concentrations of 8.5 mg/kg (i.p.), 34.1 mg/kg (p.o.) and 51.7 mg/kg (p.o.), compound **2** at concentrations of 10 mg/kg (i.p.) and 40 mg/kg (p.o.) or satraplatin at 40 mg/kg (p.o.). Data visualized in the same color correspond to equimolar concentrations. **a** Tumor volumes were calculated as described in the "Experimental" part. Each experimental group contained four animals. Data are mean ± SEM. **b** Animals were sacrificed on day 15 and tumors were collected and weighed. Data are expressed as fold change to the untreated control group of the respective experiment

1 and **2** led to a slight tumor growth delay to similar extent. In case of compound **1**, this effect was independent from the drug dose used (34.1 or 51.7 mg/kg). Unexpectedly, despite its potent anticancer activity in vitro, satraplatin was completely inactive against CT-26 cells in vivo. To the best of our knowledge, this might also explain the lack of reports on experiments with satraplatin in CT-26-bearing mice, although CT-26 is a known model for in vivo tests of platinum drugs [41–44]. In addition, the results obtained upon oral treatment with **1** and **2** are unexpected considering the in vitro IC_{50} values shown in Tables 2 and 4. Although complex **1** was more than tenfold more active against CT-26 cells in MTT assays, it did not show convincingly higher antitumor activity upon oral application in vivo and the experimental setup used (Fig. 4).

With regard to the intraperitoneal application, complex **1** displayed anticancer activity comparable to the p.o. experiments, while complex **2** was inactive when given i.p. at equimolar concentrations. Similar results were obtained upon intraperitoneal application of the novel Pt(IV) anticancer drugs in mice bearing L1210 leukemia cells (Figure S3).

Tissue distribution of platinum after multiple dose administration of investigational drugs in CT-26 tumor-bearing mice

To better understand the pharmacology and toxicology of the novel complexes, tissue samples, collected from CT-26-bearing mice (compare Fig. 4) were analyzed by ICP-MS. The platinum levels in tumor, kidney, liver, lung, and fractions of whole blood (serum and blood pellet) are shown in Fig. 5 and Table S2. As expected, the route of administration had a distinct impact on the quantitative platinum accumulation in all tissues. Platinum concentrations in tissue upon i.p. application were higher, despite the four times lower dosages administered, compared to the p.o. application. In general, this is not unexpected as usually not the full amount of the orally applied compound is bioavailable. The difference between oral and intraperitoneal treatment was most pronounced for complex **2**, where tenfold higher amounts of platinum were measured in liver, kidney and serum after i.p. administration. Nevertheless, the same trend of platinum distribution as for the single dose experiments could be observed independently from the route of administration (compare with Fig. 3). Thus, compound **1** displayed again the highest platinum levels in all samples, followed by satraplatin and compound **2** (Fig. 5, Table S2 and Figure S4) and the highest platinum concentrations were found in liver followed by kidney and lung tissue.

The repeated oral administration over 2 weeks resulted in an overall increase of platinum content in the tissues in comparison to the single dose experiments over 24 h indicating a cumulative effect (Table S2). Complex **1** was administered orally in two doses (Fig. 5a) leading to correspondingly elevated platinum levels in the investigated samples: a two times higher platinum concentration in kidney and liver was observed, whereas in tumor the platinum level increased up to 30 %. This indicates that although the total body platinum levels increased in accordance to the applied higher dose, this had a minor impact on the amount of platinum delivered to the malignant tissue. For compound **2**, platinum concentrations <0.5 µg/g could be observed for all tissues after oral application, corresponding to 10- to 50-fold lower platinum amounts compared to compound **1**. Interestingly, despite the overall significantly higher platinum levels, complex **1** did not demonstrate distinctly better in vivo anticancer activity in the CT-26 model after oral treatment, compared to complex **2**.

Overall, the outcome of the in vivo experiments was rather unexpected considering the results of the cell culture tests. Although a potent anticancer activity of compound **1** against both CT-26 and L1210 cells was observed in cell culture, the effects in vivo were rather minor. Nevertheless, compound **1** was superior to **2** after i.p. administration, which is, at least to some extent, in accordance to the cell culture experiments. In contrast, both compounds were similarly active after oral gavage and at least in the case of **1** also widely independent of the given dose. This is remarkable, especially considering the almost complete lack of activity in cell culture as well as the low platinum levels detected both in serum and tissues after oral drug treatment in the case of complex **2**. Noteworthy, compound **2** is a prodrug of the clinically used platinum(II) drug carboplatin. We have previously reported that the rate of reduction by biological reducing agents (e.g. ascorbate) of tetracarboxylatoplatinum(IV) complexes, prodrugs of carboplatin are slower than for diaminedichloridobis(carboxylato)platinum(IV) complexes (e.g. compound **1** and satraplatin) [18]. In addition, carboplatin is much less reactive than cisplatin (and its dichlorido analogs), which is reflected in slower metabolism (in vitro and in vivo) and rather low IC_{50} values in cell culture experiments. Moreover, the therapeutic dose of carboplatin is approx. four times higher than for cisplatin, as nearly 90 % of the injected dose is recovered in urine [45]. The slow metabolism of compound **2** could be an explanation for the low platinum levels detected both in serum and tissues after treatment with **2**. Our SEC-ICP-MS experiments showed that nearly no free parental species of the investigated platinum(IV) compounds could be detected in blood serum already 2 h after oral application. It may be speculated that the tested complexes in their native forms are excreted faster than their metabolites, which tend to bind to serum protein and to be retained in tissues. In addition, especially the first-pass effect, also reported for many other orally applied drugs [25] has to be considered.

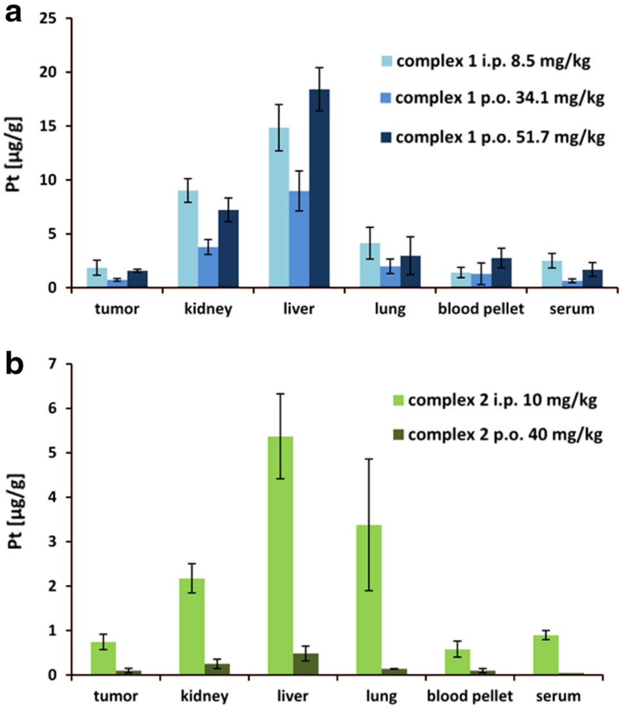

Fig. 5 Platinum accumulation after multiple dose administration (i.p. and p.o.) of complex **1** (**a**) and complex **2** (**b**) in different tissues, blood pellet and serum originating from CT-26-bearing mice. Data are based on four animals per group, average concentrations and corresponding standard deviations are given

Our data suggest that after oral gavage only a fraction of the test drugs is taken up into the body and thus is bioavailable. This is a frequent observation when using oral application and the reasons, why only part of the drug reaches the systemic circulation are complex and can be influenced by various factors [46]: (1) drugs might have insufficient stability in the gastrointestinal tract leading to degradation before drug uptake. (2) Several physicochemical factors (e.g. lipophilicity) can influence the drug absorption. This effect was minimized in our study as the compounds possess similar lipophilicity. Nevertheless, it cannot be completely ruled out that some other physicochemical parameters might impact on their bioavailability. Finally, (3) there might be insufficient drug absorption from the intestinal lumen, for example, based on drug efflux back into the gastrointestinal tract by cellular transport proteins, e.g. P-glycoprotein (ABCB1) or the breast cancer resistance protein (ABCG2). These efflux proteins are strongly expressed at the membranes of the gut epithelium and are known to impact on multiple drugs [3, 46]. To gain insights into this topic, the role of ABC transporter expression on the anticancer activity of our two test drugs (especially compound **2**) is matter of ongoing investigations.

Conclusions

The results from this study indicate that pre-experiments using cell culture can only be taken as a first indication to estimate the in vivo anticancer activity of platinum (IV)-based cytostatics. Thus, i.p. experiments were found to be in some agreement with the cell culture experiments, predicting the reduced antitumor activity of compound **2** compared to compound **1.** In contrast, the data from cell culture experiments were not at all predictive for the in vivo activity after oral gavage. Despite the low IC_{50} values demonstrated in the viability tests and the high amount of platinum detected in blood and tumor tissue, compound **1** did not show significantly enhanced activity against CT-26 cells in vivo in comparison to compound **2.** However, the mechanisms leading to this discrepancy between in vivo and cell culture experiments are so far speculative. One explanation might be rapid metabolization indicated by the serum analysis, which showed that already 2 h after oral treatment the administered drugs have been completely metabolized and/or bound to proteins in serum. In addition, cytotoxicity tests conducted solely with human cancer cell lines do not consider the complex interactions between various tissue types and their impact on pharmacokinetics and pharmacodynamics of the test compounds. Further investigations of the role and activity of diverse drug metabolites is topic of ongoing studies and will help to better understand the fate of anticancer drugs in vivo. Moreover, such detailed knowledge can improve the prediction of in vivo anticancer activity and, thus, allow selecting the best drug candidates for further (pre)clinical development.

Acknowledgments Matthias Klose and Ricarda Bugl are acknowledged for their assistance in sample preparation and ICP-MS measurements. In addition, we are thankful to G. Zeitler and S. Van Schoonhoven for animal care. This work was supported by the Austrian Science Fond grant P26603 (to P.H.). This work was performed in the surrounding of COST action CM1105.

References

1. Wheate NJ, Walker S, Craig GE, Oun R (2010) Dalton Trans 39:8113–8127
2. Yao X, Panichpisal K, Kurtzman N, Kenneth N (2007) Am J Med Sci 334:115–124
3. Heffeter P, Jungwirth U, Jakupec M, Hartinger C, Galanski M, Elbling L, Micksche M, Keppler B, Berger W (2008) Drug Resist Updat 11:1–16
4. Kelland LR (2007) Nat Rev Cancer 7:573–584
5. Jakupec MA, Galanski M, Arion VB, Hartinger CG, Keppler BK (2008) Dalton Trans 2:183–194
6. Galanski M, Arion VB, Jakupec MA, Keppler BK (2003) Curr Pharm Des 9:2078–2089
7. van Rijt SH, Sadler PJ (2009) Drug Discov Today 14:1089–1097
8. Hambley TW (2007) Dalton Trans 4929–4937

9. Hall MD, Mellor HR, Callaghan R, Hambley TW (2007) J Med Chem 50:3403–3411
10. Hall MD, Hambley TW (2002) Coord Chem Rev 232:49–67
11. Gibson D (2009) Dalton Trans 10681–10689
12. Wexselblatt E, Gibson D (2012) J Inorg Biochem 117:220–229
13. Choy H, Park C, Yao M (2008) Clin Cancer Res 14:1633–1638
14. Reithofer MR, Valiahdi SM, Jakupec MA, Arion VB, Egger A, Galanski M, Keppler BK (2007) J Med Chem 50:6692–6699
15. Reithofer M, Galanski M, Roller A, Keppler BK (2006) Eur J Inorg Chem 2006:2612–2617
16. Reithofer MR, Schwarzinger A, Valiahdi SM, Galanski M, Jakupec MA, Keppler BK (2008) J Inorg Biochem 102:2072–2077
17. Varbanov H, Valiahdi SM, Legin AA, Jakupec MA, Roller A, Galanski M, Keppler BK (2011) Eur J Med Chem 46:5456–5464
18. Varbanov HP, Valiahdi SM, Kowol CR, Jakupec MA, Galanski M, Keppler BK (2012) Dalton Trans 41:14404–14415
19. Hoffmeister BR, Adib-Razavi MS, Jakupec MA, Galanski M, Keppler BK (2012) Chem Biodivers 9:1840–1848
20. Varbanov HP, Jakupec MA, Roller A, Jensen F, Galanski M, Keppler BK (2012) J Med Chem 56:330–344
21. Giandomenico CM, Abrams MJ, Murrer BA, Vollano JF, Rheinheimer MI, Wyer SB, Bossard GE, Higgins JD (1995) Inorg Chem 34:1015–1021
22. OECD Guideline for Testing of Chemicals, 105 OECD, Paris (1995)
23. OECD guideline for testing of chemicals, 107 OECD, Paris (1995)
24. Hall MD, Telma KA, Chang K-E, Lee TD, Madigan JP, Lloyd JR, Goldlust IS, Hoeschele JD, Gottesman MM (2014) Cancer Res 74:3913–3922
25. Patrick GL (2008) An introduction to medicinal chemistry. Oxford University Press, Oxford
26. Reithofer MR, Bytzek AK, Valiahdi SM, Kowol CR, Groessl M, Hartinger CG, Jakupec MA, Galanski M, Keppler BK (2011) J Inorg Biochem 105:46–51
27. Lipinski CA (2004) Drug Discov Today Technol 1:337–341
28. Varbanov HP, Göschl S, Heffeter P, Theiner S, Roller A, Jensen F, Jakupec MA, Berger W, Galanski M, Keppler BK (2014) J Med Chem 57:6751–6764
29. Kelland LR, Abel G, McKeage MJ, Jones M, Goddard P, Valenti M, Murrer BA, Harrap KR (1993) Cancer Res 53:2581–2586
30. Perazella MA (2009) Clin J Am Soc Nephrol 4:1275–1283
31. Wallace GC, Ramsden DB, Grant HM (2012) Encyclopedia of Drug Metabolism and Interactions. Wiley, New York
32. Sulyok M, Hann S, Hartinger CG, Keppler BK, Stingeder G, Koellensperger G (2005) J Anal At Spectrom 20:856–863
33. Hartinger CG, Zorbas-Seifried S, Jakupec MA, Kynast B, Zorbas H, Keppler BK (2006) J Inorg Biochem 100:891–904
34. Groessl M, Hartinger CG, Polec-Pawlak K, Jarosz M, Keppler BK (2008) Electrophoresis 29:2224–2232
35. Allain P, Heudi O, Cailleux A, Le Bouil A, Larra F, Boisdron-Celle M, Gamelin E (2000) Drug Metab Dispos 28:1379–1384
36. Groessl M, Terenghi M, Casini A, Elviri L, Lobinski R, Dyson PJ (2010) J Anal At Spectrom 25:305–313
37. Bell DN, Liu JJ, Tingle MD, Rattel B, Meyer TU, McKeage MJ (2008) Clin Exp Pharmacol Physiol 35:1440–1446
38. Raynaud FI, Mistry P, Donaghue A, Poon GK, Kelland LR, Barnard CFJ, Murrer BA, Harrap KR (1996) Cancer Chemother Pharmacol 38:155–162
39. Sova P, Mistr A, Kroutil A, Semerád M, Chlubnová H, Hrusková V, Chládková J, Chládek J (2011) Cancer Chemother Pharmacol 67:1247–1256
40. Vouillamoz-Lorenz S, Buclin T, Lejeune F, Bauer J, Leyvraz S, Decosterd L (2003) Anticancer Res 23:2757–2765
41. Guo H-F, Huang J, Shi HS, Chen X-C, Wang Y-S (2014) PLoS One. doi:10.1371/journal.pone.0085789
42. Jungwirth U, Xanthos DN, Gojo J, Bytzek AK, Koerner W, Heffeter P, Abramkin S, Jakupec MA, Hartinger CG, Windberger U, Galanksi M, Keppler BK, Berger W (2012) Mol Pharamcol 81:719–728
43. Ge R, Ahn J-C, Shin J-I, Bahk CW, He P, Chung P-S (2011) Photomed Laser Surg 29:155–160
44. Lee JH, Lee HJ, Lee HJ, Choi WC, Yoon SW, Ko SG, Ahn KS, Choi SH, Ahn KS, Lieske JC, Kim SH (2009) Phytomedicine 16:188–197
45. Lokich J, Anderson N (1998) Ann Oncol 9:13–21
46. Stuurman FE, Nuijen B, Beijnen JH, Schellens JH (2013) Clin Pharmacokinet 52:399–414

Supporting Information

to

Comparative *in vitro* and *in vivo* pharmacological investigation of platinum(IV) complexes as novel anticancer drug candidates for oral application

Table S1. Administration regimens for the evaluation of the pharmacokinetic properties and *in vivo* anticancer activity of compound **1**, **2** and satraplatin.

drug	**tumor model**	**form of admin.**	**admin. dose [mg/kg]**	**Pt admin.** [mg/kg]**	**nr. of admin.**	**end of experiment**
satraplatin	-	p.o.	40.0	15.63	1	2 h
	-	p.o.	25.8	10.32	1	24 h
	CT-26	p.o.	40.0	15.63	4	15 days
1	-	p.o.	40.0	12.10	1	2 h
	-	p.o.	34.1	10.32	1	24 h
	CT-26	p.o.	34.1	10.32	4	15 days
	CT-26	p.o.	51.7	15.63	4	15 days
	CT-26	i.p.	8.5	2.58	4	15 days
	L1210	i.p.	10.0	3.02	3	-*
	L1210	i.p.	20.0	6.04	3	-*
2	-	p.o.	40.0	10.32	1	2 h
	-	p.o.	40.0	10.32	1	24 h
	CT-26	p.o.	40.0	10.32	4	15 days
	CT-26	i.p.	10.0	2.58	4	15 days
	L1210	i.p.	10.0	2.58	3	-*

* until sacrifice due to L1210 leukemia necessary

** calculated from applied dose

Table S2. Platinum concentrations in different mice tissues upon treatment with complex **1**, **2** and satraplatin, 2 h and 24 h after single dose administration and in CT-26-bearing mice

drug	tumor model	dose [mg/kg]	time	Pt accumulation in µg/g[a]					
				tumor	**kidney**	**liver**	**lung**	**pellet**	**serum**
satra	-	40.0	2 h	-	1.61 ± 0.33	2.96 ± 0.70	0.40 ± 0.01	0.32 ± 0.06	0.64 ± 0.18
	-	25.8	24 h	-	1.91 ± 0.51	4.47 ± 0.04	-	0.83 ± 0.06	0.25 ± 0.03
	CT-26	40.0	15 d	0.55 ± 0.18	2.53 ± 0.39	6.71 ± 1.53	1.29 ± 0.47	1.26 ± 0.78	0.30 ± 0.04
1	-	40.0	2 h	-	3.93 ± 0.48	8.61 ± 1.16	0.96 ± 0.01	1.19 ± 0.06	1.97 ± 0.07
	-	34.1	24 h	-	2.26 ± 0.29	4.24 ± 1.21	-	0.42 ± 0.05	0.24 ± 0.02
	CT-26	34.1	15 d	0.73 ± 0.13	3.78 ± 0.70	8.97 ± 1.85	1.98 ± 0.67	1.30 ± 1.00	0.63 ± 0.17
	CT-26	51.7	15 d	2.26 ± 1.38	7.23 ± 1.11	18.42 ± 2.00	2.97 ± 1.76	2.75 ± 0.91	1.69 ± 0.65
	CT-26	8.5	15 d	1.85 ± 0.69	9.02 ± 1.10	14.85± 2.14	4.14 ± 1.47	1.41± 0.48	2.50 ± 0.67
2	-	40.0	2 h	-	0.23 ± 0.11	0.37 ± 0.01	0.16 ± 0.06	0.20 ± 0.16	0.15 ± 0.01
	-	40.0	24 h	-	0.23 ± 0.02	0.36 ± 0.07	-	0. 28 ± 0.03	0.06 ± 0.01
	CT-26	40.0	15 d	0.10 ± 0.05	0.25 ± 0.10	0.49 ± 0.16	0.14 ± 0.01	0.10 ± 0.05	0.05 ± 0.01
	CT-26	10.0	15 d	0.74 ± 0.17	2.18 ± 0.33	5.37 ± 0.95	3.38 ± 1.48	0.58 ± 0.18	0.90 ± 0.10

[a] data are mean +/- standard deviation

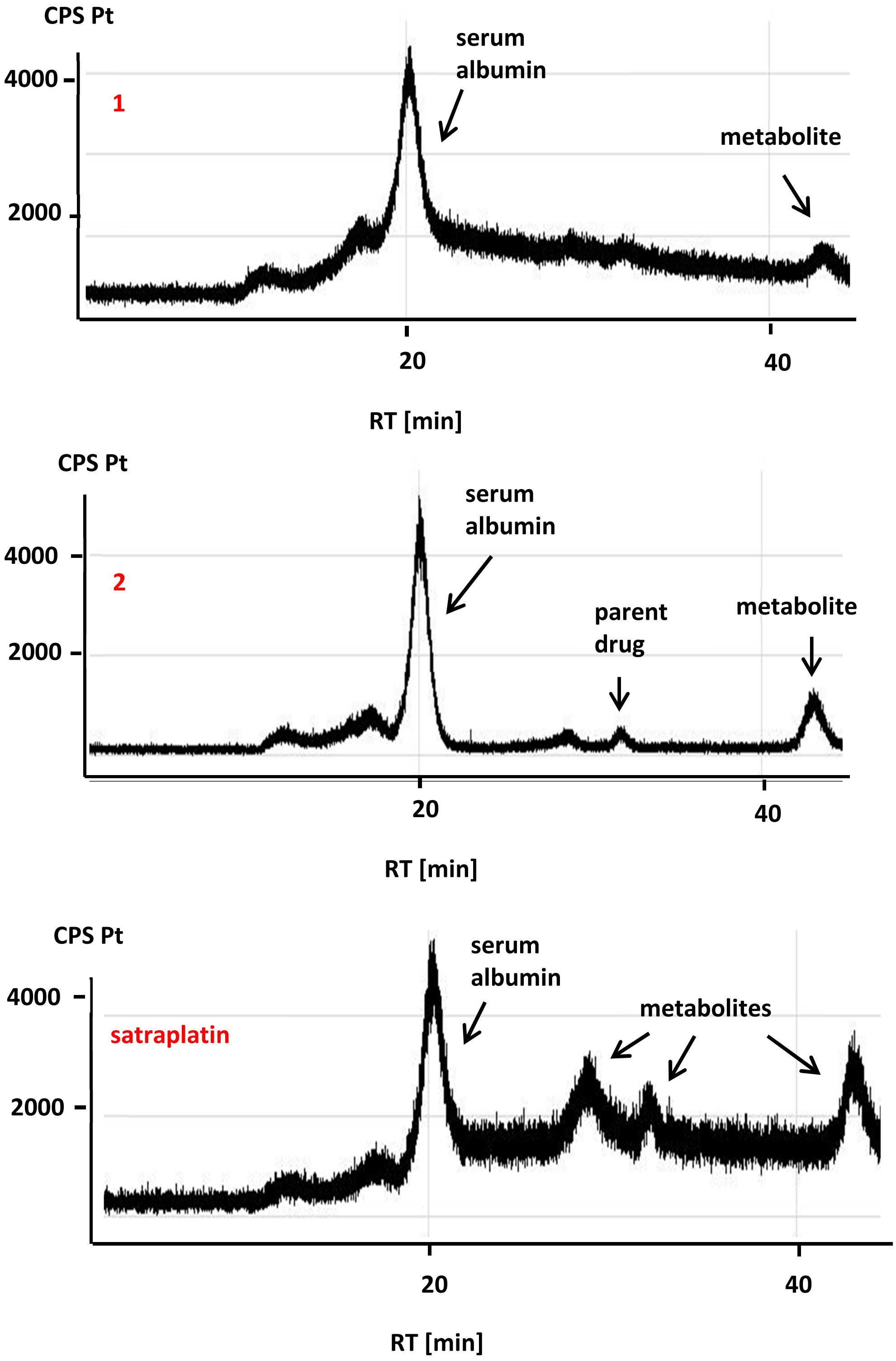

Figure S1. SEC-ICP-MS elution profiles of compound **1**, **2** and satraplatin in serum of mice 2 h after p.o. treatment with the respective complexes.

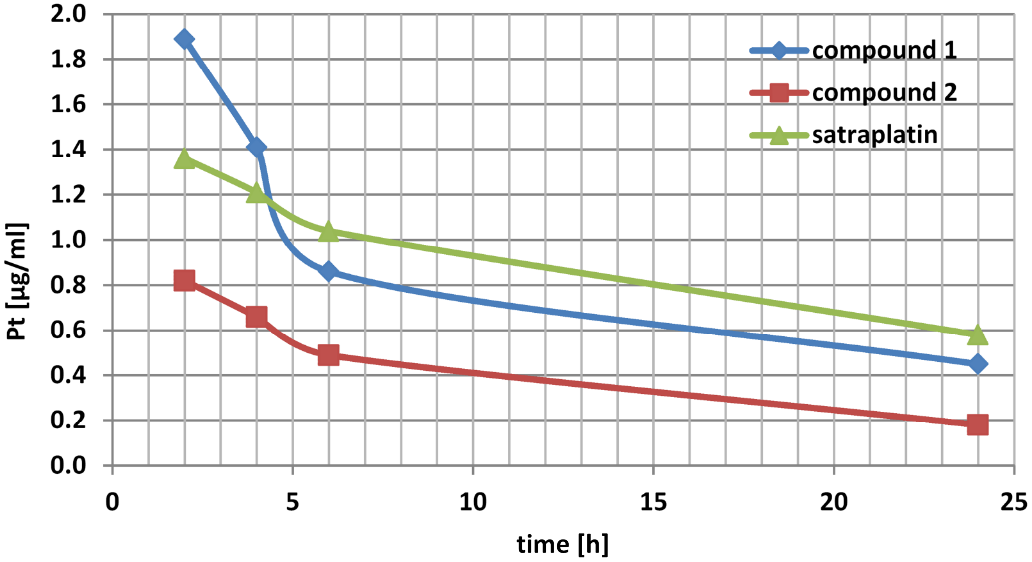

Figure S2. Platinum concentration in blood versus time curves for compound **1**, **2** and satraplatin, administered p.o. at dose 0.05 mmol/kg.

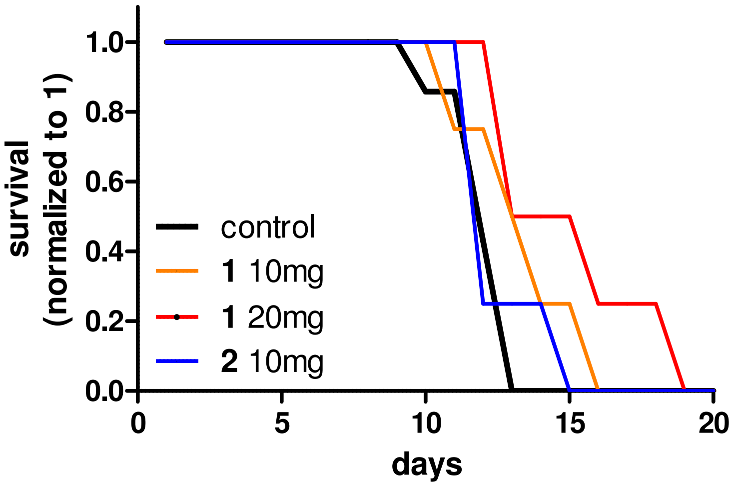

Figure S3. Anticancer activity of compound **1** and **2** *in vivo* against leukemia. Kaplan–Meier plots showing the survival (days after tumor implantation) of L1210-bearing DBA mice (n=4) treated intraperitoneally with the indicated doses in comparison to solvent-treated controls (n=8) on day 1, 5, and 9.

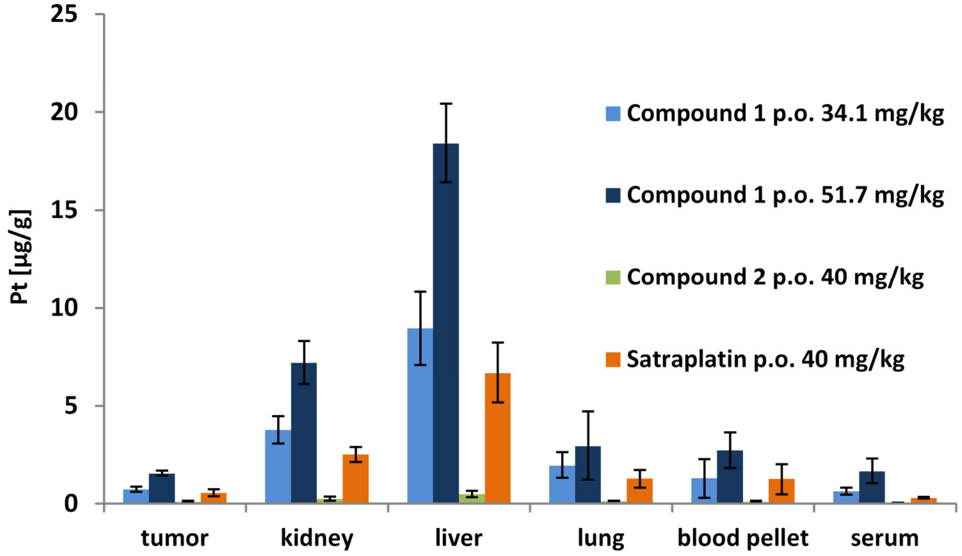

Figure S4. Platinum accumulation after oral administration of compound **1**, **2** and satraplatin in CT-26-bearing mice.

Metallomics

PAPER

View Article Online
View Journal | View Issue

Cite this: *Metallomics*, 2015, 7, 1256

Tumor microenvironment in focus: LA-ICP-MS bioimaging of a preclinical tumor model upon treatment with platinum(IV)-based anticancer agents†

Sarah Theiner,[ab] Christoph Kornauth,[c] Hristo P. Varbanov,[a] Markus Galanski,[a] Sushilla Van Schoonhoven,[bd] Petra Heffeter,[bd] Walter Berger,[bd] Alexander E. Egger*[e] and Bernhard K. Keppler[ab]

Received 28th January 2015,
Accepted 27th March 2015

DOI: 10.1039/c5mt00028a

www.rsc.org/metallomics

The selection of drug candidates for entering clinical development relies on *in vivo* testing in (solid) tumor animal models. However, the heterogeneity of tumor tissue (*e.g.* in terms of drug uptake or tissue composition) is rarely considered when testing novel drug candidates. Therefore, we used the murine colon cancer CT-26 tumor model to study the spatially-resolved drug distribution in tumor tissue upon repetitive treatment of animals over two weeks with three investigational platinum(IV)-based anticancer agents, oxaliplatin or satraplatin. A quantitative laser ablation-inductively coupled plasma-mass spectrometry (LA-ICP-MS) imaging method revealed a heterogeneous platinum distribution, which correlated well with the histologic features of the tumor and surrounding tissue at the microscopic level. In most of the cases, higher amounts of intratumoral platinum were found in the surrounding tissue than in the malignant parts of the sample. This indicates that determination of average platinum amounts (*e.g.* by microwave-assisted digestion of the sample followed by analysis with ICP-MS) might overestimate the drug uptake in tumor tissue causing misleading conclusions. In addition, we studied the platinum distribution in the kidneys of treated animals to probe if accumulation in the cortex and medulla predict potential nephrotoxicity. A 10-fold increase of platinum in the cortex of the kidney over the medulla was observed for oxaliplatin and satraplatin. Although these findings are similar to those in the platinum distribution of the nephrotoxic anticancer drug cisplatin, treatment with the compounds of our study did not show signs of nephrotoxicity in clinical use or clinical trials (oxaliplatin, satraplatin) and did not result in the alteration of renal structures. Thus, predicting the side effects based on bioimaging data by LA-ICP-MS should be considered with caution. To the best of our knowledge, this is the first LA-ICP-MS study on spatially-resolved platinum accumulation in tissues after repetitive platinum-based anticancer drug treatment of mice bearing a preclinical tumor model.

Introduction

Chemotherapy for cancer treatment frequently includes one of the worldwide-approved platinum(II)-based compounds (cisplatin, carboplatin or oxaliplatin).[1] In the last few decades, effort has been made to develop novel platinum(IV)-based cytostatics (*e.g.* tetraplatin, iproplatin and satraplatin) with a focus on the reduction of side effects, overcoming the resistance occurring in platinum(II)-based drug treatment and improvement of oral bioavailability.[2–4] Platinum(IV) complexes can exert high kinetic inertness in substitution reactions, assuming their stability in the gastrointestinal tract (GIT) and in the bloodstream.[5] A prerequisite for their anticancer activity is the formation of the active platinum(II) species upon two-electron reduction preferably in the hypoxic tumor tissue (prodrug-concept).[6] Therefore, platinum(IV) complexes could be considered as an orally applicable, safe alternative over the established platinum(II)-based chemotherapeutics.[6,7] Satraplatin ((OC-6-43)-bis(acetato)amminedichlorido(cyclohexylamine)platinum(IV)) has been the first orally active platinum-based drug evaluated in clinical trials.[8] Despite positive results

---

[a] *Institute of Inorganic Chemistry, University of Vienna, Vienna, Austria*
[b] *Research Platform 'Translational Cancer Therapy Research', University of Vienna, Vienna, Austria*
[c] *Institute of Clinical Pathology, Medical University of Vienna, Vienna, Austria*
[d] *Institute of Cancer Research, Department of Medicine I and Comprehensive Cancer Center of the Medical University, Medical University of Vienna, Vienna, Austria*
[e] *ADSI – Austrian Drug Screening Institute GmbH, Innrain 66a, 6020-Innsbruck, Austria. E-mail: alexander.egger@adsi.ac.at; Tel: +43 (0)512-507-36305*

† Electronic supplementary information (ESI) available. See DOI: 10.1039/c5mt00028a

against refractory prostate cancer, after completion of clinical phase III trial, satraplatin was not approved by the FDA, as it failed to demonstrate decisive benefits with regard to the survival rate.[9,10]

To gain information on the *in vivo* properties of novel drugs, animal models are widely used to investigate their toxicological profile, pharmacokinetic behavior and therapeutic efficacy.[11–13] Based on these data, the most promising drug candidates are then selected for further (pre)clinical development. However, due to the enormous costs of clinical trials, additional information regarding the evaluation of novel drug candidates is of high interest, *e.g.* knowledge of the spatially-resolved (<100 μm) drug accumulation in the target tissue. In case the compound of interest contains a non-physiological heteroatom (such as Pt), visualization thereof can be accomplished using micro-X-ray fluorescence (μ-XRF)[14] or laser ablation (LA) hyphenated to ICP-MS (LA-ICP-MS).[15–18] LA-ICP-MS combines fast sample preparation, visualization of elemental distributions independent of the chemical binding partner and highly sensitive quantification in the sub μg g^{-1} order in thin tissue sections.[16,19] It has become of great interest in cancer research and diagnosis to detect tumor markers with the help of metal-labelled antibodies[20,21] and to identify possible protein binding partners of metallodrugs after 2D gel electrophoresis.[22,23] However, there are only a few reports on the applications of LA-ICP-MS as imaging tool for metal-based anticancer agents in biological tissue samples. Herewith, the effect of cisplatin-treatment on mice kidneys, testis and cochlea[24–26] as well as platinum accumulation in tumors of rats after hyperthermic treatment with oxaliplatin have been investigated.[27] In addition, the quantitative platinum and ruthenium distribution of cisplatin and the investigational ruthenium complex NKP1339 in different tissues of mice have been compared using LA-ICP-MS.[28] Combined imaging techniques of LA-ICP-MS and matrix-assisted laser desorption/ionisation-mass spectrometry (MALDI-MS) have been applied to analyze patient samples from peritoneal carcinosis treated intraperitoneally with cisplatin or oxaliplatin.[29]

We have recently reported the *in vivo* anticancer activity of three novel platinum(IV)-based drug candidates in the colon cancer model CT-26 together with the average platinum levels in different mice tissues and serum upon treatment.[30,31] However, in these studies the impact of tumor heterogeneity (*e.g.* varying degrees of vascularization and necrotic areas) as well as drug distribution between malignant and adjacent benign tissue at the microscopic level was not considered. Thus, within this paper we assessed the spatially-resolved platinum distributions of compounds **1–3** (Fig. 1) in tumor and kidney tissue in comparison with satraplatin and oxaliplatin by means of LA-ICP-MS. The obtained data were compared with histological evaluations as well as total platinum levels measured using ICP-MS. To the best of our knowledge, this is the first report on quantitative spatially-resolved platinum biodistribution using LA-ICP-MS in an *in vivo* tumor model upon treatment with platinum(IV)-based anticancer agents.

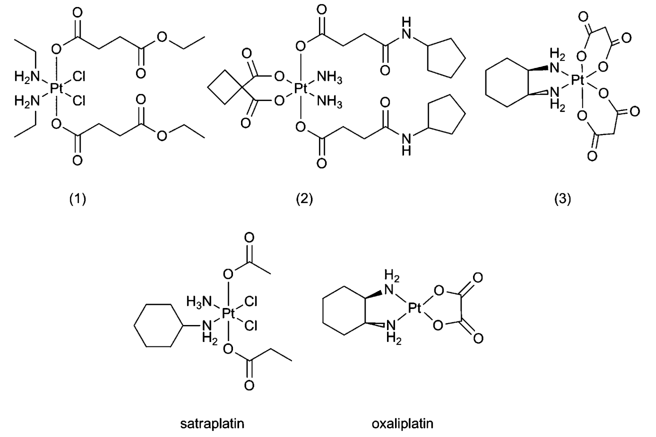

Fig. 1 Structural formulae of platinum complexes under investigation; compound **1** ((OC-6-33)-dichloridobis((4-ethoxy)-4-oxobutanoato)-bis(ethylamine)platinum(IV)), compound **2** ((OC-6-33)-diammine(cyclobutane-1,1-dicarboxylato)bis((4-cyclopentylamino)-4-oxobutanoato)platinum(IV)), compound **3** ((OC-6-22)-((1*R*,2*R*)-diaminocyclohexane)bis(malonato)-platinum(IV)), satraplatin ((OC-6-43)-bis(acetato)amminedichlorido(cyclohexylamine)platinum(IV)) and oxaliplatin ((1*R*,2*R*)-cyclohexane-1,2-diamine)-(ethanedioato-O,O′)platinum(II).

Experimental

Chemicals

The synthesis and characterization of compounds **1**, **2** and **3** was described previously.[31–33] Satraplatin was synthesized according to the method given in ref. 34; oxaliplatin was prepared using standard literature methods as described in ref. 35. Milli-Q water (18.2 MΩ cm, Milli-Q Advantage, Darmstadt, Germany) was used for all dilutions for ICP-MS measurements. Nitric acid (≥65%, p.a., Fluka, Buchs, Switzerland) was further purified in a quartz subboiling point distillation unit (Milestone-MLS GmbH, Leutkirch, Germany) before usage. Platinum and rhenium standards for ICP-MS measurements were derived from CPI International (Amsterdam, The Netherlands). Tissue-Tek medium (Sakura Finetek, The Netherlands) was used for embedding of the cryosections. All other reagents and solvents were obtained from commercial sources and were used without further purification.

Animal experiments

Animal experiments were approved by the local ethics commission and were carried out according to the Austrian and FELASA guidelines for animal care and protection. Six- to eight-week-old Balb/c mice were purchased from Harlan Laboratories (San Pietro al Natisone, Italy). The animals were kept in a pathogen-free environment and every procedure was carried out in a laminar airflow cabinet. Murine CT-26 cells (5×10^5) were injected subcutaneously into the right flank and therapy was started when tumor nodules were palpable (day 4). Mice were treated with the compounds at days 4, 7, 11, and 14 using the regimens summarized in Table S1 (ESI†). Animals were controlled for distress development every day and tumor size was assessed regularly by caliper measurements. Mice were anesthetized on day 15 approx. 24 h after the last drug application and organs were collected and stored at −20 °C for quantitative platinum determination using solution-based ICP-MS. For LA-ICP-MS measurements, the tumor and kidney of one representative mouse were collected, immediately shock-frozen in liquid nitrogen and kept at −80 °C until analysis.

Sample preparation for LA-ICP-MS, apoptosis counting and histological evaluation

For LA-ICP-MS measurements, the tumor and kidney samples were embedded in Tissue-Tek medium and cryosectioned into slices of 20 μm thickness using a cryotome (Microm HM 550, Thermo Fischer). The cryosections were placed onto glass slides, air-dried and kept at room temperature until analysis. A consecutive cryoslice of 5 μm of the respective organ was stained with haematoxylin–eosin (H&E) using standard protocols. Histological evaluation was performed on an Olympus BH2 standard light microscope. In addition, another part of the tumor/kidney was paraffin-embedded, sliced and H&E-stained using routine histological methods for apoptosis counting.

Microwave-assisted digestion of tissue samples and solution-based ICP-MS measurements

Digestion of tissue samples (approx. 10–30 mg) was performed with sub-boiled nitric acid using a microwave system Discover SP-D (CEM Microwave Technology, Germany). The following microwave parameters were used: temperature: 200 °C; ramp time: 4 min; hold time: 6 min; maximal power: 300 W. Digested samples were diluted with Milli-Q water resulting in nitric acid concentrations lower than 3% and platinum concentrations lower than 20 ng g^{-1}. The total platinum content was determined using an ICP-quadrupole MS instrument Agilent 7500ce (Agilent Technologies, Waldbronn, Germany). The ICP-MS instrument was equipped with a CETAC ASX-520 autosampler (Nebraska, USA) and a MicroMist nebulizer at a sample uptake rate of approx. 0.25 ml min^{-1}. The instrument was tuned daily in order to achieve maximum sensitivity. Rhenium served as the internal standard for platinum to account for instrumental fluctuations and matrix effects. The ICP-MS was equipped with nickel cones and operated at an RF power of 1550 W. Argon was used as the plasma gas (15 l min^{-1}) and as a carrier gas with a flow rate of ∼1.1 l min^{-1}. The dwell time was set to 0.1 s and the measurement was performed in 10 replicates. The Agilent MassHunter software package (Workstation Software, Version B.01.01, 2012) was used for data processing.

Quantitative bioimaging in tissue samples using LA-ICP-MS

Bioimaging with LA-ICP-MS, including quantification, was performed according to a previously described procedure with slight modification, using matrix-matched calibration standards.[28] For this purpose, commercially available pig liver was homogenized (homogenizer, Minilys, Peqlab, USA) and spiked with liquid platinum standards yielding platinum concentrations between 1 and 30 μg g^{-1}. The final platinum concentrations of the calibration standards were validated by ICP-MS measurements after microwave-assisted acid digestion using the same conditions as for the organs. Standards were run at the beginning and at the end of the laser experiment, and additionally in the middle when ablation time exceeded two hours in order to monitor instrumental drift.

A Nd:YAG solid state laser (NWR 213, ESI, Fremont, CA, USA) at a wavelength of 213 nm was used to obtain the spatially-resolved distribution of platinum in tumor and kidney sections. The laser beam path was equipped with a square-shaped laser spot table ensuring a constant delivery of energy onto the moving sample throughout the entire diameter of the laser beam. An optical sample map of the region of interest was generated prior to the measurement. The output laser energy was tuned daily in order to ensure complete ablation of the sample material. Ablation was performed at 10 Hz using parallel line scans, a spot size of 70 μm, scan speed of 40 μm s^{-1} and spacing of 10 μm between the lines. The energy of the laser was increased to reach the substrate (= complete ablation) latest upon 10 shots (corresponding to a movement of the sample stage of approx. half the laser diameter). Assessment of complete ablation was evaluated upon termination of the sequence using an optical microscope. The resulting sample energy was in the range of 0.13–0.16 mJ corresponding to a fluence between 2.7 and 3.2 J cm^{-2}. The ablated sample material was transferred to the ICP-MS instrument with helium (quality 5.0) at a flow rate of 400 ml min^{-1}. The warm-up time of the laser was set to 10 s and the wash-out delay to 10 s. Laser ablation data was recorded using a Triple Quadrupole ICP-MS Agilent 8800 (Agilent Technologies, Tokyo, Japan) and processed using the Agilent MassHunter software package (Workstation Software, Version B.01.03, 2013). The instrumental parameters for LA-ICP-MS are given in Table 1.

The assessment of average platinum concentrations at the microscopic level by means of LA-ICP-MS was based on a greyscale color scheme for image export in Iolite, providing a linear correlation between the grey value and the registered counts per second (CPS) of the isotope ^{195}Pt. The CPS were correlated with the concentration of the ablated standards enabling conversion of grey values to concentrations (expressed in μg g^{-1}) using ImageJ (Version 1.48v).[38] Upon calibration, the average platinum concentrations were read out using the histogram function of ImageJ.

The software Igor Pro (Wavemetrics, Igor Pro 6.34A) together with its add-on Iolite (Iolite Version 2.5) was used for further data processing and generation of platinum distribution maps.[36] The data reduction scheme ‘Trace_Elements’ including blank subtraction and no smoothing of the visualization was

Table 1 Instrumental parameters of LA-ICP-MS

	LA-ICP-MS
RF power [W]	1350
Cone material	Nickel
Carrier gas [l min^{-1}]	1.1
Make up gas [l min^{-1}]	—
Plasma gas [l min^{-1}]	15
Monitored isotopes	^{13}C, ^{195}Pt
Dwell time [s]	0.1
Number of replicates	1

applied according to the manual by the authors (Iolite User Manual, Version 2.0).[37] The aspect ratio of the image was set according to the dimensions of the ablated area in order to obtain accurately shaped pictures. In case matrix-matched standards were measured for quantitative bioimaging, the platinum concentration of each standard was assigned in the scale bar of the image to the corresponding average counts. If not otherwise stated, the thresholds in the color bar were set to 0 and a platinum concentration of approx. 1.8 μg g^{-1} for all visualizations in order to facilitate comparison of the platinum amounts between the images solely by the color. In addition, the average platinum concentration (determined by ICP-MS after microwave-assisted digestion) in tissue originating from the same sample, is marked with an asterisk to prove the validity of the obtained quantitative imaging results (Fig. 2).

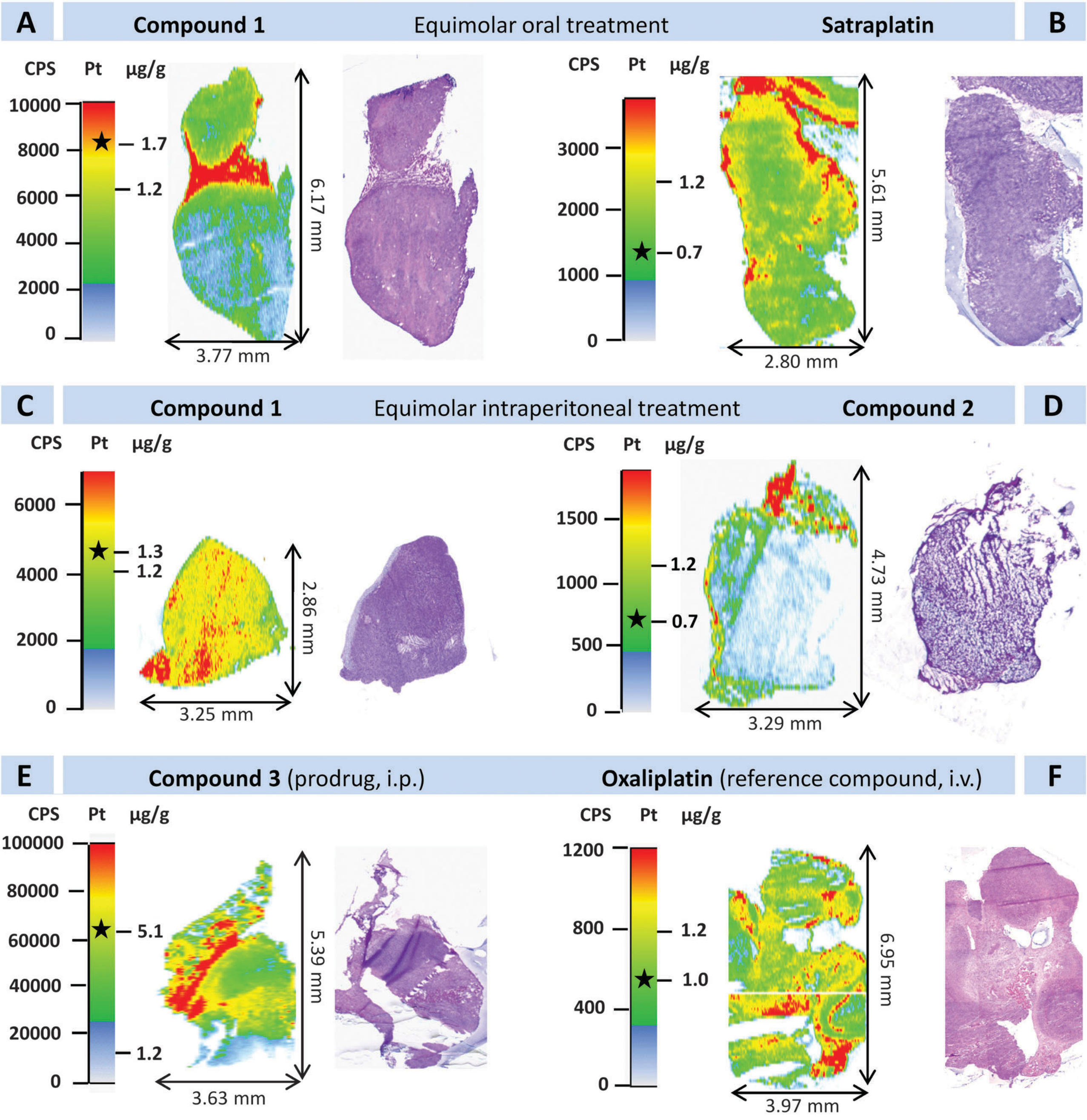

Fig. 2 Platinum distribution in CT-26 tumor sections measured by LA-ICP-MS. Mice were treated with equimolar doses of (A) compound **1** (51.7 mg kg^{-1}, p.o.) or (B) satraplatin (40 mg kg^{-1}, p.o.), (C) compound **1** (8.5 mg kg^{-1}, i.p.) or (D) compound **2** (10 mg kg^{-1}, i.p.); with (E) compound **3** (30 mg kg^{-1}, i.p.) or (F) oxaliplatin (9 mg kg^{-1}, i.v.) on days 4, 7, 11, and 14. For LA-ICP-MS measurements cryosections were used. In addition, a consecutive H&E-stained cryosection is shown for comparison. The asterisks within the intensity bars correspond to the average platinum concentration determined using ICP-MS after microwave-assisted digestion.

Results and discussion

Average platinum levels in tumor and kidney sections

The murine colon carcinoma CT-26 model was recently used to assess the *in vivo* anticancer activity and pharmacokinetics of compounds **1–3** in comparison with satraplatin and oxaliplatin.[30,31] For this purpose, CT-26-bearing mice (n = 4) were treated four times (on days 4, 7, 11, and 14) with the respective drugs. The dosages and routes of administration are summarized in detail in Table S1 (ESI†). Concentrations were chosen equimolar to satraplatin or equimolar to each other for better comparison of the platinum accumulation in tissue. In the case of compound **3**, the dose exhibiting activity on the leukemia model L1210 was administered,[31] whereas oxaliplatin-treated mice received the maximal tolerable dose.[39] Twenty-four hours after the last drug application, the mice were sacrificed and tissue samples were collected. The average platinum concentrations in tumor and several organs (including kidney, liver, lung; determined by ICP-MS) have recently been published[30,31] and are summarized in Table S1 (ESI†). Table 2 shows the average platinum levels of the tumor and kidney samples of the individuals used for the here presented study. In all cases, a representative animal was chosen for LA-ICP-MS bioimaging, which did not differ more than 25% and 30% in the case of tumor and renal platinum content, respectively, from the previously reported mean values. Consequently, in accordance with recently published data,[30,31] the rank of the platinum concentrations in tumor and kidney increased in the following order: compound **2** < satraplatin < oxaliplatin < compound **1** (i.p. and p.o.) < compound **3**.

In order to obtain quantitative information using LA-ICP-MS, matrix-matched standards (consisting of pig liver, spiked with liquid platinum standard solutions) were prepared for calibration.[28] The experimentally determined platinum concentrations of the standards were used to plot calibration curves yielding in all cases correlation coefficients >0.99 (for example see Fig. S1, ESI†).

Platinum distribution in tumor sections using LA-ICP-MS

The platinum distribution in the CT-26 tumors after treatment with the respective platinum compounds was determined at the microscopic level using LA-ICP-MS (Fig. 2) and correlated with the local tissue histology (visualized by H&E stain of a consecutive slide) as well as the previously determined average platinum content of the tumors. For the LA-ICP-MS experiments, the upper threshold of the intensity bars of all visualizations was scaled to platinum concentrations of ~1.8 μg g^{-1}, with the exception of compound **3** (Fig. 2E) which was scaled to ~8.2 μg g^{-1}. In general, the LA-ICP-MS data were in good agreement with the average platinum content assessed previously using ICP-MS (indicated by an asterisk inserted into the color legend).

The detailed measurements using LA-ICP-MS revealed that due to morphological heterogeneity of the tumor sections, the average platinum concentration and the spatially-resolved platinum distribution pattern differed. Thus, although the majority of the ablated sample area exhibited a relatively homogeneous platinum distribution, larger islets of increased platinum levels (indicated by red color) could also be observed in all tumor sections. The following causes for this finding have to be considered: (1) artifacts resulting from the sample preparation (*e.g.* tissue compressions or duplicates) (2) heterogeneity of tumor tissue (*e.g.* due to varying degrees of necrosis/apoptosis, vascularization or susceptibility to the applied drug) (3) non-tumor tissue originating from the treated animal (*e.g.* connective tissue, muscle tissue). In order to further enlighten the nature of these regions, a combined interpretation of grey-scaled images taken prior to ablation of the tissue samples and of H&E-stained consecutive tissue sections was conducted. In addition, ablation of ^{13}C was used as an indication for varying degrees of organic matter to rule out artifacts originating from different tissue types. A representative ^{13}C image (compound **1**, corresponding to Fig. 2A) showed a homogeneous distribution of organic matter over the whole tumor tissue (Fig. S2, ESI†).

In detail, compound **1** (dosed orally; Fig. 2A) exhibited areas of platinum enrichment corresponding to loose soft tissue sparsely infiltrated by tumor cells and striated muscle from the treated mouse. The adjacent regions, which accumulated platinum to a lesser extent, could be assigned to more solid areas of the tumor. According to the analysis using LA-ICP-MS, the tumor itself accumulated platinum at concentrations of approx. 0.5–1.2 μg g^{-1}, whereas loose soft tissue exhibited increased platinum levels of around 2.0–3.5 μg g^{-1} (Fig. 3, top; dotted regions). The average platinum concentration of this sample was ~1.7 μg g^{-1} (Table 2), indicating that the platinum enrichment in the non-malignant tumor areas also

Table 2 Average platinum concentrations in tumor and kidney samples of the treated mouse selected for bioimaging using LA-ICP-MS. Values were determined using ICP-MS after microwave-assisted digestion and the results are given as mean ± standard deviation (samples from one mouse were measured in triplicates). In addition, the average concentration was determined by LA-ICP-MS using the histogram function of ImageJ as described in the Experimental section

			Pt concentration [μg g^{-1}]		
Compound	Route of admin.	Pt admin. [μg g^{-1}]	Tumor (ICP-MS)	Kidney (ICP-MS)	Tumor (LA-ICP-MS)
Satraplatin	p.o.	15.63	0.70 ± 0.06	2.37 ± 0.18	0.81
1	p.o.	15.63	1.66 ± 0.18	8.54 ± 0.45	0.90
1	i.p.	2.58	1.29 ± 0.24	8.15 ± 0.38	1.18
2	i.p.	2.58	0.72 ± 0.15	2.16 ± 0.56	0.66
3	i.p.	11.04	5.06 ± 0.14	12.78 ± 0.33	4.60
Oxaliplatin	i.v.	4.42	0.96 ± 0.08	4.54 ± 0.17	1.15

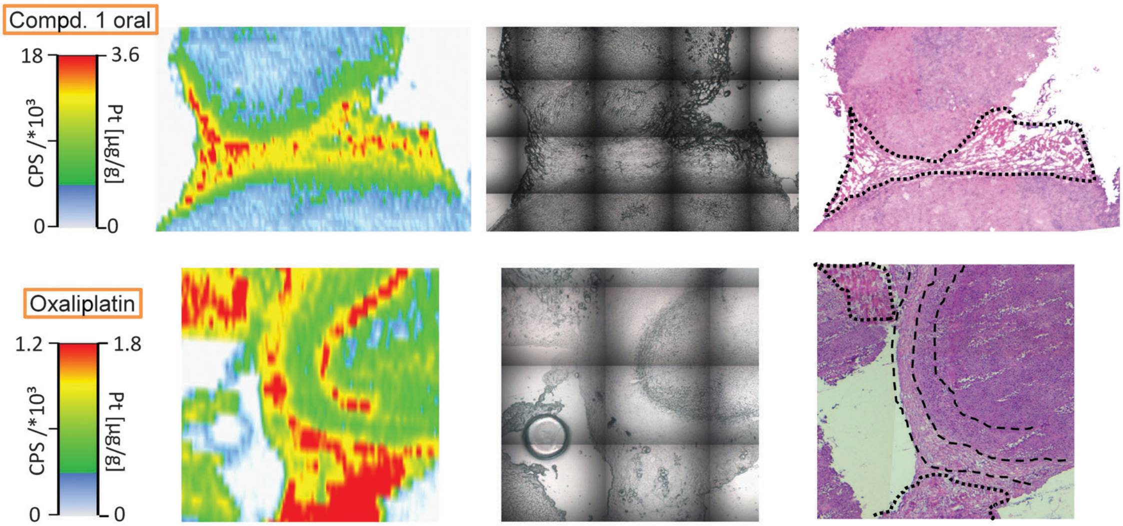

Fig. 3 Detailed view of ablated tumor samples after treatment with compound **1** (p.o., top) and oxaliplatin (i.v., bottom); laser platinum image (left), sample map taken prior to laser ablation (middle) and H&E-stained section (right). The dotted spots in the H&E-stained slides correspond to loose connective tissue with sparsely scattered tumor cells. The dashed lines indicate areas of necrotic tissue within the tumor nodule.

distinctly affects quantitative measurements of total organ levels. The ablated sample after intraperitoneal administration of compound **1** (Fig. 2C) revealed solely unstructured tumor tissue containing platinum levels of ~1.4 μg g^{-1}. This is in accordance with the average platinum concentration (~1.3 μg g^{-1}, Table 2) analyzed using ICP-MS. An overestimation of the tumor-specific platinum levels determined using ICP-MS was also found in other investigated platinum(IV) samples. Compound **2** (Fig. 2D and Fig. S3, middle, ESI†) exhibited a similar platinum accumulation profile to compound **1** after p.o. administration. Increased platinum amounts could be observed in areas of soft tissue with a lower density of infiltrating tumor cells, most probably corresponding to host tissue (approx. 0.7–1.5 μg g^{-1}) surrounding the tumor and lower, but relatively homogeneously distributed platinum levels in tumor tissue (~0.1–0.3 μg g^{-1}). The administered platinum amount upon intraperitoneal treatment with compound **3** was around 4.5-times higher than for compounds **1** and **2**, which resulted in higher platinum accumulation in the tumor (Fig. 2E and Fig. S3, bottom, ESI†). The tissue section exhibited areas of distinctly different platinum amounts ranging from ~1.2 to ~8.2 μg g^{-1}. Most parts of the ablated sample area showed platinum concentrations between 4.5 and 5 μg g^{-1}, whereas areas with elevated platinum levels of ~8 μg g^{-1} (indicated by red color) could also be found.

For comparison, mice were treated orally with satraplatin (Fig. 2B) and intravenously with oxaliplatin (Fig. 2F), which corresponds to the respective clinically-relevant administration route. In contrast to the experimental compounds, increased platinum levels could be detected not only in areas of loose non-malignant soft tissue but also in some areas of tumor tissue (Fig. 3, bottom and Fig. S3, top, ESI†). For satraplatin, these regions were found mainly at the edge of the tumor with platinum amounts of ~1.5 to 1.8 μg g^{-1}, whereas the rest of the tumor tissue exhibited platinum levels of ~0.7 μg g^{-1}. Treatment with oxaliplatin resulted in a relatively heterogeneous platinum distribution pattern with platinum concentrations ranging from ~0.8 to 1.5 μg g^{-1}. In these samples, the platinum enrichment (~1.0 to 1.5 μg g^{-1}) clearly correlated with tumor nodules composed of mitotically active, highly atypical cells as observed in H&E-stained tissue sections (Fig. 3, bottom; dashed lines and Fig. S4, ESI†). Still, platinum was highly concentrated in soft tissue containing a lower density of tumor cells.

In general, areas of (loose) soft tissue within and/or surrounding the tumor comprise increased amounts of platinum. The histologic nature of this tissue (*e.g.* microvessels or connective tissue) is matter of ongoing studies.

As a next step, we addressed the question whether these differences in intratumoral drug distribution correlate with the anticancer activity of the tested platinum drugs. In addition to the previously published tumor growth throughout the experiment (time-span of two weeks),[30,31] the final tumor weight at day 15 is displayed in Fig. S5 (ESI†). Based on the reported tumor growth kinetics, compound **2** and satraplatin were inactive under the experimental conditions used, while compound **1** (administered i.p. or p.o.) showed activity to some extent. On the other hand, oxaliplatin as well as compound **3** exhibited the highest activity of the investigated compounds. In the case of compound **3**, preliminary results of histological evaluations indicated that this activity was based on both apoptosis induction as well as reduction of the mitotic cell population in the malignant tissue (Fig. S6, ESI†).

Equimolar dosages of satraplatin and compound **1** as well as of compound **1** and compound **2** (Table 2) were administered p.o. and i.p., respectively, which allows direct comparison of their spatially-resolved platinum distribution in tumor tissue.

In the case of compound **2** (Fig. 2D), the comparison of the laser image with the histological stains showed that the platinum influx seemed to be restricted mainly to peritumoral (connective) tissue with elevated platinum levels of ~0.7 to

1.5 µg g^{-1}. In cancerous tissue only lower amounts of platinum (~0.1 to 0.3 µg g^{-1}) could be detected. These findings could be an explanation for the lack of anticancer activity of this compound for the CT-26 model. In contrast, compound **1** (Fig. 2C) administered at an equimolar dose to compound **2** (Fig. 2D) deeply penetrates into the malignant tissue, probably explaining its activity.

The third generation platinum(II)-based anticancer drug oxaliplatin is part of the standard therapeutic strategy against colon cancer in clinics and was therefore used as the positive control in our study.[40,41] In addition, we compared it with compound **3**, a platinum(IV) prodrug that is expected to form identical active metabolites like oxaliplatin.[31] Both compounds were active in the CT-26 tumor model and accumulated not only in soft tissue surrounding the tumor but also penetrated and accumulated in tumor tissue. However, due to varying dosages and routes of administration between oxaliplatin and compound **3**, their concentrations in tissue cannot be compared in our study. Our data show that LA-ICP-MS seems to be a promising tool to better investigate and understand the response of tumor models to metal-based anticancer drug treatment.

So far, only a few reports have been published, dealing with metal-based anticancer drug uptake (cisplatin and oxaliplatin) in tumor tissues and their visualization by LA-ICP-MS.[27,29] Both studies aimed to investigate the treatment of peritoneal carcinosis by hyperthermic intraperitoneal chemotherapy. Thus, mass spectrometry was used to study the penetration depth of the applied platinum-based drugs in tumor tissue of rat[27] or human samples[29] up to a treatment time of 60 min. In these investigations, the platinum influx was restricted mainly to the tumor periphery which is a logical consequence of the direct contact of the tumor tissue with the highly-concentrated perfusion solution.[27,29] In the experiments performed here, in contrast, drug transport to the tumor tissue has to be considered as exclusively *via* the bloodstream, as it is the case for the vast majority of anticancer treatment regimens in clinics. Additionally, we applied repetitive treatments over a time-span of two weeks to gain deeper information on drug response in preclinical *in vivo* experiments. The extent of drug penetration into cancerous tissue in correlation with the anticancer activity can be of importance to estimate the potential of novel metal-based anticancer drug candidates, but cannot be assessed solely by microwave-assisted digestion and ICP-MS analysis. Spatially-resolved information on the platinum distribution revealed differences compared to the total platinum content in tumor tissue for some of the analyzed compounds. Consequently, we have demonstrated that LA-ICP-MS analysis is capable of determining platinum levels located specifically in the malignant parts of the tumor tissue.

Platinum distribution in kidney sections using LA-ICP-MS

In addition to the tumor samples, the platinum distribution in kidneys was also investigated. This is of interest for metal-based anticancer drugs, as cisplatin treatment (which is routinely employed in half of the standard oncological treatment regimens in clinics)[9] is frequently associated with nephrotoxicity (one out of three patients).[42] In order to better understand the mechanisms involved in cisplatin-induced nephrotoxicity, several LA-ICP-MS studies have already focused on platinum imaging in murine kidney sections upon treatment with cisplatin.[24–26,28] However, there are so far no LA-ICP-MS investigations on the renal distribution of other platinum-based drugs like *e.g.* oxaliplatin and satraplatin. This is especially of interest, as nephrotoxicity has not been observed as major adverse effect for these two compounds during preclinical evaluation and/or in treatment regimens in clinics.[8,43,44] Consequently, in order to assess whether the renal platinum distribution of oxaliplatin (9 mg kg^{-1}, i.v.) and satraplatin (40 mg kg^{-1}, p.o.) differed from the published data on cisplatin, platinum accumulation maps were obtained using LA-ICP-MS (Fig. 4). The upper threshold in the color code bar was set to a platinum concentration of ~5.2 µg g^{-1} for oxaliplatin and ~4.2 µg g^{-1} for satraplatin. In general, both compounds exhibited 8- to 10-times higher platinum levels in the cortex and corticomedullary region than in the medulla of the kidney. The higher platinum accumulation in these regions is in good correlation with the LA-ICP-MS studies in the renal sections of cisplatin-treated rats

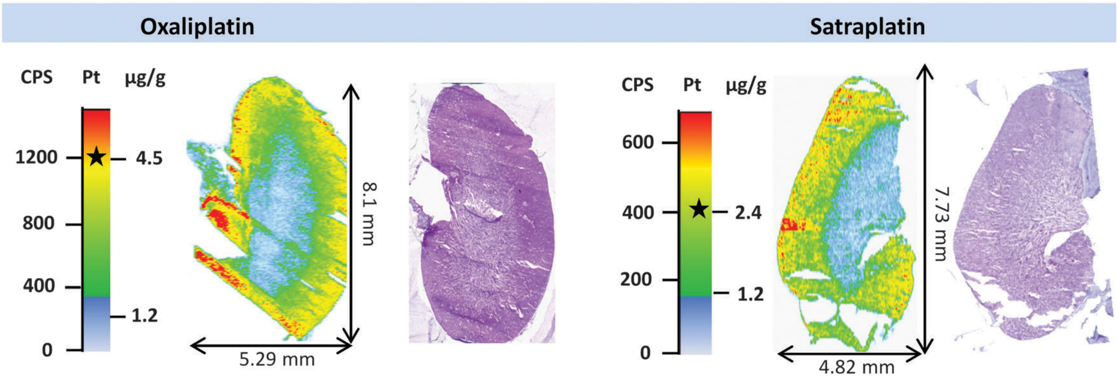

Fig. 4 Distribution of platinum in kidney sections of CT-26-bearing mice treated either with oxaliplatin (9 mg kg^{-1}, i.v.) (left) or satraplatin (40 mg kg^{-1}, p.o.) (right). A consecutive H&E-stained cryosection is shown for comparison. The asterisks within the intensity bars correspond to the average platinum concentration determined using ICP-MS after the microwave-assisted digestion.

and mice.[24–26,28] However, in contrast to the obvious signs of nephrotoxicity observed in the cisplatin samples,[24–26,28] no signs of cell damage such as tubular necrosis was observed in H&E-stained samples of the animals, tested in this study (Fig. S7, ESI†). Together with a recent report on mice treated with the clinically-tested ruthenium compound KP1339, where no correlation between the ruthenium distribution in renal tissue and nephrotoxicity was found,[28] this raises the question of whether LA-ICP-MS is an appropriate tool for the indication of toxic kidney damage. More detailed knowledge on the structure and toxicity of the species (intact parent compound and/or metabolites) present in renal tissue is required. Consequently, drawing conclusions about the possible renal toxicity of platinum-based drug treatment solely based on the quantitative platinum accumulation pattern might not be appropriate. Thus, during preclinical evaluation the assessment of indicative blood serum parameters are still needed in order to estimate the nephrotoxic potential of investigational metal-based anticancer drug candidates.

Conclusions

A quantitative bioimaging method using LA-ICP-MS was successfully applied to the tumor and kidney sections of CT-26-bearing mice upon treatment with platinum-based chemotherapeutics to compare spatially-resolved drug accumulation with histological structures. The platinum distribution maps of tumor samples (originating from six mice) obtained by LA-ICP-MS correlated with the histological pictures, which allowed discerning the platinum localization in cancerous and non-malignant tissue. Interestingly, (loose) soft tissue (*e.g.* connective tissue or microvessels) exhibited higher platinum contents than the malignant parts, especially for the experimental compounds. Tumor heterogeneity observed histologically was reflected in the obtained platinum distributions as well. This information is lost in case drug accumulation is studied solely by determination of total platinum tissue levels *e.g.* using ICP-MS analysis. Thus, histologically assigned quantitative data on drug uptake could contribute to a better understanding on the efficacy of metal-based antitumor compounds at an early preclinical stage. Therefore, knowledge of the spatially-resolved metal distribution in tumor tissue could become an essential part in the lead compound selection for further metal-based anticancer drug development.

In addition, this study addressed the local platinum distribution in kidneys of treated animals. Oxaliplatin and satraplatin exhibited higher platinum levels in the cortex of kidneys than in the medulla, a pattern which was also observed previously in the case of cisplatin. In contrast to cisplatin, the compounds included in our study have not been shown to induce nephrotoxicity, to the best of our knowledge. This indicates that predictions on the possible renal toxicity of platinum-based drug treatment solely based on the quantitative platinum accumulation pattern might not be appropriate.

Acknowledgements

We are thankful to G. Zeitler for animal care and Anita Brandstetter for support with the histological evaluations. We acknowledge Luca Bamonti for proof-reading this paper. This work was supported by the Austrian Science Fund grant P26603 (to P.H.). This work was performed in the surroundings of COST action CM1105.

References

1 L. R. Kelland, *Nat. Rev. Cancer*, 2007, **7**, 573–584.
2 T. W. Hambley, *Dalton Trans.*, 2007, 4929–4937.
3 M. Galanski, V. B. Arion, M. A. Jakupec and B. K. Keppler, *Curr. Pharm. Des.*, 2003, **9**, 2078–2089.
4 S. H. van Rijt and P. J. Sadler, *Drug Discovery Today*, 2009, **14**, 1089–1097.
5 D. Gibson, *Dalton Trans.*, 2009, 10681–10689.
6 E. Wexselblatt and D. Gibson, *J. Inorg. Biochem.*, 2012, **117**, 220–229.
7 M. D. Hall and T. W. Hambley, *Coord. Chem. Rev.*, 2002, **232**, 49–67.
8 H. Choy, C. Park and M. Yao, *Clin. Cancer Res.*, 2008, **14**, 1633–1638.
9 N. J. Wheate, S. Walker, G. E. Craig and R. Oun, *Dalton Trans.*, 2010, **39**, 8113–8127.
10 C. N. Sternberg, D. P. Petrylak, O. Sartor, J. A. Witjes, T. Demkow, J. M. Ferrero, J. C. Eymard, S. Falcon, F. Calabro, N. James, I. Bodrogi, P. Harper, M. Wirth, W. Berrry, M. E. Petrone, T. J. McKearn, M. Noursalehi, M. George and M. Rozencweig, *J. Clin. Oncol.*, 2009, **27**, 5431–5438.
11 M. V. S. Varma, Z. A. Radi, C. J. Rotter, J. Litchfield, A. F. El-Kattan and A. V. Lyubimov, *Encyclopedia of Drug Metabolism and Interactions*, John Wiley & Sons, Inc., 2011.
12 G. C. Wallace, D. B. Ramsden and H. M. Grant, *Encyclopedia of Drug Metabolism and Interactions*, John Wiley & Sons, Inc., 2012.
13 B. Gammelgaard, S. Stürup, C. Møller and A. V. Lyubimov, *Encyclopedia of Drug Metabolism and Interactions*, John Wiley & Sons, Inc., 2011.
14 M. West, A. T. Ellis, P. J. Potts, C. Streli, C. Vanhoof, D. Wegrzynek and P. Wobrauschek, *J. Anal. At. Spectrom.*, 2012, **27**, 1603–1644.
15 J. S. Becker and N. Jakubowski, *Chem. Soc. Rev.*, 2009, **38**, 1969–1983.
16 J. S. Becker, M. Zoriy, A. Matusch, B. Wu, D. Salber, C. Palm and J. S. Becker, *Mass Spectrom. Rev.*, 2010, **29**, 156–175.
17 I. Konz, B. Fernández, M. Fernández, R. Pereiro and A. Sanz-Medel, *Anal. Bioanal. Chem.*, 2012, **403**, 2113–2125.
18 J. S. Becker, A. Matusch and B. Wu, *Anal. Chim. Acta*, 2014, **835**, 1–18.
19 D. Drescher, C. Giesen, H. Traub, U. Panne, J. Kneipp and N. Jakubowski, *Anal. Chem.*, 2012, **84**, 9684–9688.
20 C. Giesen, T. Mairinger, L. Khoury, L. Waentig, N. Jakubowski and U. Panne, *Anal. Chem.*, 2011, **83**, 8177–8183.

21 J. Seuma, J. Bunch, A. Cox, C. McLeod, J. Bell and C. Murray, *Proteomics*, 2008, **8**, 3775–3784.

22 E. Moreno-Gordaliza, D. Esteban-Fernandez, C. Giesen, K. Lehmann, A. Lazaro, A. Tejedor, C. Scheler, B. Canas, N. Jakubowski, M. W. Linscheid and M. M. Gomez-Gomez, *J. Anal. At. Spectrom.*, 2012, **27**, 1474–1483.

23 I. Khalaila, A. Bergamo, F. Bussy, G. Sava and P. J. Dyson, *Int. J. Oncol.*, 2006, **29**, 261–268.

24 M. Zoriy, A. Matusch, T. Spruss and J. S. Becker, *Int. J. Mass Spectrom.*, 2007, **260**, 102–106.

25 E. Moreno-Gordaliza, C. Giesen, A. Lázaro, D. Esteban-Fernández, B. Humanes, B. Cañas, U. Panne, A. Tejedor, N. Jakubowski and M. M. Gómez-Gómez, *Anal. Chem.*, 2011, **83**, 7933–7940.

26 O. Reifschneider, C. A. Wehe, I. Raj, J. Ehmcke, G. Ciarimboli, M. Sperling and U. Karst, *Metallomics*, 2013, **5**, 1440–1447.

27 D. Gholap, J. Verhulst, W. Ceelen and F. Vanhaecke, *Anal. Bioanal. Chem.*, 2012, **402**, 2121–2129.

28 A. E. Egger, S. Theiner, C. Kornauth, P. Heffeter, W. Berger, B. K. Keppler and C. Hartinger, *Metallomics*, 2014, **6**, 1616–1625.

29 J. Bianga, A. Bouslimani, N. Bec, F. Quenet, S. Mounicou, J. Szpunar, B. Bouyssiere, R. Lobinski and C. Larroque, *Metallomics*, 2014, **6**, 1382–1386.

30 S. Theiner, H. Varbanov, M. Galanksi, A. Egger, W. Berger, P. Heffeter and B. K. Keppler, *J. Biol. Inorg. Chem.*, 2015, **20**, 89–99.

31 H. P. Varbanov, S. Göschl, P. Heffeter, S. Theiner, A. Roller, F. Jensen, M. A. Jakupec, W. Berger, M. Galanski and B. K. Keppler, *J. Med. Chem.*, 2014, **57**, 6751–6764.

32 H. Varbanov, S. M. Valiahdi, A. A. Legin, M. A. Jakupec, A. Roller, M. Galanski and B. K. Keppler, *Eur. J. Med. Chem.*, 2011, **46**, 5456–5464.

33 H. P. Varbanov, S. M. Valiahdi, C. R. Kowol, M. A. Jakupec, M. Galanski and B. K. Keppler, *Dalton Trans.*, 2012, **41**, 14404–14415.

34 C. M. Giandomenico, M. J. Abrams, B. A. Murrer, J. F. Vollano, M. I. Rheinheimer, S. B. Wyer, G. E. Bossard and J. D. Higgins, *Inorg. Chem.*, 1995, **34**, 1015–1021.

35 L. Habala, M. Galanski, A. Yasemi, A. A. Nazarov, N. G. von Keyserlingk and B. K. Keppler, *Eur. J. Med. Chem.*, 2005, **40**, 1149–1155.

36 C. Paton, J. Hellstrom, B. Paul, J. Woodhead and J. Hergt, *J. Anal. At. Spectrom.*, 2011, **26**, 2508–2518.

37 http://www.iolite.org.au/Iolite.html.

38 http://imagej.nih.gov/ij/.

39 U. Jungwirth, D. N. Xanthos, J. Gojo, A. K. Bytzek, W. Koerner, P. Heffeter, S. Abramkin, M. A. Jakupec, C. G. Hartinger, U. Windberger, M. Galanksi, B. K. Keppler and W. Berger, *Mol. Pharmacol.*, 2012, **81**, 719–728.

40 R. Akhtar, S. Chandel, P. Sarotra and B. Medhi, *J. Gastrointest. Oncol.*, 2014, **6**, 177–183.

41 G. Yothers, M. J. O'Connell, C. J. Allegra, J. P. Kuebler, L. H. Colangelo, N. J. Petrelli and N. Wolmark, *J. Clin. Oncol.*, 2011, **29**, 3768–3774.

42 X. Yao, K. Panichpisal, N. Kurtzman and N. Kenneth, *Am. J. Med. Sci.*, 2007, **334**, 115–124.

43 A. J. Armstrong and D. J. George, *Ther. Clin. Risk Manage.*, 2007, **3**, 877–883.

44 J. Cassidy and J.-L. Misset, *Semin. Oncol.*, 2002, **29**, 11–20.

Electronic Supplementary Material (ESI) for Metallomics.

Supporting Information

to

Tumor microenvironment in focus: LA-ICP-MS bioimaging of a preclinical tumor model upon treatment with platinum(IV)-based anticancer drugs

Sarah Theiner[1,2], Christoph Kornauth[3], Hristo P. Varbanov[1], Markus Galanski[1], Sushilla Van Schoonhoven[2,4], Petra Heffeter[2,4], Walter Berger[2,4], Alexander E. Egger[5*], Bernhard K. Keppler[1,2]

[1] Institute of Inorganic Chemistry, University of Vienna, Vienna, Austria

[2] Research Platform 'Translational Cancer Therapy Research', University of Vienna, Vienna, Austria

[3] Institute of Clinical Pathology, Medical University of Vienna, Vienna, Austria

[4] Institute of Cancer Research, Department of Medicine I and Comprehensive Cancer Center of the Medical University, Medical University of Vienna, Vienna, Austria

[5] ADSI – Austrian Drug Screening Institute GmbH, Innsbruck, Austria

[*]Corresponding author: Alexander E. Egger; ADSI-Austrian Drug Screening Institute GmbH, Innrain 66a, 6020-Innsbruck, Austria; alexander.egger@adsi.ac.at;

Tel.: +43(0)512-507-36305

Table S1. Administration regimens for satraplatin, compound **1**, **2**, **3** and oxaliplatin and platinum concentrations in tumor and kidney of CT-26 bearing mice (n=4) after treatment with the respective compounds.

compound	form of admin.	admin. dose [mg/kg]	Pt admin.* [mg/kg]	Pt accumulation in μg/g	
				tumor** (n=4)	kidney** (n=4)
satraplatin	p.o.	40.0	15.63	0.55 ± 0.18	2.53 ± 0.39
1	p.o.	51.7	15.63	2.26 ± 1.38	7.23 ± 1.11
1	i.p.	8.5	2.58	1.85 ± 0.69	9.02 ± 1.10
2	i.p.	10.0	2.58	0.74 ± 0.17	2.18 ± 0.33
3	i.p.	30.0	11.04	4.96 ± 0.89	10.49 ± 1.73
oxaliplatin	i.v.	9.0	4.42	0.98 ± 0.34	4.54 ± 0.72

* calculated from applied dose

** values taken from ref.[29] for satraplatin, compound **1** and **2**; and from ref.[30] for oxaliplatin and compound **3**

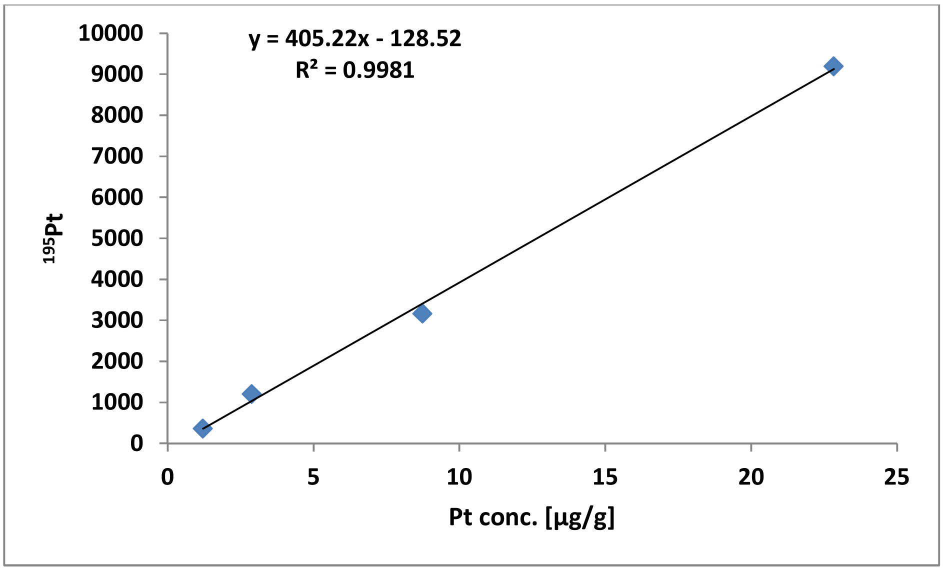

Figure S1. Representative calibration curve (valid for tumor upon treatment with compound **2**, 10 mg/kg, i.p.) for the quantification of platinum in tumor and kidney sections by LA-ICP-MS. Counts per second (CPS) of the registered isotope ^{195}Pt are plotted against the experimentally determined platinum concentrations by ICP-MS in the matrix-matched standards.

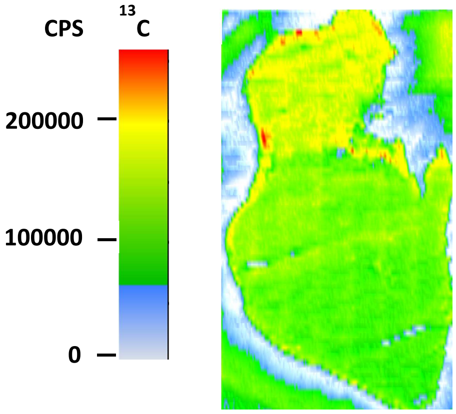

Figure S2. ^{13}C distribution as indication of organic matter in an ablated tumor section upon treatment with compound 1 (51.7 mg/kg, p.o.). Organic matter outside the tumor originates from the embedding medium.

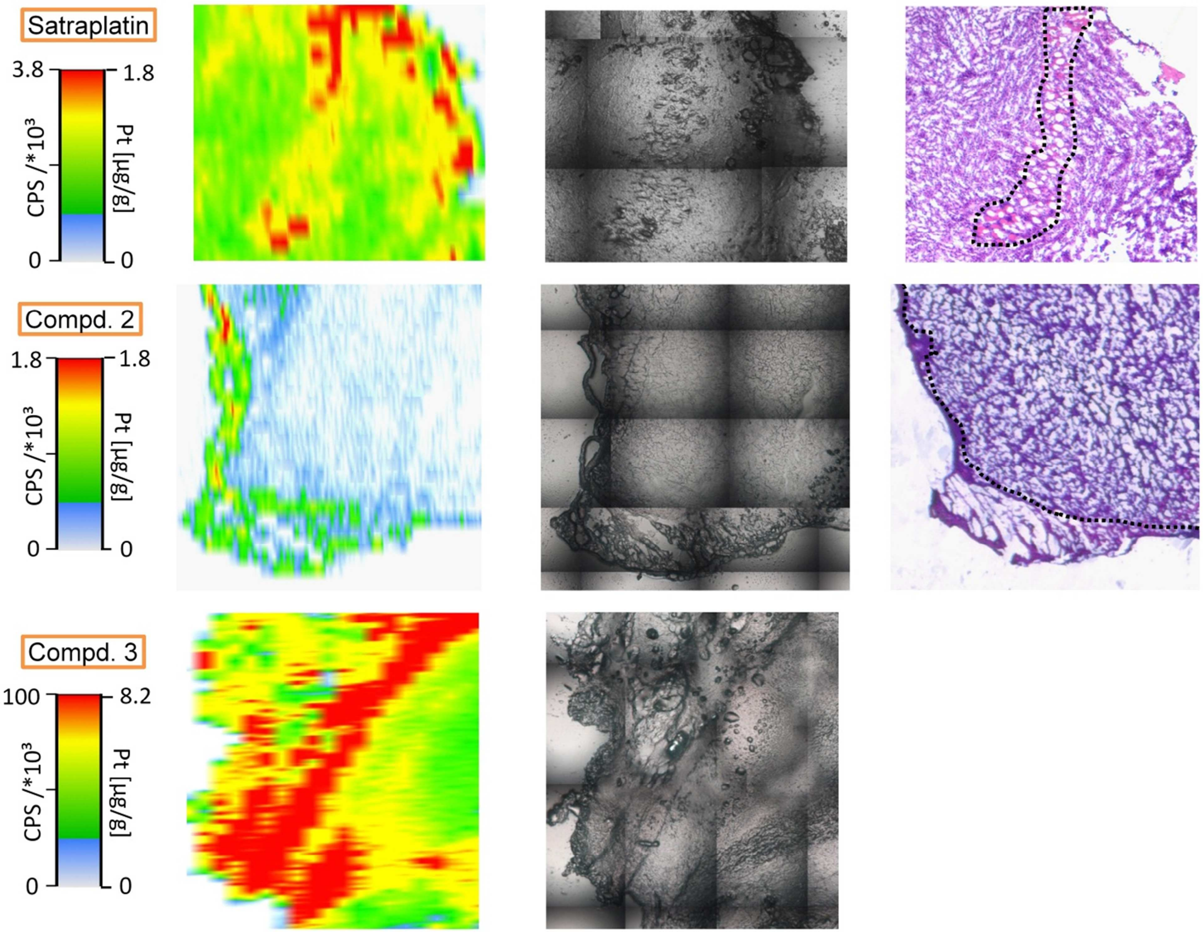

Figure S3. Detailed view of ablated tumor samples after treatment with satraplatin (p.o., top), compound **2** (i.p., middle) or compound **3** (i.p., bottom); laser platinum image (left), sample map taken prior to laser ablation (middle) and H&E-stained cryosection (right). The dotted spots in the H&E-stained slides correspond to loose connective tissue.

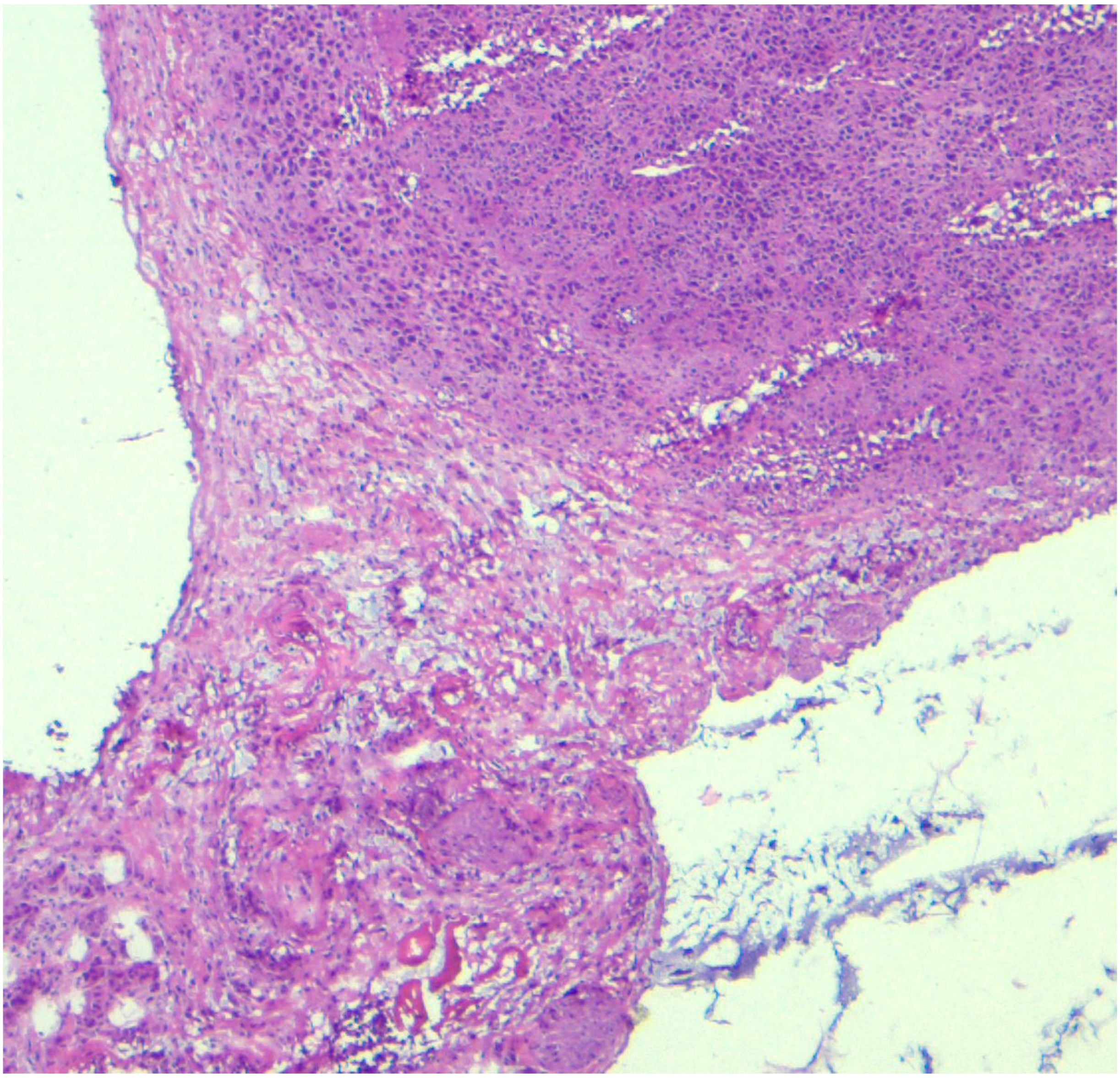

Figure S4. HE stained, enlarged image of the tumor treated with oxaliplatin (i.v.), corresponding to Figure 3, bottom. Loose connective tissue with sparsely scattered tumor cells (lower part) and areas of necrotic tissue as well as tumor nodules composed of mitotically active, highly atypical cells (upper part) are displayed.

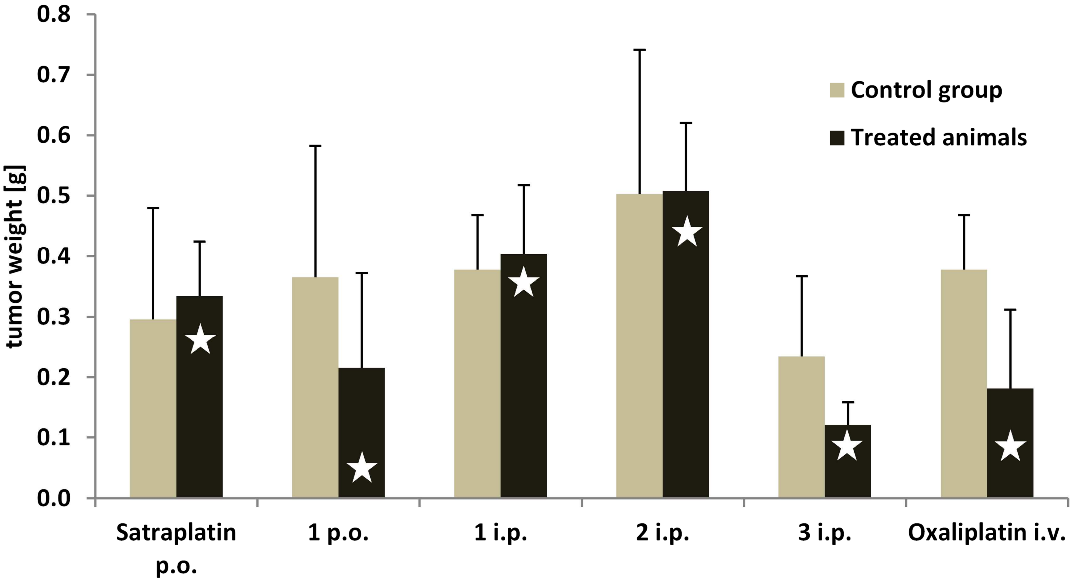

Figure S5. Anticancer activity of the test compounds. CT-26 cells were injected subcutaneously into the right flank of BALB/c mice. Mice were treated on day 4, 7, 11, and 14 with the indicated compounds. Animals were sacrificed on day 15 and tumors were collected. The white stars indicate the tumor weight of the single mouse subjected to LA-ICP-MS analysis after treatment with the respective compound.

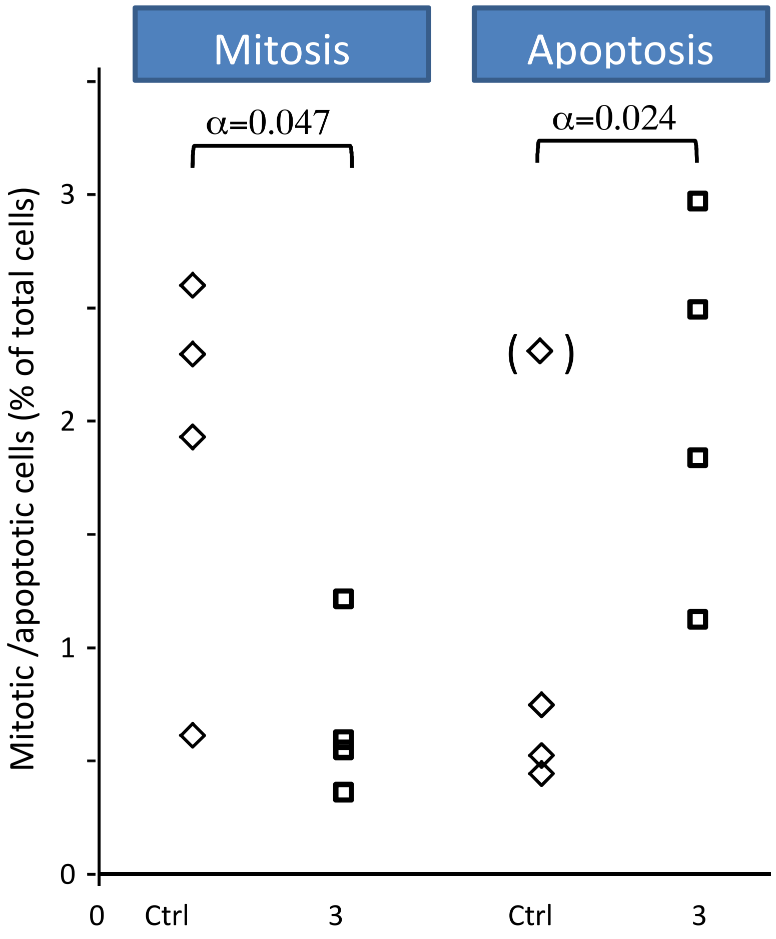

Figure S6. Fraction of mitotic and apoptotic cells in control animals (n=4, ◊) and animals treated with compound 3 (n=4, □). (◊) indicates an outlier. Rates of mitosis and apoptosis differed significantly from control animals (α<0.05 based on ANOVA analysis).

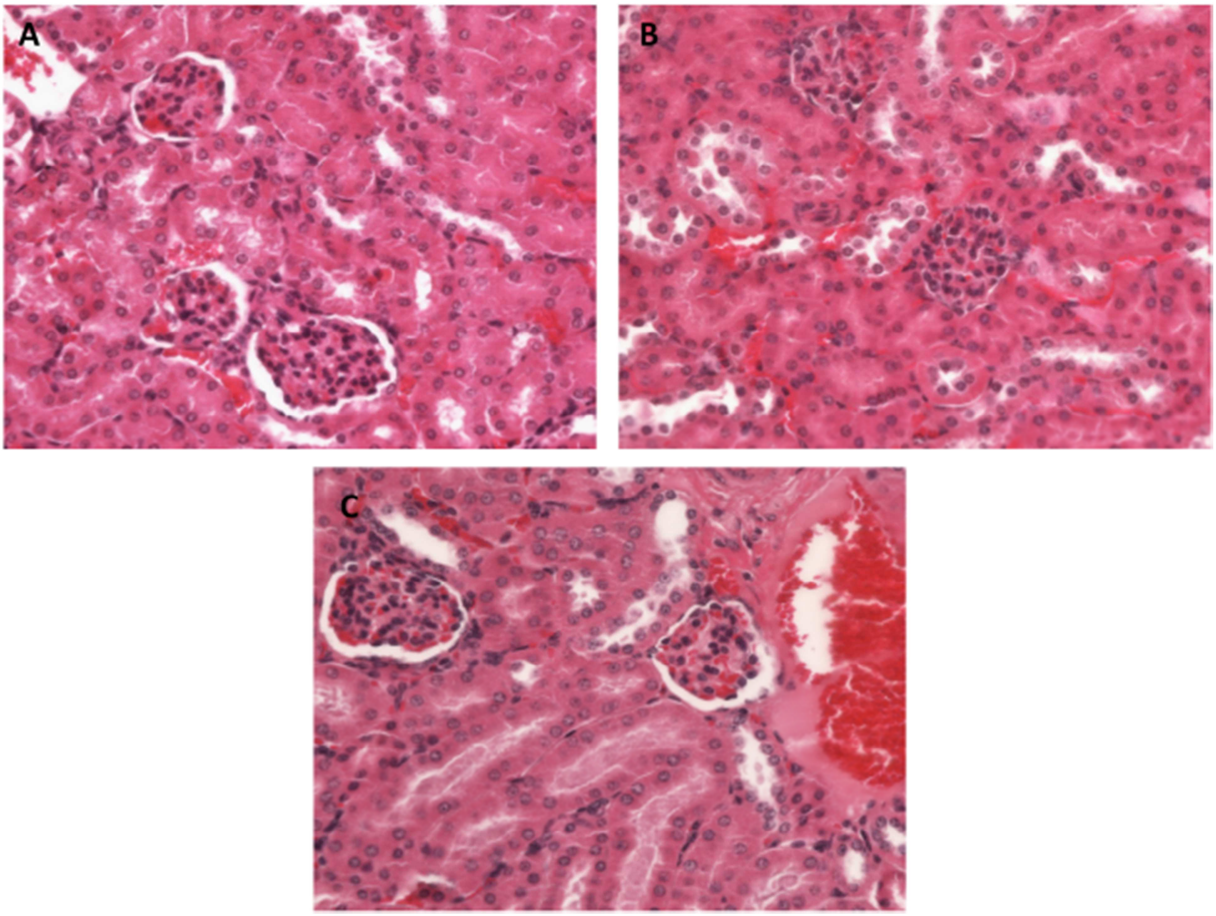

Figure S7. H&E-stained mouse kidney sections, cortex (40x). (A) control mouse (B) oxaliplatin (C) satraplatin.

Metallomics

PAPER

View Article Online
View Journal | View Issue

Cite this: *Metallomics*, 2014, **6**, 1616

Quantitative bioimaging by LA-ICP-MS: a methodological study on the distribution of Pt and Ru in viscera originating from cisplatin- and KP1339-treated mice†

Alexander E. Egger,*[ab] Sarah Theiner,[bc] Christoph Kornauth,[d] Petra Heffeter,[ce] Walter Berger,[ce] Bernhard K. Keppler[bc] and Christian G. Hartinger*[bcf]

Received 10th March 2014,
Accepted 30th April 2014

DOI: 10.1039/c4mt00072b

www.rsc.org/metallomics

Laser ablation-inductively coupled plasma-mass spectrometry (LA-ICP-MS) was used to study the spatially-resolved distribution of ruthenium and platinum in viscera (liver, kidney, spleen, and muscle) originating from mice treated with the investigational ruthenium-based antitumor compound KP1339 or cisplatin, a potent, but nephrotoxic clinically-approved platinum-based anticancer drug. Method development was based on homogenized Ru- and Pt-containing samples (22.0 and 0.257 μg g^{-1}, respectively). Averaging yielded satisfactory precision and accuracy for both concentrations (3–15% and 93–120%, respectively), however when considering only single data points, the highly concentrated Ru sample maintained satisfactory precision and accuracy, while the low concentrated Pt sample yielded low recoveries and precision, which could not be improved by use of internal standards (^{115}In, ^{185}Re or ^{13}C). Matrix-matched standards were used for quantification in LA-ICP-MS which yielded comparable metal distributions, *i.e.*, enrichment in the cortex of the kidney in comparison with the medulla, a homogenous distribution in the liver and the muscle and areas of enrichment in the spleen. Elemental distributions were assigned to histological structures exceeding 100 μm in size. The accuracy of a quantitative LA-ICP-MS imaging experiment was validated by an independent method using microwave-assisted digestion (MW) followed by direct infusion ICP-MS analysis.

Introduction

Metal-based drugs possess a long and successful history in cancer treatment, starting in 1978 with the worldwide approval of cisplatin (Fig. 1).[1,2] Despite being highly efficient in treatment of testicular, head, neck and ovarian tumors, patients suffer from severe side effects such as emesis, neurotoxicity and myelosuppression as well as nephrotoxicity, which is often dose-limiting.[3,4] Nevertheless, cisplatin and its second and third generation compounds carboplatin and oxaliplatin are still among the most frequently prescribed anticancer agents nowadays.[5,6] Promising alternatives to platinum-based therapeutics aim for reduced side effects and efficacy in resistant tumors. These include ruthenium-based anticancer complexes, for example sodium *trans*-[tetrachloridobis(1*H*-indazole)ruthenate(III)], KP1339 (Fig. 1), which is currently undergoing a clinical phase I/II trial.[7–11]

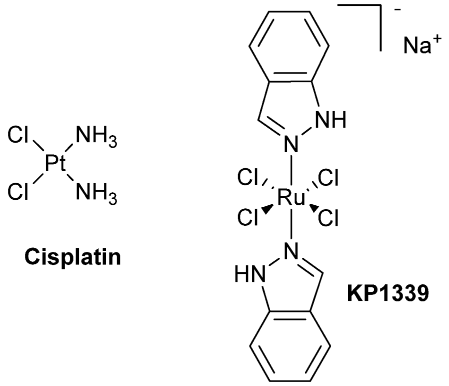

Fig. 1 Chemical structures of the clinically-established anticancer compound cisplatin as well as the investigational ruthenium complex KP1339.

---

[a] *ADSI – Austrian Drug Screening Institute GmbH, Innrain 66a, A-6020 Innsbruck, Austria. E-mail: alexander.egger@adsi.ac.at; Tel: +43-512-507-36305*
[b] *Institute of Inorganic Chemistry, University of Vienna, Vienna, Austria*
[c] *Research Platform 'Translational Cancer Therapy Research', University of Vienna, Vienna, Austria*
[d] *Institute of Clinical Pathology, Medical University of Vienna, Vienna, Austria*
[e] *Institute of Cancer Research, Department of Medicine I, and Comprehensive Cancer Center, Medical University of Vienna, Vienna, Austria*
[f] *School of Chemical Sciences, University of Auckland, Private Bag 92019, Auckland 1142, New Zealand. E-mail: c.hartinger@auckland.ac.nz; Fax: (+64)9 373 7599 ext 87422*

† Electronic supplementary information (ESI) available. See DOI: 10.1039/c4mt00072b

Despite intensive preclinical testing, the main reasons causing abandonment of clinical trials include issues with the pharmacokinetics of drug candidates, low efficacy and unexpected side effects.[12,13] Bioimaging techniques in preclinical *in vivo* studies could improve the success rate by visualizing the distribution of a drug in the target tissue with high spatial resolution in the micrometre scale at an early stage in the drug development process. Highly sensitive imaging techniques based on mass spectrometry such as laser ablation-inductively coupled plasma-mass spectrometry (LA-ICP-MS), matrix-assisted laser desorption ionization-mass spectrometry (MALDI-MS), and secondary ion mass spectrometry (SIMS) serve as analytical tools in biomedical studies as well as in the fields of medicinal and bioinorganic chemistry.[14–18] LA-ICP-MS has become the method of choice in elemental bioimaging as it combines the high spatial resolution of laser ablation (spot size down to 4 μm) with the high sensitivity of mass spectrometric detection by ICP-MS yielding detection limits in the sub $\mu g\ g^{-1}$ range, especially for transition metals.[17,19] Furthermore, the sample preparation is straightforward, as the tissue samples are either paraffin-embedded or cryosectioned onto glass slides, with the tissue thickness varying in the range from 5 to 200 μm.[18,20] A general work-flow for a bioimaging experiment is depicted in the ESI† (Scheme S1).

One of the major challenges of LA-ICP-MS in bioimaging studies is the development of reliable and validated quantification strategies.[18,21] Quantification is mainly hampered by the lack of appropriate certified reference materials for the analyte of interest in the respective tissue-based matrix and a standardized approach for the application of internal standards has not been established. Several quantification procedures have been proposed in the literature including online-addition of solution-based calibration standards[19,22] and standards spiked in polymers followed by coating on slides.[23] Most commonly, matrix-matched calibration standards are individually prepared for each analytical problem by homogenization of the matrix (*e.g.*, whole blood/blood serum, chicken breast, liver and rat brain tissues) and addition of a defined amount of the analytes of interest.[19,24–26] As the analysis time per sample is typically in the range of several hours, the development of strategies to account for variations of the elemental response are challenging. They are caused by, *e.g.*, varying water content in the sample and different sample thickness, fluctuations in the laser chamber during the ablation process and during quantification by ICP-MS. To account for these issues, a suitable internal standard needs to be used, which ideally is a naturally occurring and homogenously distributed element within the biological matrix. Consequently, the isotope ^{13}C has been shown to be the element of choice for tissue samples. The main drawbacks of ^{13}C are the significantly different atomic mass and first ionization potential compared to most analytes as well as its insensitivity to instrumental fluctuations of the ICP-MS.[27,28] Iodine as an internal standard has been proposed upon iodination of cell nuclei in fibroblast cells and has allowed correction for tissue inhomogeneities.[29,30] Further strategies involve spin-coating of the glass slide with solutions of the internal standard and placing the sample tissue on top.[23] Alternatively, a thin layer of a gold standard can be deposited directly on the tissue.[31] Both strategies yield simultaneous ablation of the sample and the internal standard.

In biomedical studies, LA-ICP-MS has shown high potential to improve the understanding of the distribution of trace elements involved in complex biological processes at tissue and cellular level. Especially analysis of metal-based nanoparticles yielded spatially-resolved elemental distributions in the nanometre scale allowing assignment to subcellular structures.[29,32–34] Several studies have focussed on bioimaging of brain samples from animal models for Parkinson's, Alzheimer's and Wilkinson's diseases and disease-induced alterations of elements were monitored.[19,22,35–38] In cancer research, LA-ICP-MS has been used to map the metabolism and pathogenesis of primary brain tumours,[39,40] to identify metastatic melanoma in lymph nodes,[41] and to detect tumor markers in breast cancer tissue.[20] In the field of platinum-based anticancer drugs, metal distribution in tissues being targeted by cisplatin (testis, kidney and cochlea) has recently been determined by LA-ICP-MS.[42–44] Furthermore, ICP-MS and LA-ICP-MS have been combined to study the uptake of oxaliplatin during hyperthermic intraperitoneal chemotherapy in rats.[45]

Within this paper, we compared for the first time the (quantitative) spatially-resolved biodistribution of Ru and Pt in viscera (kidney, liver, muscle, and spleen) of KP1339- or cisplatin-treated Balb/c mice. Additionally, the validation of the method is reported. This includes analysis of homogenates of known metal concentrations by LA-ICP-MS as well as the application of microwave digestion followed by direct infusion ICP-MS measurements as an independent method for proving the validity of the data.

Experimental

Chemicals

Cisplatin and KP1339 were prepared according to literature procedures.[46,47] Nitric acid (≥65%, p.a.) was purchased from Fluka (Buchs, Switzerland) and further purified in a quartz sub-boiling point distillation unit (Milestone-MLS GmbH, Leutkirch, Germany). All dilutions were gravimetrically prepared with Milli-Q water (18.2 MΩ cm, Milli-Q Advantage, Darmstadt, Germany). Indium, platinum, rhenium, and ruthenium standards were obtained from CPI International (Amsterdam, The Netherlands). Tissue-Tek medium (Sakura Finetek, Netherlands) was used for the embedding of the cryosections.

Animal experiments

Eight-week-old Balb/c mice were purchased from Harlan Laboratories (San Pietro al Natisone, Italy). The animals were kept in a pathogen-free environment and every procedure was done in a laminar airflow cabinet. Animal experiments were approved by the ethics committee of the Medical University of Vienna and the Bundesministerium für Wissenschaft und Forschung Ref. II/10b (Gentechnik und Tierversuche), application Nr. BMWF-66.009/0337-II/3b/1011, and were carried out according to the Austrian and FELASA guidelines for animal care and protection in order to minimize distress for the animals. Mice (n = 2 for each treatment) were treated with 15 mg kg^{-1} cisplatin intraperitoneally (in 0.9% NaCl) or 50 mg kg^{-1} KP1339 intravenously (in citrate buffer pH 3.5). Mice were sacrificed after 18 and 24 h for KP1339 and cisplatin, respectively. The entire liver of one mouse per group was removed and stored at −20 °C for method development. Organs of the second mouse (liver, kidney, muscle and spleen) were used for the determination of the biodistribution of Pt and Ru, and its quantification by LA-ICP-MS and ICP-MS after MW digestion. Tissues for imaging were either immediately frozen in dry ice-cooled methylbutane or stored at 4 °C if cryosectioning could be performed within 5 h. Additional samples of all organs were stored at −20 °C for quantitative determination of the respective average metal concentration by means of MW and ICP-MS analysis. Half of a kidney from each animal group was formalin-fixed and paraffin-embedded for detailed histopathological evaluation *via* periodic acid Schiff (PAS) stain.

Preparation of standards and controls

Commercially available pig liver (approx. 5 g) was used for the preparation of matrix-matched standards, spiked with In and Re (10 μg g^{-1} each) and homogenized with a ball homogenizer (Schwingmuehle Retsch MM2000) with a single ceramic ball for 5 min at 40% and 5 min at 90% intensity. Aliquots were spiked with liquid Ru and Pt standards yielding final concentrations ranging from 1 to 50 μg g^{-1}. In order to minimize dilution of the matrix, the total amount of added standard solution never exceeded 10% (w/w). Mixing of homogenates with standard solutions was performed in Eppendorf tubes together with 3 balls made from steel at 70% energy for 15 min.

In order to check the accuracy of the method in general, control samples containing a known concentration of analyte were prepared independently of the standards in the following manner: liver (approx. 1 g) from cisplatin- or KP1339-treated mice, which was not subjected to bioimaging experiments and thus independent, was spiked with In and Re (10 μg g^{-1} each) and homogenized following the protocol for the preparation of the standards. Samples were pelletized in an Eppendorf centrifuge at 80 rpm for 1 min. Subsequently, the standards and control samples were prepared by microwave-assisted digestion for direct infusion ICP-MS to verify the concentration of the standards and to determine the target value ("true value") for the LA-ICP-MS control samples (Scheme 1). The remaining homogenates were stored at −20 °C.

Quantification of the average metal content by ICP-MS

An ETHOS microwave digestion system (MLS, Leutkirch, Germany), equipped with an MR-10 rotor for 30 QS-3 teflon tubes was used. Prior to sample digestion, all tubes were cleaned with equal volumes of water and nitric acid of subboiled quality at 180 °C for 20 min under temperature control of one vessel. Consecutively, the samples with a moist mass of 20–40 mg (*i.e.*, tissues from animal experiments, standards, and controls; see Scheme 1) were digested with 35% nitric acid using the conditions given in Table S1 (see ESI†). Samples were diluted with Milli-Q water yielding a nitric acid concentration of approx. 3.5% and metal concentrations not exceeding 15 ng g^{-1}. An ICP-MS (Agilent 7500ce, Waldbronn, Germany) equipped with a CETAC ASX-520 autosampler (Nebraska, USA) and a MicroMist nebulizer at a sample uptake rate of approximately 0.25 ml min^{-1} was used for quantification. In and Re served as internal standards for Ru and Pt, respectively, in samples originating from animal experiments. As the homogenates (standards and control samples) already contained In and Re, Ce was used in that case alternatively. The internal standard was added *via* a peristaltic pump and merged with the solution of the analyte *via* a T-piece previous to the nebulizer. Experimental parameters are summarized in Table 1. Data processing was conducted with the MassHunter software package (Agilent, Workstation Software, Version B.01.01, 2012). If not otherwise stated, reported data is based on digestions performed in triplicates. As a certified reference material for Ru and Pt in mammalian tissue is to the best of our knowledge not available, three to five samples, which were analyzed on different days with independently prepared calibration standards, were used as control samples for the current calibration to ensure lab-internal long term comparability of measured data.

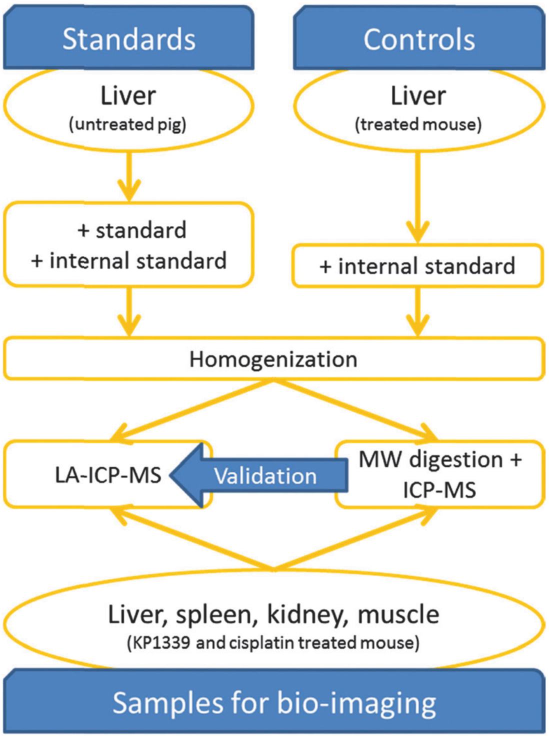

Scheme 1 Simplified overview of sample preparation. Standards (spiked with known amounts of Ru or Pt as well as internal standards) and control samples (originating from a treated animal) were homogenized and analyzed *via* LA-ICP-MS and MW digestion followed by ICP-MS measurement for method development and validation. The metal content in samples originating from animal experiments was quantified by these two methods in the same manner using MW digestion as reference for proving validity of the data obtained by LA-ICP-MS.

Table 1 Parameters for the quantification of liquid samples by ICP-MS and for the hyphenation with a laser ablation system

	ICP-MS	LA-ICP-MS
RF-power [W]	1500	1350
Cones	Ni	Ni
Registered isotopes	^{101}Ru, ^{102}Ru, ^{115}In, ^{140}Ce, ^{194}Pt, ^{195}Pt, ^{185}Re	^{13}C^{a}, ^{102}Ru, ^{115}In^{a}, ^{185}Re^{a}, ^{195}Pt
Dwell time [s]	0.1	0.1
Replicates	10	—
Carrier gas [l min^{-1}]	0.9	1.0
Make up gas [l min^{-1}]	0.2	—
Plasma gas [l min^{-1}]	15	15

[a] Internal standards were only registered in spiked, homogenized samples used for method development.

Laser ablation and data processing

Sample preparation. Matrix-matched homogenous liver standards, homogenized liver originating from cisplatin- or KP1339-treated mice as well as organs of treated mice were embedded in Tissue-Tek medium and cryocut into slices of 20 μm thickness with a cryotom (Microm HM 550, Thermo Fischer). The slices were placed on glass object dishes and air dried. A slice of 5 μm was stained with haematoxylin eosin (HE) for the histological evaluation.

General setup for LA. Laser ablation was performed with a solid state laser (Nd:YAG) at a wavelength of 213 nm (NWR 213, ESI, Fremont, CA, USA), equipped with a 2 volume ablation cell. Enhancing the performance for bioimaging applications, the laser was detuned yielding a reduced maximum energy of 2 mJ in the ablation chamber, thus enabling improved fine-tuning of the applied energy. Furthermore, the laser beam path was equipped with a square-shaped laser spot table ensuring a constant delivery of energy onto the moving sample throughout the entire diameter of the laser beam. An optical sample map of the region of interest was generated and the ablation pattern (parallel line scans) was defined. Ablation was performed at a spot size of 70 μm and a scan speed of 40 μm s^{-1}. The ablated material was transferred to the ICP-MS with He at a flow rate of 400 ml min^{-1}. Further parameters for the laser ablation process are summarized in Table 2 and for LA-ICP-MS in Table 1.

Method development and validation. The matrix-matched standards from pig liver and the control samples were ablated in line-scans of 2 mm in length in the following order: standards (0, 1, 5, 10, 50 μg g^{-1}, two lines per concentration level), control samples (5 lines each), standards (two lines per concentration level), control samples (5 lines each), standards (two lines per concentration level). The laser and ICP-MS parameters are summarized in Table 1 and 2, respectively. The average gas blank was calculated for each isotope and subtracted from each individually registered data point. Additionally, the ^{102}Ru/^{115}In, ^{195}Pt/^{185}Re, ^{102}Ru/^{13}C and ^{195}Pt/^{13}C ratio for each data point and averages over all data points (90–110) within a line scan were calculated. The resulting average counts (or ratios) per line-scan were averaged over the six line-scans per concentration level and plotted against the concentration obtained by MW/ICP-MS yielding the respective calibration curves. The raw data of the ten lines per control sample were processed in the same manner, and their average counts (or ratios) as well as their precision were converted into concentrations and corresponding standard deviations using the calibration curve from the LA-ICP-MS experiment. Concentrations of the homogenized control samples, obtained independently by LA-ICP-MS and by MW/ICP-MS were compared to verify accuracy and precision.

Quantitative bioimaging of mouse organs. Each standard was analyzed in triplicate line scans (length: 1.5–3 mm) at least before and after scanning of a tissue section. In case the analysis time exceeded 2 h, standards were additionally measured within the ablation experiment. Length and width of the ablated area were measured for scaling purpose. The recorded files were imported into Iolite (Version 2.15)[48] as an add-on to Igor Pro (Wavemetrics, Igor Pro 6.22A). The maps of the metal distribution (^{195}Pt and ^{102}Ru) were generated with the data reduction scheme Trace_Elements following the procedures described in the manual (Iolite User Manual, Version 2.0)[49] including background subtraction and no smoothing of the visualization. The aspect ratio of the image was set according to the length and width of the ablated area to obtain accurately shaped pictures. The visualized metal distribution was scaled proportionally and superimposed on the histologic image.

Assignment of concentrations to the resulting color-coded Ru or Pt maps was performed and validated in the following manner: The instrumental drift was monitored by the standards that were run before and after the ablation experiment. In case the drift of the counts exceeded 15%, no quantitative calculations were performed; otherwise the concentration of each standard was assigned in the scale bar of the image to the corresponding average counts. In order to validate the spatially-resolved, quantitative biodistribution, the average concentration determined by MW/ICP-MS was assigned in the scale-bar as well. The quantitative image was considered to be valid, if the concentration determined by MW/ICP-MS was within the concentration pattern determined by bioimaging.

Table 2 Instrumental parameters used in laser ablation experiments

Sample energy [mJ]	0.08–0.10
Fluence [J cm^{-2}]	2.1–2.5
Repetition rate [Hz]	10
Laser beam shape	Square
Spot size [μm]	70
Scan speed [μm s^{-1}]	40
Transfer gas and flow rate [ml min^{-1}]	He, 400
Length per line (standards) [mm]	2
Spacing between lines [μm]	10
Warm up [s]	10
Wash out delay [s]	15

Results and discussion

A method for obtaining quantitative information on the metal distribution in organs of cisplatin- and KP1339-treated mice was developed and validated. Metal concentrations in organs originating from a single mouse were determined independently by two methodologies: LA-ICP-MS and MW followed by quantification with ICP-MS.

Method development and validation

Pig liver is well suited for the preparation of matrix-matched standards due to the absence of fascia and connective tissue as well as its availability. Details on the concentration of the standards, determined by MW/ICP-MS, and typical calibration curves for LA-ICP-MS, obtained by ablating cryosections of the matrix-matched standards, are available in the ESI† (Table S2 and Fig. S1, respectively).

In order to validate the calibration for LA-ICP-MS, a tissue slice of known concentration originating from homogenized liver of a treated mouse was prepared. Homogenization is required to ensure a uniform distribution of the spiked internal standards (In, Re), to identify the best suited internal standard. This process circumvents any impact of inhomogeneous drug distribution in liver originating from animal experiments. The concentrations of the control samples (approx. 20–40 mg) were determined in triplicates by means of MW/ICP-MS as 0.257 ± 0.039 μg g^{-1} and 22.0 ± 1.2 μg g^{-1} for Pt and Ru, respectively. These values were considered as target values for the quantification of these elements in tissue sections of the same samples by LA-ICP-MS. The results for two slices of the homogenized mouse liver (homogenate 1 and homogenate 2) are depicted in Fig. 2. Quantification only *via* raw counts results in recoveries for both elements in the range of 93–120% (Table S3, ESI†). Internal standards, spiked to the homogenate (^{115}In, ^{185}Re) did not improve the recovery, while an internal standard being present intrinsically in the sample (^{13}C), yielded improved data in the case of Ru. For Pt, recovery was worse when In was used as the internal standard, which may be due to their different masses and first ionization energies (9.0 *vs.* 5.8 eV, respectively). Although being much lighter than Pt, ^{13}C (11.3 eV), performed better as internal standard than In, maybe due to their similar first ionization potential. Additionally, analysis of homogenates originating from the same tissue type and use of an internal standard intrinsically present, such as ^{13}C, were considered as best prerequisites to ensure uniform distribution within the sample as well as identical concentration of the internal standard between different samples. Using this approach, biased results due to inconstant internal standard concentrations were ruled out.

Ten line-scans per homogenate were conducted and the precision (expressed as relative standard deviation) ranged from 3 to 8% in case of Ru and 8 to 15% in case of Pt (Table S3, ESI†), whereas none of the internal standards improved precision significantly. The higher uncertainty for Pt might be explained by its 100-fold lower concentration in liver tissue compared to the Ru sample.

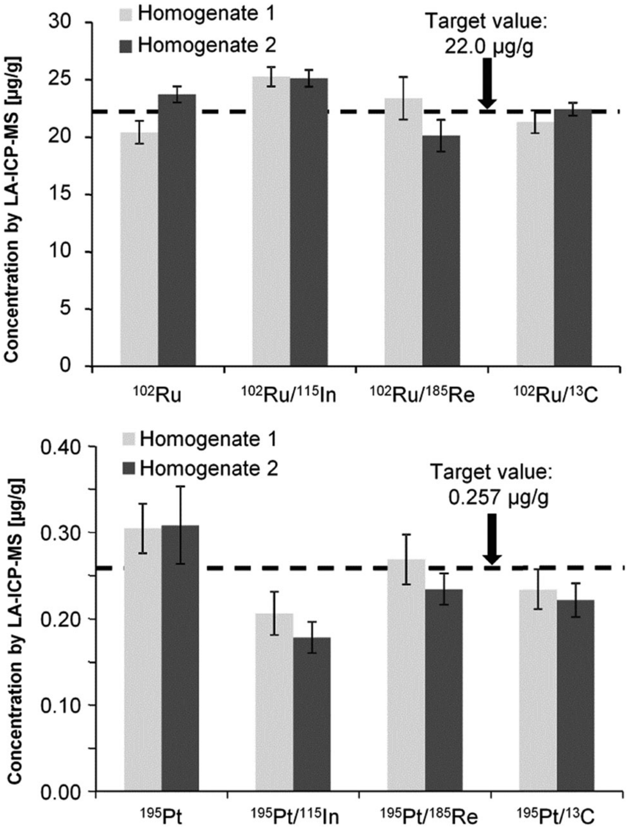

Fig. 2 LA-ICP-MS-based quantification of ruthenium (top) and platinum (bottom) in homogenized liver originating from mice treated with either KP1339 or cisplatin, respectively. The dashed lines indicate the target value, obtained by quantification *via* MW/ICP-MS of liver samples. LA-ICP-MS based quantifications *via* raw counts of the metal as well as the use of internal standards ^{115}In, ^{185}Re and ^{13}C were compared with respect to their accuracy and precision (standard deviation calculated from 10 line scans of 1950 μm length each).

However, accuracy and precision based on averages (ten line-scans, each approx. 90 data points) are not valid for bioimaging experiments. Laser ablation imaging experiments are usually optimized *via* scan speed of the laser, laser diameter and registration time per datapoint[20,50] but do not allow for collection of a large number of data points to obtain an average. Hence, we randomly selected one line-scan of the ruthenium and one of the platinum homogenate (Fig. 3 and Fig. S2, ESI†). Concentrations scatter symmetrically along the scans, indicating well-homogenized samples and the absence of a concentration gradient. In case of the higher concentrated ruthenium sample, single spikes ranged from 10 up to 40 μg g^{-1} and precision over the entire line was approx. 20% giving a more realistic picture on the interpretation of bioimaging data. Analysis of the Pt sample (< 0.5 μg g^{-1}) showed that spatially-resolved quantitative data is not meaningful in the experimental setting: although the average over ten line-scans was still satisfactory with regard to precision and accuracy (Table S3, ESI†), precision within a single line-scan was lower than 30% and spikes ranged from 0.05 to 0.8 μg g^{-1} (target concentration: 0.257 μg g^{-1}), which equals recoveries from 19 to 311%. Hence, intensities of

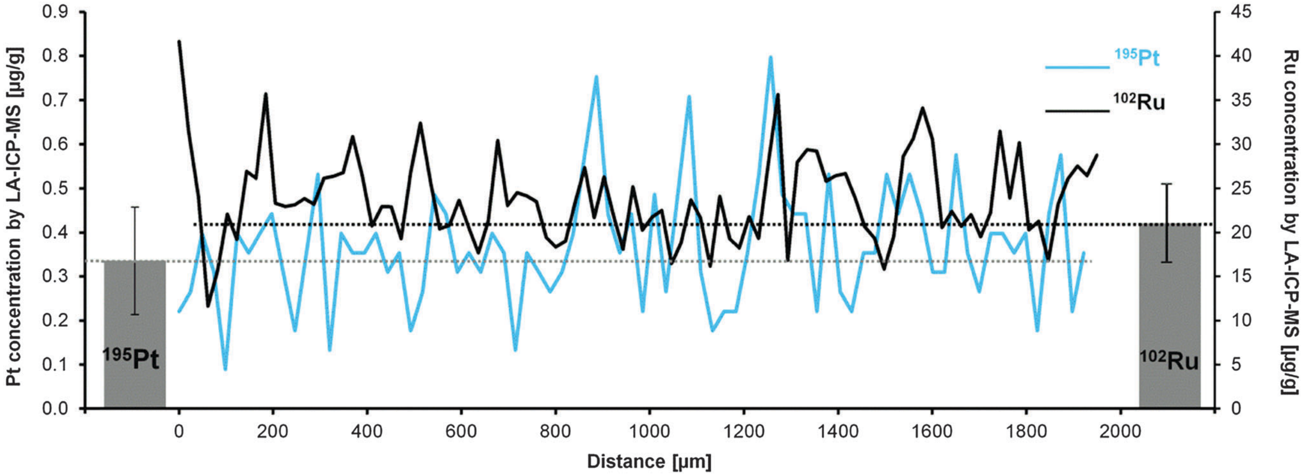

Fig. 3 Concentrations of Ru and Pt along a single line-scan (1950 µm) as determined by LA-ICP-MS in homogenized mouse liver originating from mice treated with either KP1339 or cisplatin, respectively. The bar charts represent the average and standard deviation of the line-scan. The target concentrations are 22.0 µg g^{-1} for Ru and 0.257 µg g^{-1} for Pt. The impact of internal standardization (^{13}C, ^{115}In, ^{185}Re) is visualized in Fig. S2 (ESI†) in the same manner.

peaks being distinctly different from neighbouring ones in bioimaging experiments should be interpreted with caution, especially in low concentrated samples (sub µg g^{-1} range).

Data analysis employing internal standards (^{13}C, ^{115}In, ^{185}Re) demonstrated that neither of them improved the precision significantly (Fig. S2, ESI†), thus, supporting that quantification solely *via* raw counts and matrix-matched standards is feasible.[36,39,42,51] Hence, we decided to perform quantitative LA experiments without internal standard, but ensured that instrumental drift during the ablation experiments was monitored by running calibration standards at least three times (at the beginning, during the ablation experiment and at the end of the sample run) and evaluated their precision. In case precision exceeded 15%, raw counts are reported instead of quantitative data.

In order to estimate the spatial resolution of the experimental setting, ablation was performed in parallel, horizontal line-scans. Hence, the diameter of the laser limits the vertical resolution to 70 µm with the laser parameters used. The horizontal resolution (along the line) was mainly impacted by the scan speed and dwell time (40 µm s^{-1} and 0.1 s). Thus, the theoretical limit equals a pixel size of 70 × 4 µm. A detailed picture of a KP1339-treated kidney (Fig. 4) features a tissue structure of approximately 100 × 100 µm in size (red circle). This structure is clearly visible in the corresponding laser ablation image, indicating that meaningful imaging data is obtained for structures exceeding 100 µm in size (Fig. 4).

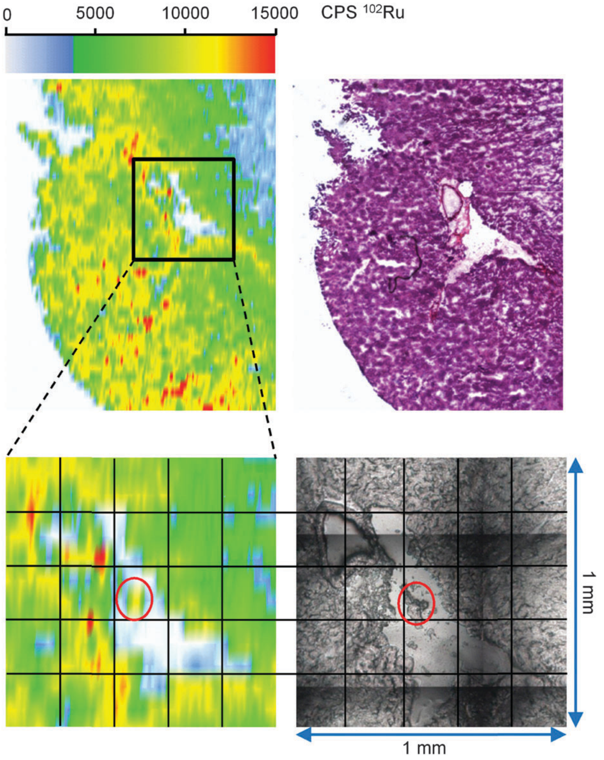

Fig. 4 Pictures of the LA-ICP-MS scan (left) and a consecutive HE stained slice (right) of kidney originating from a KP1339-treated mouse. The applied parameters for LA (70 µm laser diameter, 40 µm s^{-1} scan speed) allowed identification of a small piece of tissue (100 µm, red circles) within a tissue free area (greyscale picture prior to ablation).

Bioimaging of cisplatin- and KP1339-treated viscera

Viscera of mice treated either with KP1339 or cisplatin were obtained and the respective distribution of the metal, expressed as counts per second (CPS), was determined within kidney and spleen (Fig. 5) as well as muscle and liver (Fig. S3, ESI†). In order to validate the concentrations determined with LA-ICP-MS, 20–40 mg of tissue was digested in a microwave using half-concentrated nitric acid and analyzed by ICP-MS. The resulting average metal concentrations for each organ are summarized in Table 3. Despite the ablation was performed on different days, the rank order of average CPS in bioimages followed the concentrations determined by MW/ICP-MS: Ru concentrations from MW/ICP-MS experiments decreased in the

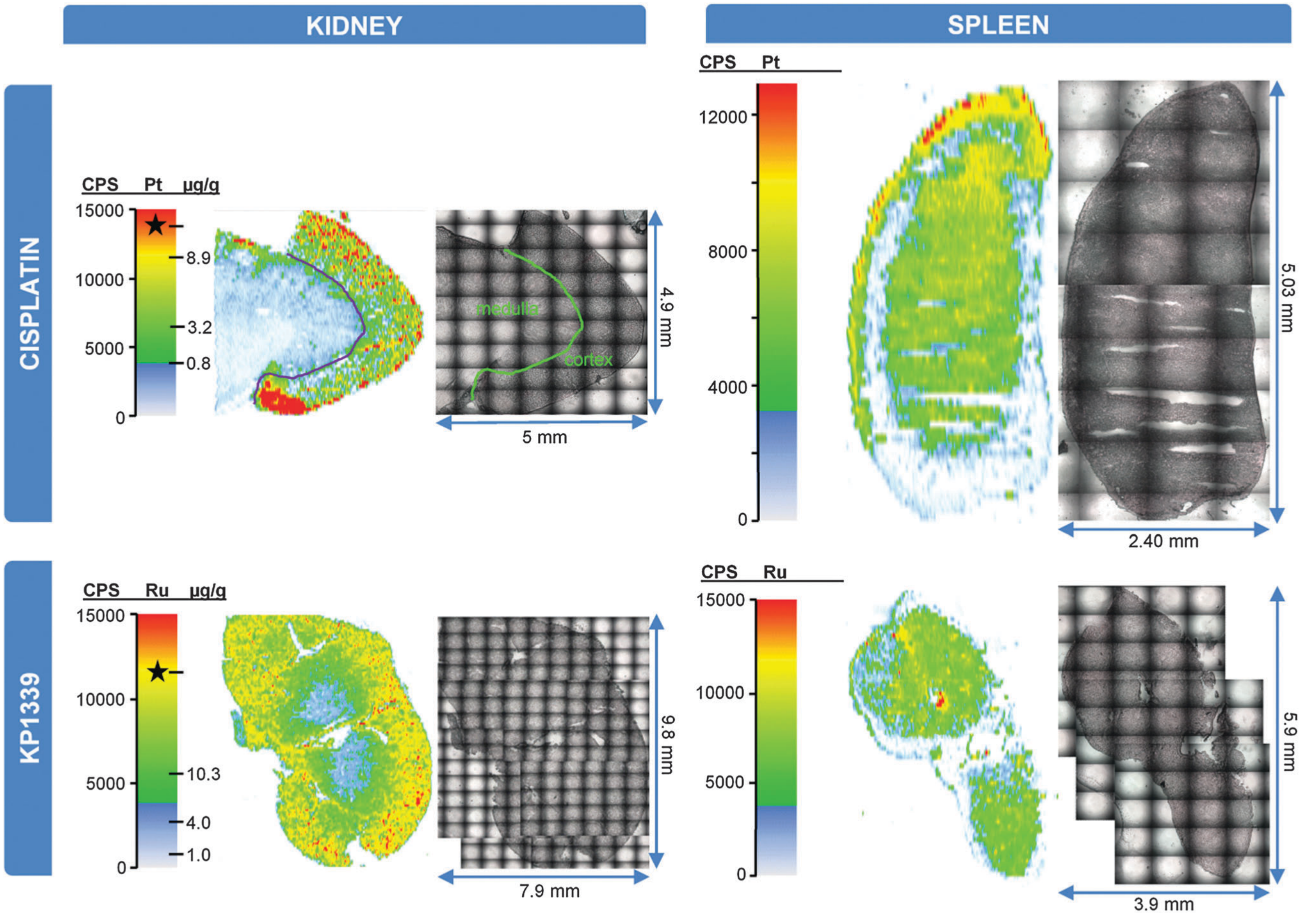

Fig. 5 Distribution of ^{195}Pt and ^{102}Ru in kidney and spleen of mice treated either with cisplatin or KP1339. Visualization was based on 128 and 76 parallel line scans (scan direction left to right, alignment of the lines from top to bottom) for Ru-containing viscera and 63 and 64 for the Pt samples. The corresponding greyscale images were recorded with the built-in camera of the laser ablation system prior to ablation of the sample. The color scales represent the recorded counts per second (CPS) of the registered metal ion isotopes by LA-ICP-MS. Quantitative amounts of Pt and Ru in kidney were obtained by ablating matrix-matched standards within the same run. In these cases, concentrations obtained by MW/ICP-MS were appropriately assigned to the color scale bar with an asterisk. Their corresponding colors according to the scale are in good accordance with the colors available in pictures obtained by LA-ICP-MS, proving validity of the method in real samples. Analysis of spleen was performed without simultaneous ablation of standards.

order liver ≥ kidney ≫ spleen > muscle and average CPS recorded by LA were estimated as 12 000 for liver and kidney, 7000 for spleen, and 3000 for muscle. Additionally, the MW/ICP-MS procedure was used as an independent methodology to assess the accuracy of the quantitative Pt distribution in kidney and Ru distribution in liver and kidney in the following manner: the average Ru concentration determined by MW/ICP-MS (*e.g.* 22.6 ± 0.8 µg g^{-1} in liver, Table 3) was indicated with an asterisk in the color bar (Fig. 5 and Fig. S3, ESI†), which shows that the concentration from MW/ICP-MS is in accordance with the concentrations determined by LA-ICP-MS. In case of the kidneys, the Ru and Pt concentrations determined by MW/ICP-MS corresponded to concentrations found in the cortex, hence again proving validity of the approach. When determining the quantitative distribution of Pt in a liver originating from a cisplatin-treated mouse the instrumental drift exceeded 15% and the quantitative data was therefore considered not valid.

Table 3 Metal concentrations in organs of mice treated either with cisplatin or KP1339. Concentrations were determined by ICP-MS after MW digestion of the samples. The data correspond to the same mice that were cryosectioned and ablated as depicted previously. The results are given as mean ± standard deviation in case of cisplatin and as mean ± span in case of KP1339. Concentrations of Pt in muscle and spleen were not determined (n.d.) due to insufficient sample material

	Concentration [µg g^{-1}]	
Organ	Cisplatin (Pt, n = 3)	KP1339 (Ru, n = 2)
Liver	3.9 ± 1.2	22.6 ± 0.8
Kidney	11.2 ± 0.6	20.5 ± 2.2
Muscle	n.d.	2.9 ± 0.3
Spleen	n.d.	6.5 ± 0.4

Both metals were found to be homogenously distributed in liver tissue, whereas the metal distribution in kidney tissue correlated with the functional differentiation of the organ. The Pt concentration in the cortex was found to be about 10-times higher than in the medulla (9 and <0.8 µg g^{-1}, respectively). Note that the reported absolute values do not consider biological variations as they are based on experiments with a single mouse per metal compound. However, our data obtained for cisplatin-treated mice is in good agreement with most data reported previously, using also LA-ICP-MS,[42–44] although treatment regimens as well as preparation of samples and standards varied significantly (see Table S4, ESI†). So far, only two literature reports dealt with spatially-resolved, quantitative bioimaging:[42,44] Zoriy *et al.* studied Pt distribution in frozen sections of kidney originating from cisplatin-treated mice (3 mg kg^{-1} for 60 min) and reported highest concentrations in the medulla and progressively decreasing amounts to the periphery.[42] In contrast, Reifschneider *et al.* not only investigated murine kidney and cochlea tissue affected by cisplatin treatment but also the testes as therapeutic target tissue and reported Pt biodistribution quantitatively. Samples were obtained from mice treated with cisplatin (15 mg kg^{-1}) for 1 h and 4 days and embedded in a cold polymerizing resin, which was used for preparation of standards as well. The highest concentrations of 85 and 2 μg g^{-1} were detected in the cortico-medullary region upon treatment for 1 h and 4 days, respectively, and no significant Pt accumulation was detected in the medulla.[44] These findings are in good agreement with our data (approx. 9 μg g^{-1} in the cortex), considering the treatment time of 24 h in our case. Moreno-Gordaliza *et al.* investigated formalin-fixed paraffin-embedded (FFPE) kidneys.[43] In this study, Pt was found to be enriched by a factor of 10 in cortex in comparison with the medulla, which is also in accordance with our results. On the other hand, quantitative Pt concentrations differ substantially despite comparable dosages (16 mg kg^{-1} for 3 days *vs.* 15 mg kg^{-1} for 1 day in our study) and identical route of applications (i.p.). While quantification is based on LA-ICP-MS in both cases, the sample and standard preparation varied considerably (*e.g.* FFPE tissue) yielding loss of quantitative spatial resolution and some experimental details remain ambiguous. Our approach (treatment 15 mg kg^{-1}, 1 day) based on the LA-ICP-MS analysis of cryosections and matrix-matched standards for calibration was chosen to obtain spatially-resolved quantitative information. The reported concentrations of <0.8 μg g^{-1} in the medulla and approximately 9 μg g^{-1} in the cortex, as estimated from Fig. 5, correspond to wet tissue. Furthermore, this was independently confirmed by determining the Pt content of the same kidney used for preparation of cryosections by MW/ICP-MS, which yielded an average Pt concentration of 11.2 ± 0.6 μg g^{-1} (Table 3), thereby proving the accuracy of our quantitative laser ablation procedure.

The observed accumulation of Pt in cortex of the kidney is in accordance with its toxicity for proximal tubule cells, located in the cortico-medullary junction.[52] However, drawing conclusions on potential side effects solely on the basis of accumulation is not justified: Ru originating from KP1339 possesses a comparable distribution pattern in kidneys, but in contrast to cisplatin no severe side effects (such as nephrotoxicity) have been observed in preclinical or clinical trials.[10,11] Additionally, we compared stained kidney sections from cisplatin and KP1339-treated mice histologically and no pathologic alterations indicating acute tubular damage were observed (Fig. S4 and S5, ESI†). Studies focusing on cisplatin nephrotoxicity report visible histologic damage in renal tissue after cisplatin treatment of rats (5 mg kg^{-1} for 5 days[52] or 16 mg kg^{-1} for 3 days).[43] As degenerative changes in proximal tubule tissue become visible after 3–5 days at earliest,[53] the short treatment-time with cisplatin in our experiment (24 h) explains the discrepancy at histologic level.

Pt and Ru are homogenously distributed in muscle tissue (Fig. S3, ESI†) and distribution in spleen exhibited regions with enriched amounts of metals for both compounds (Fig. 5, left).

Conclusion

Quantification of elemental distributions in biological samples studied by LA-ICP-MS suffers from a lack of certified reference materials for the analyte of interest and currently no standardized approach for the application of internal standards is available. Therefore we focused in this paper on the method development and validation of a quantitative LA-ICP-MS bioimaging experiment in organs of mice treated with the anticancer agents KP1339 or cisplatin. Analysis of liver homogenates by a single line-scan resulted in a realistic estimation of the precision for tissue imaging with a relative standard deviation of approximately 20%, while averaging over line-scans only pretended high accuracy (70–120%) and precision (3–15%). Applying internal standards such as ^{115}In, ^{185}Re and ^{13}C did not improve the quality of the data and was not mandatory given instrumental response is stable over time with a drift of less than 15% during the entire ablation experiment. The experimental resolution of the elemental distributions was determined to be approximately 100 μm *via* corresponding histological structures in optical images of the ablated area.

Using this method, the spatially-resolved biodistribution of KP1339 in a series of organs was studied for the first time, exhibiting distribution patterns similar to cisplatin. Because of the low number of test animals used, the absolute values on organ distributions have to be taken carefully. Both compounds were enriched in the cortex of the kidney in comparison with the medulla, a homogenous distribution was determined in the liver as well as in muscle tissue and areas of the spleen showed also higher metal concentrations. The viscera were additionally digested in a microwave and the concentrations as determined by direct infusion ICP-MS confirmed those determined by LA-ICP-MS imaging. Therefore the validity of the data in real world samples was demonstrated in an independent experiment. Moreover, our data reveal that no toxic alterations at histologic level are observed after treatment of mice with KP1339, although the ruthenium concentration in tissue was much higher than the platinum concentration. This is in good agreement with the lack of severe side effects observed in clinical trials with KP1339.[11]

Acknowledgements

C.G.H. is grateful for the financial support provided by the Austrian Science Fund (Project Number I496-B11; postdoctoral fellowship to A.E.E.), the University of Auckland, Genesis

Oncology Trust, and the Royal Society of New Zealand. We would like to thank the members of the COST actions D39 and CM1105 for useful discussions. The authors are indebted to Dr Michael Reithofer and Dr Werner Ginzinger for preparation of cisplatin and KP1339, respectively. Lucas Prieto Gonzáles-Posada is acknowledged for assisting in sample preparation, Gerlinde Grabmann for fruitful discussion and Ute Jungwirth for providing the picture of the mouse in Scheme S1 (ESI†).

References

1 J. Reedijk, *Chem. Rev.*, 1999, **99**, 2499–2510.

2 N. P. E. Barry and P. J. Sadler, *Chem. Commun.*, 2013, **49**, 5106–5131.

3 M. A. Jakupec, M. Galanski and B. K. Keppler, *Rev. Physiol., Biochem. Pharmacol.*, 2003, **146**, 1–53.

4 X. Yao, K. Panichpisal, N. Kurtzman and N. Kenneth, *Am. J. Med. Sci.*, 2007, **334**, 115–124.

5 D. Lebwohl and R. Canetta, *Eur. J. Cancer*, 1998, **34**, 1522–1534.

6 M. A. Jakupec, M. Galanski, V. B. Arion, C. G. Hartinger and B. K. Keppler, *Dalton Trans.*, 2008, 183–194.

7 C. G. Hartinger, S. Zorbas-Seifried, M. A. Jakupec, B. Kynast, H. Zorbas and B. K. Keppler, *J. Inorg. Biochem.*, 2006, **100**, 891–904.

8 C. G. Hartinger, M. A. Jakupec, S. Zorbas-Seifried, M. Groessl, A. Egger, W. Berger, H. Zorbas, P. J. Dyson and B. K. Keppler, *Chem. Biodiversity*, 2008, **5**, 2140–2155.

9 A. Bergamo, C. Gaiddon, J. H. M. Schellens, J. H. Beijnen and G. Sava, *J. Inorg. Biochem.*, 2012, **106**, 90–99.

10 D. S. Thompson, G. J. Weiss, S. F. Jones, H. A. Burris, R. K. Ramanathan, J. R. Infante, J. C. Bendell, A. Ogden and D. D. Von Hoff, *J. Clin. Oncol.*, 2012, **30**(suppl), abstr 3033.

11 R. Trondl, P. Heffeter, C. R. Kowol, M. A. Jakupec, W. Berger and B. K. Keppler, *Chem. Sci.*, 2014, DOI: 10.1039/C3SC53243G.

12 J. Arrowsmith, *Nat. Rev. Drug Discovery*, 2011, **10**, 1.

13 J. Arrowsmith and P. Miller, *Nat. Rev. Drug Discovery*, 2013, **12**, 569.

14 C. S. Allardyce, P. J. Dyson, F. R. Abou-Shakra, H. Birtwistle and J. Coffey, *Chem. Commun.*, 2001, 2708–2709.

15 I. Khalaila, A. Bergamo, F. Bussy, G. Sava and P. J. Dyson, *Int. J. Oncol.*, 2006, **29**, 261–268.

16 J. S. Becker and N. Jakubowski, *Chem. Soc. Rev.*, 2009, **38**, 1969–1983.

17 J. S. Becker, M. Zoriy, A. Matusch, B. Wu, D. Salber, C. Palm and J. S. Becker, *Mass Spectrom. Rev.*, 2010, **29**, 156–175.

18 I. Konz, B. Fernández, M. Fernández, R. Pereiro and A. Sanz-Medel, *Anal. Bioanal. Chem.*, 2012, **403**, 2113–2125.

19 J. S. Becker, M. V. Zoriy, C. Pickhardt, N. Palomero-Gallagher and K. Zilles, *Anal. Chem.*, 2005, **77**, 3208–3216.

20 C. Giesen, T. Mairinger, L. Khoury, L. Waentig, N. Jakubowski and U. Panne, *Anal. Chem.*, 2011, **83**, 8177–8183.

21 D. Hare, C. Austin and P. Doble, *Analyst*, 2012, **137**, 1527–1537.

22 D. Pozebon, V. L. Dressler, M. F. Mesko, A. Matusch and J. S. Becker, *J. Anal. At. Spectrom.*, 2010, **25**, 1739–1744.

23 C. Austin, D. Hare, T. Rawling, A. M. McDonagh and P. Doble, *J. Anal. At. Spectrom.*, 2010, **25**, 722–725.

24 H. Sela, Z. Karpas, H. Cohen, Y. Zakon and Y. Zeiri, *Int. J. Mass Spectrom.*, 2011, **307**, 142–148.

25 J. A. T. Pugh, A. G. Cox, C. W. McLeod, J. Bunch, B. Whitby, B. Gordon, T. Kalber and E. White, *J. Anal. At. Spectrom.*, 2011, **26**, 1667–1673.

26 K. Jurowski, S. Walas and W. Piekoszewski, *Talanta*, 2013, **115**, 195–199.

27 C. Austin, F. Fryer, J. Lear, D. Bishop, D. Hare, T. Rawling, L. Kirkup, A. McDonagh and P. Doble, *J. Anal. At. Spectrom.*, 2011, **26**, 1494–1501.

28 D. A. Frick and D. Gunther, *J. Anal. At. Spectrom.*, 2012, **27**, 1294–1303.

29 C. Giesen, L. Waentig, T. Mairinger, D. Drescher, J. Kneipp, P. H. Roos, U. Panne and N. Jakubowski, *J. Anal. At. Spectrom.*, 2011, **26**, 2160–2165.

30 L. Waentig, N. Jakubowski, H. Hayen and P. H. Roos, *J. Anal. At. Spectrom.*, 2011, **26**, 1610–1618.

31 I. Konz, B. Fernández, M. L. Fernández, R. Pereiro, H. González, L. Álvarez, M. Coca-Prados and A. Sanz-Medel, *Anal. Bioanal. Chem.*, 2013, **405**, 3091–3096.

32 D. Drescher, C. Giesen, H. Traub, U. Panne, J. Kneipp and N. Jakubowski, *Anal. Chem.*, 2012, **84**, 9684–9688.

33 H. A. O. Wang, D. Grolimund, C. Giesen, C. N. Borca, J. R. H. Shaw-Stewart, B. Bodenmiller and D. Günther, *Anal. Chem.*, 2013, **85**, 10107–10116.

34 A. J. Managh, S. L. Edwards, A. Bushell, K. J. Wood, E. K. Geissler, J. A. Hutchinson, R. W. Hutchinson, H. J. Reid and B. L. Sharp, *Anal. Chem.*, 2013, **85**, 10627–10634.

35 B. Jackson, S. Harper, L. Smith and J. Flinn, *Anal. Bioanal. Chem.*, 2006, **384**, 951–957.

36 A. Matusch, C. Depboylu, C. Palm, B. Wu, G. U. Höglinger, M. K. H. Schäfer and J. S. Becker, *J. Am. Soc. Mass Spectrom.*, 2010, **21**, 161–171.

37 J. S. Becker, *Int. J. Mass Spectrom.*, 2010, **289**, 65–75.

38 D. J. Hare, J. K. Lee, A. D. Beavis, A. van Gramberg, J. George, P. A. Adlard, D. I. Finkelstein and P. A. Doble, *Anal. Chem.*, 2012, **84**, 3990–3997.

39 M. V. Zoriy, M. Dehnhardt, G. Reifenberger, K. Zilles and J. S. Becker, *Int. J. Mass Spectrom.*, 2006, **257**, 27–33.

40 M. V. Zoriy, M. Dehnhardt, A. Matusch and J. S. Becker, *Spectrochim. Acta, Part B*, 2008, **63**, 375–382.

41 D. Hare, F. Burger, C. Austin, F. Fryer, R. Grimm, B. Reedy, R. A. Scolyer, J. F. Thompson and P. Doble, *Analyst*, 2009, **134**, 450–453.

42 M. Zoriy, A. Matusch, T. Spruss and J. S. Becker, *Int. J. Mass Spectrom.*, 2007, **260**, 102–106.

43 E. Moreno-Gordaliza, C. Giesen, A. Lázaro, D. Esteban-Fernández, B. Humanes, B. Cañas, U. Panne, A. Tejedor, N. Jakubowski and M. M. Gómez-Gómez, *Anal. Chem.*, 2011, **83**, 7933–7940.

44 O. Reifschneider, C. A. Wehe, K. Diebold, C. Becker, M. Sperling and U. Karst, *J. Anal. At. Spectrom.*, 2013, **28**, 989–993.

45 D. Gholap, J. Verhulst, W. Ceelen and F. Vanhaecke, *Anal. Bioanal. Chem.*, 2012, **402**, 2121–2129.

46 S. C. Dhara, *Indian J. Chem.*, 1970, **8**, 193–194.

47 B. Keppler, Method of manufacturing an alkali metal salt of *trans*-[tetrachlorobis(1*H*-indazole)ruthenate(III)]), EP 2152084 B1, Niiki Pharma Inc., USA, 2008.

48 C. Paton, J. Hellstrom, B. Paul, J. Woodhead and J. Hergt, *J. Anal. At. Spectrom.*, 2011, **26**, 2508–2518.

49 http://www.iolite.org.au/Iolite.html.

50 J. Lear, D. Hare, P. Adlard, D. Finkelstein and P. Doble, *J. Anal. At. Spectrom.*, 2012, **27**, 159–164.

51 J. S. Becker, U. Breuer, H.-F. Hsieh, T. Osterholt, U. Kumtabtim, B. Wu, A. Matusch, J. A. Caruso and Z. Qin, *Anal. Chem.*, 2010, **82**, 9528–9533.

52 D. Sheikh-Hamad, W. Cacini, A. Buckley, J. Isaac, L. Truong, C. Tsao and B. Kishore, *Arch. Toxicol.*, 2004, **78**, 147–155.

53 J. P. Fillastre and G. Raguenez-Viotte, *Toxicol. Lett.*, 1989, **46**, 163–175.

Electronic Supplementary Material (ESI) for Metallomics.

Supporting Information

to

Quantitative bioimaging by LA–ICP-MS: a methodological study on the distribution of Pt and Ru in viscera originating from cisplatin- and KP1339-treated mice

Alexander E. Egger*[1,2], Sarah Theiner[2,3], Christoph Kornauth[4], Petra Heffeter[3,5], Walter Berger[3,5], Bernhard K. Keppler[2,3], Christian G. Hartinger*[2,3,6]

[1] ADSI – Austrian Drug Screening Institute GmbH, Innsbruck, Austria

[2] Institute of Inorganic Chemistry, University of Vienna, Vienna, Austria

[3] Research Platform 'Translational Cancer Therapy Research', University of Vienna, Vienna, Austria

[4] Institute of Clinical Pathology, Medical University of Vienna, Vienna, Austria

[5] Institute of Cancer Research, Department of Medicine I, and Comprehensive Cancer Center, Medical University of Vienna, Vienna, Austria

[6] School of Chemical Sciences, University of Auckland, Auckland, New Zealand

* Corresponding Authors: ADSI, Innrain 66a, A-6020 Innsbruck, Austria, E-Mail: alexander.egger@adsi.ac.at, Tel.: +43-512-507-36305 (A.E.E); University of Auckland, School of Chemical Sciences, Private Bag 92019, Auckland 1142, New Zealand E-mail: c.hartinger@auckland.ac.nz, Fax: (+64)9 373 7599 ext 87422 (C.G.H.)

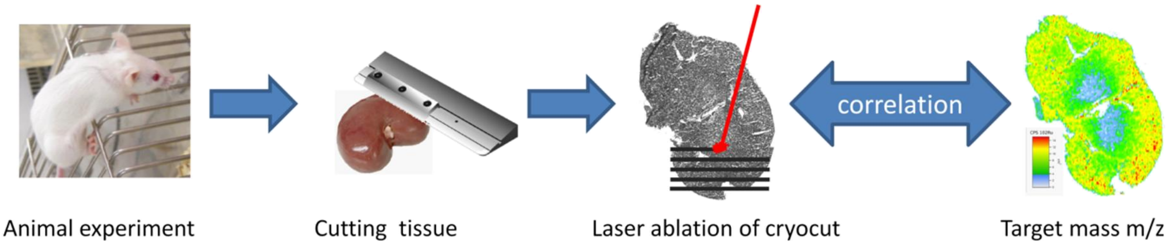

Scheme S1: Work-flow in mass spectrometry-based bioimaging experiments. The frozen animal tissue is cryocut into slices and ablated by a high energetic laser beam. The generated aerosol is transferred into the ICP-MS, recorded, and visualized in an intensity-dependent manner reflecting the shape of the ablated area.

Table S1: Conditions used for microwave-assisted acid digestion of samples and standards.

Step	t [min]	Max. E [W]	T [°C]
1	2	700	85
2	5	700	135
3	4	1000	180
4	12	1000	180
Ventilation	10	0	

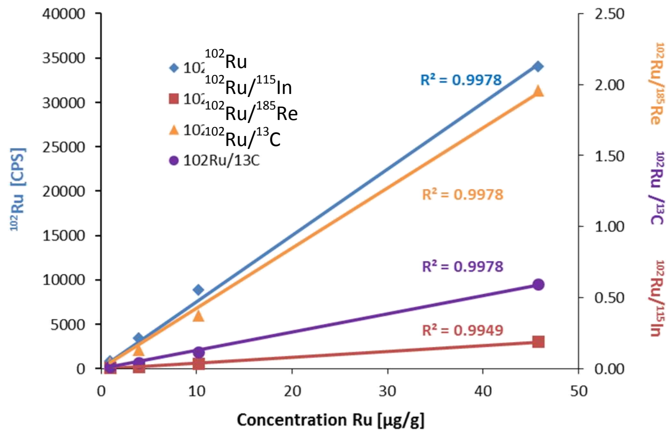

Figure S1: Comparison of the calibration curves for the quantification of Ru in tissue homogenates. The calculation is based on counts per second (CPS) of the registered isotope ^{102}Ru (♦, left ordinate) and compared with ^{102}Ru/^{195}Re (▲), ^{102}Ru/^{13}C (●) and ^{102}Ru/^{115}In (■), right ordinate.

Table S2: Comparison between theoretical Ru and Pt concentrations in spiked liver homogenates and experimentally determined values upon microwave digestion/ICP-MS.

	Concentration / [µg/g]		
Standard	**Pt, Ru (theoretical)**	**Pt (experimental)**	**Ru (experimental)**
1	0.98	0.79 ± 0.05	0.96 ± 0.03
5	4.96	3.17 ± 0.70	3.96 ± 0.08
10	9.70	8.93 ± 0.10	10.25 ± 0.77
50	45.53	39.24 ± 0.92	45.72 ± 1.01

Table S3: Precision and recovery of Ru and Pt, determined by LA-ICP-MS in two samples of homogenized liver (Homo1 and Homo2) originating from mice treated either with KP1339 or cisplatin, respectively. Recovery is referenced to microwave digestion of the sample followed by ICP-MS analysis. LA-ICP-MS data is based on averaged line scans. The range for the observed accuracy and precision for each element is given in bold numbers.

		^{102}Ru				^{195}Pt			
	Internal Standard	none	^{115}In	^{185}Re	^{13}C	none	^{115}In	^{185}Re	^{13}C
Homo1	**Recovery [%]**	93	**116**	106	97	119	81	105	91
	RSD [%]	4.9	3.3	**7.8**	4.7	9.4	12.1	10.7	9.8
Homo2	**Recovery [%]**	108	114	**92**	102	**120**	**70**	91	86
	RSD [%]	2.9	**2.8**	6.9	2.5	**14.6**	10.1	**7.6**	8.8

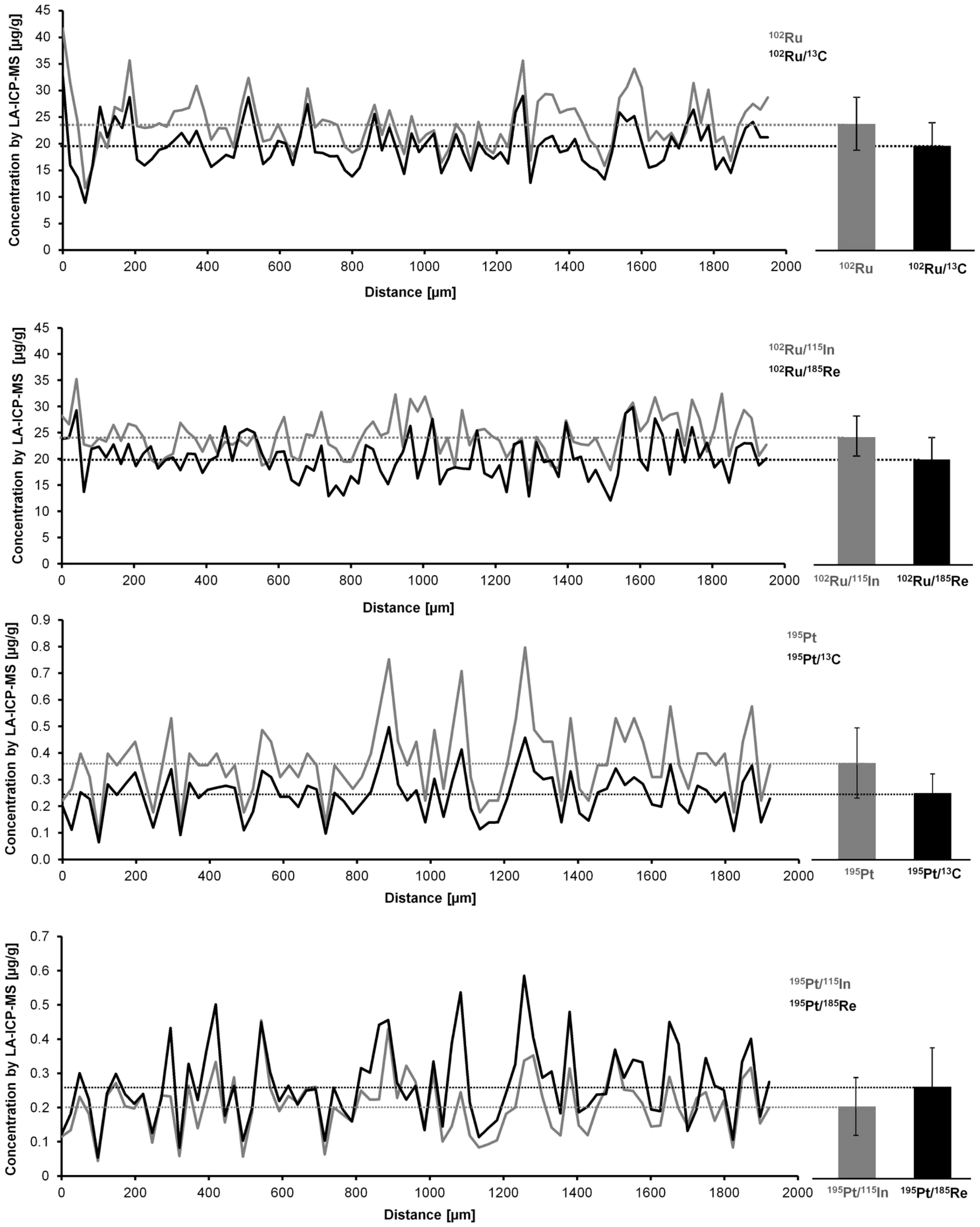

Figure S2: Concentrations of Ru and Pt along a single line-scan (1950 µm) as determined by LA–ICP-MS in homogenized mouse liver originating from mice treated with either KP1339 or cisplatin, respectively. The bar charts on the right represent the average and standard deviation of the line-scan. The target concentrations are 22.0 µg/g for Ru and 0.257 µg/g for Pt.

Table S4: Overview of studies dealing with LA-ICP-MS imaging of kidneys originating from cisplatin treated animals

Study	Animal	treatment	Sample preparation	LA-ICP-MS [µg/g]	verified
Zoriy [1]	NMRI mice	3 mg/kg (i.p.) 60 min	Cryocut, quantification via matrix matched standards	Cortex: 6-14 Medulla: ~26	No
Moreno-Gordaliza [2]	Wistar rats	5 mg/kg (i.p.) 5 d	FFPE, quantification by spiking standard onto control tissue slice	average: 14 medulla << cortex	No
		16 mg/kg (i.p.) 3 d		average: 144 medulla << cortex	
Reifschneider [3]	C57BL/6N mice	15 mg/kg 1 h	Bouin's fixative, embedded in polymerizing resin Technovit 7100, Standards prepared in Technovit 7100	Cortex: 85 Medulla << cortex	No
		15 mg/kg 4 d		Cortex: 2 Medulla << cortex	
this paper	Balb/C mice	15 mg/kg (i.p.) 24 h	Cryocut, quantification via matrix matched standards	Cortex: ~9 Medulla: <0.8	MW/ICP-MS: 11.2±0.6

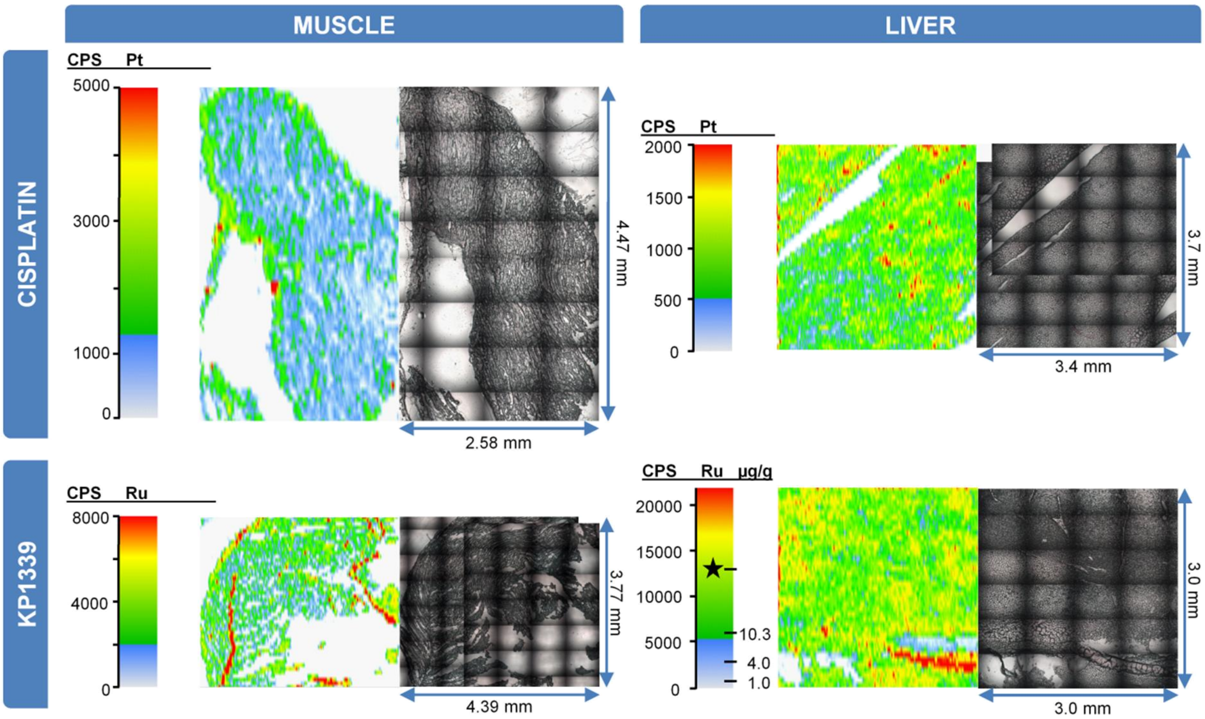

Figure S3: Distribution of ^{195}Pt and ^{102}Ru in liver and muscle of mice treated either with cisplatin or KP1339. Visualization was based on 44 and 48 parallel line scans (scan direction left to right, alignment of the lines from top to bottom) for Ru-containing viscera and 46 and 56 for Pt. The corresponding greyscale images were recorded with the built-in camera of the laser ablation system prior to ablation of the sample. The color scales represent the recorded counts per second (CPS) of the registered metal ion isotopes by LA–ICP-MS. Red colored areas of apparent Ru enrichment in liver and muscle are due to tissue duplication according to the histological image and the fact that their intensity is twice as high compared to neighbouring tissue. Quantitative amounts of Ru in liver, was obtained by ablating matrix matched standards within the same run. In this case, the concentration obtained by MW/ICP-MS was appropriately assigned to the color scale bar with an asterisk. Its corresponding color according to the scale is in good accordance with the color available in the picture obtained by LA–ICP-MS, proving validity of the method in real samples. Analysis of muscle was performed without simultaneous ablation of standards.

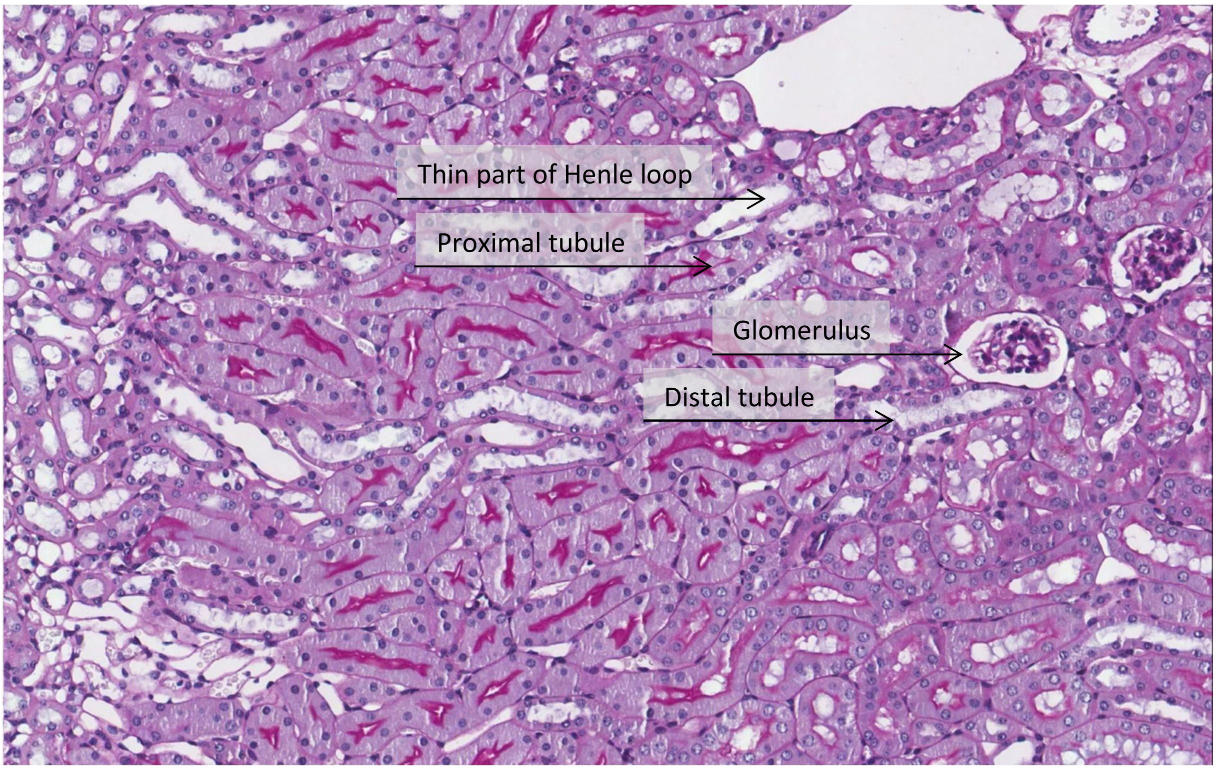

Figure S4: Kidney section (PAS staining) of a KP1339-treated mouse (50 mg/kg, i.v., 18 h).

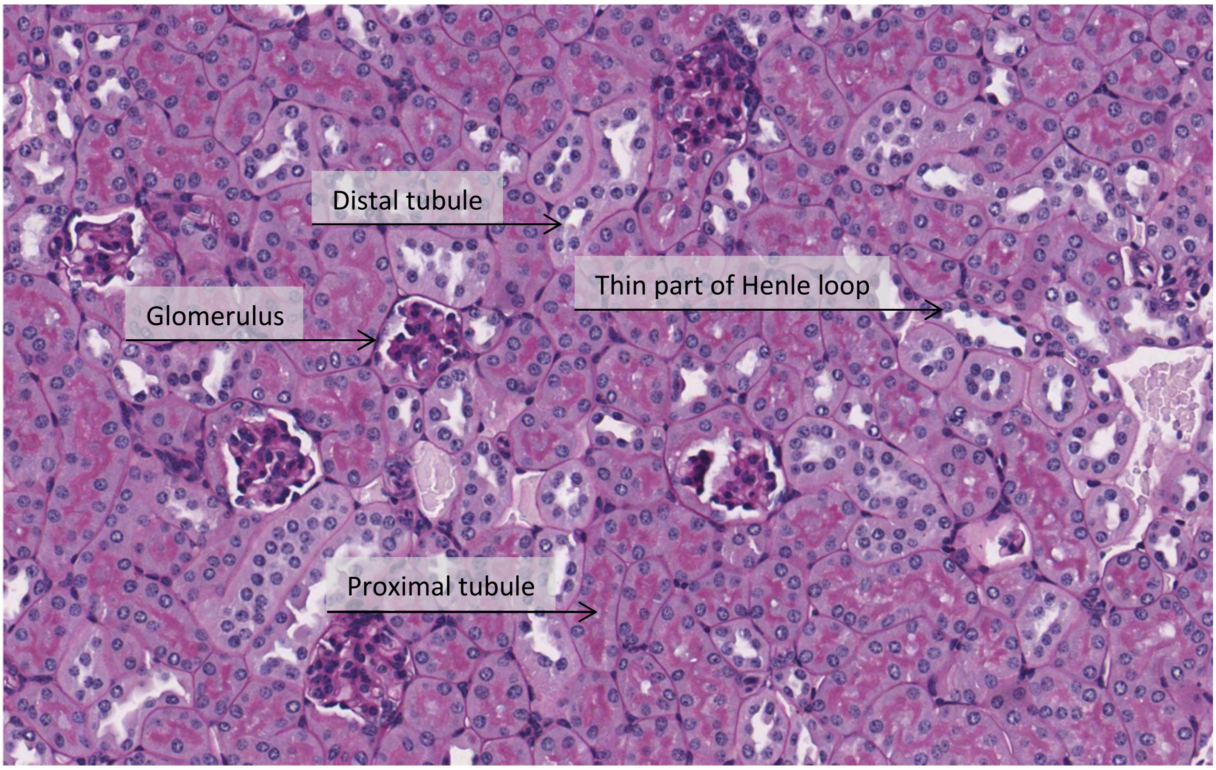

Figure S5: Kidney section (PAS staining) of a cisplatin-treated mouse (15 mg/kg, i.p., 24 h).

References

1. M. Zoriy, A. Matusch, T. Spruss and J. S. Becker, *Int. J. Mass Spectrom.*, 2007, **260**, 102-106.
2. E. Moreno-Gordaliza, C. Giesen, A. Lázaro, D. Esteban-Fernández, B. Humanes, B. Cañas, U. Panne, A. Tejedor, N. Jakubowski and M. M. Gómez-Gómez, *Anal. Chem.*, 2011, **83**, 7933-7940.
3. O. Reifschneider, C. A. Wehe, K. Diebold, C. Becker, M. Sperling and U. Karst, *J. Anal. At. Spectrom.*, 2013, **28**, 989-993.

Analysis of Pt- and Ru-based anticancer drugs – new developments.

Sarah Theiner[1,2], Luis Galvez Montano[3], Gunda Koellensperger[3], Bernhard K. Keppler[1,2]

[1] Department of Inorganic Chemistry, Faculty of Chemistry, University of Vienna, Währinger Strasse 42, 1090 Vienna

[2] Research Platform 'Translational Cancer Therapy Research', University of Vienna, Währinger Strasse 42, 1090 Vienna

[3] Department of Analytical Chemistry, Faculty of Chemistry, University of Vienna, Währinger Strasse 38, 1090 Vienna

1. Imaging techniques in metal-based anticancer drug research

The development and application of mass spectrometry imaging (MSI) techniques has become of great interest in cancer research and diagnosis to study elemental distributions in biological tissue samples at microscopic level. The ability to record spatial accumulation of multiple analytes in tissue samples under native conditions and to directly correlate obtained images with histological features has turned MSI into an invaluable analytical tool [1,2].

1.1. Imaging of metal-based anticancer drugs at tissue level

Laser ablation (LA) hyphenated to ICP-MS (LA-ICP-MS) has become the method of choice to produce quantitative images of detailed, regionally specific element distributions in biological tissue [3-5]. LA-ICP-MS combines high spatial resolution power (low µm range) with the multielement capabilities and high sensitivity of ICP-MS detection [1,3]. In addition, the sample preparation process for bioimaging by LA-ICP-MS is relatively simple and fast. Most studies rely on cryosections to preserve the biological material and elemental distributions in native physiological conditions. In this case, the biological tissue is cut under frozen conditions into thin sections (typically between 5 and 30 µm) and mounted on glass slides. For elemental mapping and conventional histological stains storage at room temperature is sufficient [3,4]. However, for routine histological evaluations, usually paraffin-embedding is used. In this case, the sample undergoes several washing steps and formalin fixation, which can result in elemental leaching. A kinetic study was carried out using rat heart showing a decrease in concentrations of biological relevant elements (such as Fe, S, P, Cu, Zn, etc.) [6]. In addition, the sample section is subjected to dehydration in a series of increasing concentrations of alcohol for paraffin embedding leading to shrinkage of the tissue.

The thin tissue section is ablated with a focused laser beam and the sample material is transferred with an ablation/carrier gas (usually He, Ar or a mixture of them) to the ICP-MS system. The elemental composition is analyzed as a function of laser beam position employing quadrupole, sector field or time-of-flight (TOF) mass analyzer. The ion intensities of each analyte are recorded as counts per second against time along the course of a laser scanning and images are generated [4].

1.2 State of the art of quantification by LA-ICP-MS

The development of unified, validated and reliable quantification strategies for bioimaging by LA-ICP-MS is still part of ongoing research and several different approaches have been proposed in literature [7,8]. Elemental fractionation during ICP-MS analysis is strongly matrix dependent and therefore, single-point calibration using certified standard reference materials (CRMs) with defined elemental concentrations would be the method of choice. In addition, the quantification process can be traced back to a certified value and can be therefore validated. However, CRMs have to match the exact matrix composition of the sample subjected to LA-ICP-MS and their limited availability for bioimaging offers only few applications [7]. Therefore, most commonly, matrix-matched calibration standards are prepared individually for each analytical problem and sample material. For this purpose, homogenates of analogous tissue are spiked with known amounts of analytes. The elemental concentrations are verified by an independent method (e.g. microwave-assisted digestion followed by ICP-MS analysis) and the prepared standards are analyzed under the same experimental conditions as the sample [8]. Different matrices have been used in literature such as liver, chicken breast, brain tissue, whole human blood, etc. [9-12].

Another approach focused on thin polymeric films spiked with analytes, which are then spin-coated on glass slides [13]. In this context, also gelatin-based standards were proposed for quantification [14,15]. However, in both cases the calibration standards do not possess the same features as biological tissues, which can have impact on the signal obtained during the laser ablation process.

An on-line solution-based calibration method has been investigated for bioimaging by LA-ICP-MS. In this case, the laser-generated aerosol is combined with a second stream of aerosol (containing the calibration standard) generated by solution nebulization. The standard aerosol can either be introduced with the help of a micro-nebulizer placed in the laser ablation cell or directly into the injector tube of the ICP-MS torch [16,17]. Applying online addition of multi-element standard solutions can lead to more standardized plasma conditions, but can also cause more bias and polyatomic interferences [16]. In addition, it is independent from the ablation source and hence does not consider possible tissue inhomogeneity and different interaction between the laser beam and the tissue sample [8].

In order to monitor instrumental drift over the measurement time of LA-ICP-MS bioimaging experiments (which can last up to several hours) the use of an internal standard is recommended. One class of internal standards comprises elements intrinsically present in the sample. In this context, the most commonly employed isotope is ^{13}C, but also phosphorus, sulfur and calcium have been proposed as normalization elements for selected applications [7,18]. Carbon may account for differences in sample thickness (as indication for organic matter), but its signal can be affected by differing water contents of the ablated tissue. In addition, ^{13}C is not always homogenously distributed within the different structures of soft tissue. Moreover, it has different mass and first ionization potential and is less sensitive to instrumental fluctuations compared to most analytes under investigation [8,19].

Alternatively, the use of thin films spiked with internal standard elements that are spin-coated on glass slides was proposed[13]. The sample section is placed on the top of the polymeric film enabling simultaneous ablation of the tissue and internal standard layer. Recently, it was shown that the use of gold layers for signal normalization compensates for instrumental drift and matrix-related differences in ablation [20,21]. Another study reported on iodine as an elemental dye for fibroblast cells and for thin tissue sections for single cell and cell nucleus imaging. In course of this study, it was also concluded that iodine would be a suitable internal standard to correct for tissue inhomogeneity [22].

1.3 LA-ICP-MS imaging in metal-based anticancer drug development

In the field of metal-based anticancer drug research, the rational behind the development of LA-ICP-MS methods is to resolve keystone questions regarding metallodrug-protein interactions, tumor response to drug treatment, as well as underlying mechanisms of therapy-related side effects. The first LA-ICP-MS study in this context analyzed the platinum content of bacterial proteins upon treatment with cisplatin after separation with gel electrophoresis [23]. In addition, protein-interactions of the investigational ruthenium complex NAMI-A were studied in comparison to cisplatin using native PAGE, SDS-PAGE and 2D gel electrophoresis followed by identification of the binding partners by LA-ICP-MS [24]. An overview of LA-ICP-MS imaging studies involving the vizualisation metal-based anticancer drugs in biological tissues is shown in Table 1. In all studies, quantification was performed using matrix-matched standards.

Table 1. Applications of LA-ICP-MS in metal-based anticancer drug research

Metallodrug	Organ	Spatial resolution	Elements	Reference
cisplatin	kidney	8 µm	Pt, Zn, Cu	Moreno-Gordaliza et al. [25]
cisplatin	kidney	50 µm	Pt, Zn, Cu	Zoriy et al. [26]
cisplatin	kidney, cochlea, testis	50 µm	Pt	Reifschneider et al. [27]
cisplatin, KP1339	kidney, liver, spleen, muscle	70 µm	Pt, C	Egger et al. [9]
oxaliplatin	tumor	70 µm	Pt, P, C	Gholap et al. [15]
oxaliplatin, satraplatin, Pt(IV) complexes	tumor, kidney	70 µm	Pt	Theiner et al. [28]
cisplatin, oxaliplatin	muscle, nerve, connective, fat tissue	70 µm	Pt	Egger et al. [29]
cisplatin, oxaliplatin	tumor	200 µm	Pt	Bianga et al. [30]

Several studies have focused on the investigation of elemental depositions in affected organs with the aim to design improved treatment regimens with reduced toxicity to healthy organs. The complex relation between kidney functionality and platinum drug chemotherapy, which limits the applicable dosage in the case of cisplatin, makes this organ ideally suited to develop LA-ICP-MS setups. In this context, a LA-ICP-MS-based methodology was evaluated for bioimaging of Pt, Cu and Zn in whole kidney sections of rats upon treatment with pharmacological doses of cisplatin [25]. The obtained results suggested a correlation of renal damage with platinum accumulation in the cortex and corticomedullarly region. In addition, lower copper and zinc levels were detected in the presence of platinum, indicating possible displacement of these elements in renal cells [25]. Interestingly, the first LA-ICP-MS study on cisplatin-induced renal damage revealed higher platinum accumulation in the medulla compared to the cortex [26]. The reason for the different observations in platinum distribution in the two studies could be related to differences in the *in vivo* setting including the applied doses, routes of administration and the time point of sacrificing. In the first case, mice were sacrificed 3 and 5 days after administration, whereas the second study relied on platinum mapping after only 1 h treatment [25,26]. For the clinically evaluated platinum- and ruthenium-based complexes oxaliplatin, satraplatin and NKP1339, a similar renal metal accumulation pattern as for cisplatin was observed, with elevated metal deposition in the cortex [9,28]. As these complexes have not shown nephrotoxic potential so far, the use of metal accumulation maps as only indicator for possible side effects might be not sufficient [28]. An investigation of the platinum distribution in therapy-affected organs (kidney, cochlea and testis) 1 h and 4 days after cisplatin infusion in mice, revealed a 95 % decrease of platinum levels [27]. Highest platinum accumulation was observed in areas with high blood supply in the outer capsule of the testis and in the bone areas in the cochlea. Regarding ototoxicity as one of the side effects of cisplatin-based chemotherapy, long-time exposure of the inner ear part to high platinum concentrations was related to degradation of sensory cells [27]. In addition, the quantitative platinum and ruthenium distribution was compared in different mice tissues (kidney, liver, muscle and spleen), upon treatment with cisplatin and the investigational ruthenium complex NKP1339 [9].

Two studies aimed to develop appropriate LA-ICP-MS imaging procedures to address tumor response to metal-based anticancer drug treatment [15,28]. In this context, a quantitative LA-ICP-MS approach was validated to study the penetration depth of oxaliplatin into rat tumor tissue of peritoneal carcinosis upon hyperthermic intraperitoneal chemotherapy. Platinum enrichment was observed mainly at the periphery of the tumor sections, which can be attributed to the direct contact with the drug perfusate [15]. In another study, the spatially-resolved platinum accumulation was analyzed by LA-ICP-MS in an *in vivo* preclinical murine tumor model upon treatment with platinum(II)- and platinum(IV)-based complexes [28]. Histologic features were reflected in the obtained platinum distribution maps. Interestingly, higher platinum accumulation was observed in soft tissue, sparsely infiltrated with tumor cells than in parts with densely packed tumor cells [28].

Only few LA-ICP-MS imaging studies so far have concentrated on clinical samples upon platinum-based chemotherapy [29,30]. In detail, patient samples from peritoneal carcinosis treated intraperitoneally with cisplatin or oxaliplatin were investigated by LA-ICP-MS in combination with MALDI-MS, as proof-of-principle study [30]. In another study, the quantitative cisplatin and oxaliplatin extravasation was studied by means of LA-ICP-MS in different tissue types (muscle, nerve tissue, connective tissue and fat tissue) derived from patients [29].

1.4 Recent developments and future trends in LA-ICP-MS bioimaging

In most LA-ICP-MS imaging studies scanning mass analyzers (quadrupole or sector field) are employed, usually recording few isotopes and using ablation parameters that yield spatial resolution in the tens of µm scale [3]. Recent developments aimed to improve lateral resolution without compromising sensitivity and scan time, as well as to achieve parallel detection of trace and major elements [4,31]. In this context, small inner volume laser ablation cells were developed to minimize measurement time and increase signal intensity. The use of small volume cells result in significant reduction of the wash out time and allow employing smaller spot sizes and applying laser impulses more frequently. The lowest dispersion cells for elemental imaging developed so far, deliver signal-pulse-signal duration of 30 ms [32] and 6 ms [33](full width at 1 % maximum). The advances in fast aerosol transport from the laser also require a fast mass analyzer for analyte detection. However, scanning frequencies of most of the sequential instruments (ICP-Q-MS or ICP-SF-MS) are usually not sufficient for detecting the signal of more analytes in short transient signals. In addition, the number of analytes has impact in time resolved analysis mode on the lateral resolution and sensitivity when using scanning mass analyzers. For this purpose, laser ablation hyphenated to ICP-MS with a TOF mass analyzer was introduced [34]. The quasi-simultaneous multielement capability of high mass resolution ICP-TOF-MS has already proven its applicability in the field of single particle analysis [35,36]. Recently, its combination with a high-washout LA cell provided sensitivities for trace and major elements down to a spot size of 1.5 µm [37]. The resulting improvement in lateral resolution was in parallel with fast analysis times, making this technology superior to conventional LA-ICP-MS systems. These developments in laser and ICP-MS technology enabled to scale down the analysis from tissue level to single cells [38]. In this context, biomarkers were detected upon antibody labeling in breast cancer tissue with a spatial resolution of around 1 µm [32]. With the aim to perform single cell analysis, a bioimaging method for gold and silver nanoparticle distribution in individual fibroblast cells was developed, using the high spatial resolution power of LA-ICP-SF-MS [39]. Optimization of ablation parameters (scan speed, ablation frequency, laser energy) yielded spatial resolution, which allowed distinguishing between nanoparticle accumulations in different cell compartments. Quantification was achieved by matrix-matched standards based on nitrocellulose membranes spiked with nanoparticle suspensions [39]. However, in the field of metal-based anticancer drug research, the potential of LA-ICP-MS using recent developments in laser technology is still far from being fully exploited in terms of single cell imaging, high spatial resolution and fast acquisition times.

1.5 Imaging of metal-based drugs at cellular and sub-cellular level

In approaching the in situ localization, speciation and determination of the oxidation state of metal-based anticancer drugs within individual cells and multi-cellular tumor models, powerful analytical techniques are required. It is essential to employ imaging methods, which allow the direct mapping of the sub-cellular distribution of metal-based anticancer drugs, without compromising the cellular morphology [40]. In general, microanalytical methods are used including synchrotron-based X-ray fluorescence microscopy (SXRF, SRIXE, or micro-XRF) and nano-scale secondary-ion mass spectrometry (NanoSIMS) [2,40]. A comparison of the main features of imaging methods including LA-ICP-MS is given in Table 2. Micro-XRF provides lateral resolution of 10-0.1 µm with moderate sensitivity, but requires access to large synchrotrons and particle-accelerator facilities [2]. In comparison to X-ray methods, LA-ICP-MS offers lower detection limits and mapping of a broader range of elements, as well as access to isotopic information [3]. (Nano)SIMS is comparable to LA-ICP-MS as in both cases the sample surface is ablated/sputtered, providing lateral resolution of 10-0.1 µm (standard SIMS) and down to 50 nm (NanoSIMS). However, samples are in contrast to LA-ICP-MS sputtered under high vacuum, requiring vacuum compatible sample preparation [41]. The main common advantage of these imaging techniques is that no drug modification for visualization is required. Thus, no possible alterations of pharmacological properties and biological behavior are caused, as could be the case by e.g. tethering chemical tags (such as fluorophores) to the metal center [42]. In general, the metal imaging methods shown in Table 2 are complementary to each other and their use depends on the application as well as on the desired information.

Table 2. Comparison of different metal imaging techniques [2,3,40,43]. Typical values are given from routine settings, but the parameters can vary depending on the individual application.

	LA-ICP-MS	**SIMS**	**NanoSIMS**	**SXRF**
Application	Metal distribution in tissues	Metal distribution in cells		Oxidation states in cells
Selectivity	Multielemental, isotopic	Multielemental, isotopic		Chemical species
Spatial resolution (µm)	5-50	0.1-10	0.05	0.1-10
Sensitivity (g/g)	10^{-7}-10^{-8}	10^{-7}-10^{-8}	10^{-2}	10^{-5}
Dynamic range	10^{9}	10^{5}	10^{2}	10^{3}
Quantification	(semi-) quantitative imaging	(semi-) quantitative imaging difficult due to matrix-effects		quantitative imaging

1.6 NanoSIMS

In the case of NanoSIMS, a primary ion beam is focused on the sample surface to ionize and sputter analytes, which are then detected by a mass analyzer. The ion yield and sensitivity can vary depending on the analyte, the sample type and the conditions used. The simultaneous multielement imaging capabilities together with the outstanding spatial resolution power (up to 50 nm) renders NanoSIMS an invaluable tool to gain insights into the mode of action of metal-based drugs and to reveal possible targets in cellular compartments [40,44]. Due to the high vacuum requirements of SIMS analysis, live cells can not be imaged and the sample preparation has to be adapted accordingly. During sample preparation process, both the structural as well as chemical integrity of cells has to be preserved and the occurrence of artifacts such as the loss or redistribution of analytes has to be avoided [39]. Sample preparation methods proposed in literature include chemical fixation followed by resin embedding, cryo-fixation and freeze substitution followed by resin embedding [41]. The latter one has been proven to be applicable for drug distribution studies in conventional cell culture systems, but due to the exposure to the substitute liquids, washout effects are likely to occur. Freeze drying might keep the chemical integrity, but resin embedding is not possible, as well as pre-characterization with other imaging techniques such as TEM (Tansmission electron microscopy) [41].

The successful mapping of platinum in eukaryotic cells by NanoSIMS opened the way for subcellular tracking of platinum-based anticancer drugs [45]. In this context, the intracellular fate of a ^{15}N labeled polynuclear platinum compound and cisplatin was studied by visualizing both the metal center, as well as isotopically labeled ligands [46,47]. In the case of cisplatin, co-localization of platinum was detected with sulfur-rich structures in nucleus and cytoplasm and with phosphor-rich chromatin regions in human colon cancer cells. These observations are consistent with the general high affinity of cisplatin to sulfur donors and its cellular target DNA [47].

1.7 X-ray-based imaging techniques

Each element has a unique fluorescence, a feature, which is used in SXRF microscopy, where an X-ray beam excites the inner shell electrons to generate measurable fluorescence. The technique provides qualitative and quantitative information on the topography, concentration and oxidative state of metal cations [40]. In particular, X-ray absorption near edge spectroscopy (XANES) has become of interest to simultaneously monitor Pt species in biological systems [48]. It was successfully shown, that Pt(II) and Pt(IV) complexes can be differentiated based on the height of their edges and their proportions can be determined using the peak-height ratio of XANES spectra [48]. Despite the prevalent consensus that kinetically inert Pt(IV) complexes are reduced to their active Pt(II) analogues in the hypoxic tumor environment, a comprehensive understanding of their cellular processing still remains elusive [49]. The application of XANES enabled following the reduction of platinum(IV) prodrugs of cisplatin and transplatin in human ovarian cancer cells. The extent of intracellular reduction was found to correlate directly with the reduction potentials and cytotoxicity [50]. Another study, using the combination of SRIXE and µXANES measurements revealed the presence of both, Pt(II) and Pt(IV) species in human ovarian cancer cells [51]. These results indicate that platinum(IV) complexes can enter tumor cells in their intact form. In addition, platinum was found to be localized mainly in the nucleus and to lesser extent in the surrounding cytoplasm of cisplatin- and platinum(IV)-treated ovarian carcinoma cells [51,52]. Keppler et al. investigated the Ru complex KP1019 using XANES in different model systems, as well as *in vivo* [53]. Microprobe X-ray fluorescence of tumor thin sections showed deep penetration of Ru into malignant tissue. Highest concentrations were observed near blood vessels and in the edge regions of the tissue samples [53].

Information on cell uptake and cellular trafficking of metal-based drugs is usually derived from *in vitro* studies in monolayer cell cultures that are generally exposed to uniform conditions and concentrations of drugs [42]. Tumor microenvironment, in contrast is complex and suspected to large concentration gradients of the drug. In order to mimic solid tumors without using animal experiments, multicellular spheroids (3D spherical aggregates of tumor cells) have been evaluated in literature [54]. X-ray fluorescence microtomography was used to investigate the penetration of cisplatin and platinum(IV) complexes in DLD-1 human colon carcinoma spheroids. Elevated platinum levels were observed in the exterior regions, whereas the core exhibited a uniform platinum distribution [55].

2 Elemental speciation analysis in metal-based anticancer drug research

In early stages of preclinical metal-based anticancer drug development, the thorough understanding of the *in vitro* and *in vivo* drug's behaviour (e.g. in terms of interactions with other molecules, hydrolysis and metabolism), is of significant importance to select an effective and selective lead compound [56-60].Elemental speciation analysis involves the versatile combination of inorganic mass spectrometry with separation techniques enabling the quantification of intact drugs and their reactions products on the basis of a metal signal (e.g. Pt or Ru), without the need for species specific standards. In the following section, the state of the art in elemental speciation analysis addressing complementary inorganic and organic mass spectrometry for studying metallodrugs is discussed. The most important achievements regarding analytical method development are summarized considering the last five years. As the methodological platforms of elemental speciation analysis are still a matter of research, development and applications of elemental speciation analysis of clinically established and candidate drugs are considered. The period before 2010 is comprehensively reviewed elsewhere [58,61-64].

2.1 Elemental speciation analysis regarding clinically established metallodrugs

2.1.1 Metallodrug-protein interactions

The role of proteins in the mode of action of anticancer metallodrugs is an ongoing matter of debate [61,65-67]. Most of the metal-based anticancer drugs applied in clinics or tested in clinical trials are administered intravenously and are therefore immediately subjected to reactive plasma constituents. Metallodrug-protein interactions can have significant impact on drug deactivation, the toxic profile of a drug, drug delivery to the tumor tissue, as well as on drug uptake into tumor cells. Accordingly, metal adduct formations with serum proteins have been extensively studied in literature employing different bioanalytical approaches [58,64,67]. A general overview of analytical figures of merit of the different applied analytical techniques [68-82] is given in Table 3. The use of inorganic mass spectrometry requires powerful on-line separation of proteins prior to detection. In most studies, the interaction of the metallodrug with the two transporter proteins human serum albumin (HSA) and transferrin (Tf) is addressed [83,84]. Taking into account their molecular weights (80 kDa and 70 kDa, respectively) HSA and Tf cannot be separated by the application of size exclusion chromatography (SEC) only [84]. Liquid chromatography (LC) separation of the two serum proteins is challenging, while capillary electrophoresis (CE) separations showed to be superior in terms of separation power. However, the combination of capillary electrophoresis with ICP-MS (CE-ICP-MS) falls short regarding sensitivity and robustness [58,61,62,64].

A recent study reported the use of monolithic discs combined with ICP-MS detection for studying cisplatin, carboplatin and oxaliplatin upon incubation in human serum [70]. Monoliths are functionally different from porous particle-based columns making the chromatographic resolution nearly independent from the flow rate. In addition, the reduced void volume facilitates the mass transfer between the mobile and stationary phase [85]. As a major advantage, the technique concedes the combination of different chromatographic separations in a single chromatographic run [70,85]. Martinčič et al. combined affinity and anion exchange chromatography in series with a column recovery of 95 %. In the first separation step immunoglobulins were retained, whereas in the second step free Pt, Pt-HSA and Pt-Tf adducts were separated. Species-unspecific isotope dilution was accomplished by post-column addition of a ^{194}Pt spike [70]. The presented chromatographic separation scheme was straightforward and hence easier to accomplish than previously published on-line 2D heart cutting chromatography [83]. In the latter approach, size exclusion chromatography (SEC) followed by ion exchange (IE) was combined with ICP-MS detection (SEC-IE-ICP-MS) for separation of albumin and transferrin in serum samples [83]. In another related study, monolithic columns have been implemented as second separation dimension in an on-line two dimensional LC X LC separation scheme [71]. Each fraction separated by conventional size exclusion chromatography was separated by anion exchange based on two parallel monolith discs. The parallel columns in the second dimension allowed a reduced separation time, while the first monolithic disc was loaded, the second one was used for IC-ICP-MS analysis. The developed method was used to study the interaction of cisplatin with serum proteins by measuring metal to sulfur ratios. The dual monolithic column method showed a higher throughput than SEC-IE-ICP-MS [71].

In the last five years, the extent of CE applications in serum samples (either *ex vivo* incubations or *in vivo* studies) has decreased. Nguyen et al. developed a CE-ICP-MS method addressing novel liposomal Pt drug formulations[72,73]. Free cisplatin, liposome-encapsulated cisplatin and cisplatin bound to human plasma proteins was separated by CE-ICP-MS with an LOD of around 40 ng/mL for Pt. Platinum to phosphorus ratio determination allowed to address the stability of the liposomal drug formulation in plasma [86]. The same authors accomplished complementary analysis of liposomal drug formulations using SEC-ICP-MS [78].

2.1.2 Methods for DNA-adduct studies

DNA is the primary target of the clinically established Pt-based anticancer drugs [56,77]. Hence, the development of elemental speciation methods for studying this type of interaction has always been a topical research theme [87-89]. Recently, Sar et al. reviewed this topic comprehensively in the case of cisplatin DNA adduct formation comparing different quantitative methods suitable for *in vivo* studies using animal models [90]. The same group investigated cisplatin-DNA adducts formation *in vivo* using Drosophila melanogaster as model. The authors developed a capillary LC-ICP-MS method and used species unspecific isotope dilution analysis for accurate quantification [91]. Different repair conditions were addressed by combining elemental speciation analysis with biochemical assays such as the Comet and SMART assay [68]. Employing this approach, complementary information was obtained on DNA strand-breaks and *in vivo* mutagenic activity of chemicals to the quantitative data on adducts formation. In addition, the adduct formation was studied by LC coupled to electrospray ionization mass spectrometry (LC-ESI-MS) [68].

Zayed et al. investigated oxaliplatin adducts with DNA nucleotides *in vitro* with A and G mono-nucleotides, GG and AG di-nucleotides [69]. The method was subsequently applied to human colorectal cancer lines. The importance of sensitivity and linear dynamic range of analysis was emphasized in this work. The application of sector field ICP-MS (ICP-SFMS) was crucial for studying cell models. The work also exemplifies the complementarity of ESI-MS and ICP-MS for studying DNA adducts by ESI-MS and ICP-MS. The developed chromatographic separations was based on polar-reversed phase columns (RP-columns) and hence compatible with both MS platforms [69].

2.1.3 Quantification of drugs and their hydrolysis products

Interestingly, elemental speciation analysis traditionally focused on environmental samples regarding the quantification of intact drugs and their hydrolysis products [92-94]. More recently, cisplatin hydrolysis was investigated in hospital wastewaters by hydrophilic interaction liquid chromatography (HILIC) hyphenated to ICP-MS [74]. N-propanol was used as HILIC eluent to tackle the inherently poor compatibility of HILIC with ICP-MS compatibility. Species-unspecific IDA using post-column addition of a ^{194}Pt spike was used for quantification. The obtained LODs are excellent (especially considering that HILIC-ICP-MS was employed) with LOD of 0.0273 ng/mL Pt and 0.1726 ng/mL Pt for monoaqua hydroxyl cisplatin and cisplatin, respectively [74].

Ultrafast LC-ICP-MS has been developed for studying oxaliplatin in human urine. The method implemented an RP- column with a silica-based stationary phase based on sub-2-µm particle size [75]. Excellent LODs were obtained; i.e. 0.05 µg/L for oxaliplatin. The analytical cycle time was lower than 1 min [75].

Falta et al. studied the quantification of intact cisplatin in cancer cell models by LC-ICP-MS and species specific IDMS [76]. For cross validation two different separations were combined, based on porous graphitized carbon and a pentafluorophenyl phase, followed by ICP-MS detection. Proteins were removed from lysed cancer cells using centrifugal ultrafiltration. As a major breakthrough, intact cisplatin could be quantified addressing preclinically relevant drug concentration levels (i.e. drug incubation for several hours at low µM concentrations) [76]. The method was successfully applied in a metallomic study regarding the dynamics of cisplatin accumulation and distribution in cancer cell models [77]. The binding of cisplatin to low molecular weight proteins was indirectly quantified by relating the intact cisplatin concentration (LC-ICP-MS) to the total Pt concentration (FI-ICP-MS) assessed in the cancer cell cytosol after protein removal. The difference in cytosolic Pt content before and after ultrafiltration gave the amount of drug–protein binding [77].

2.2 Elemental speciation analysis regarding metal-based anticancer drug candidates

Approaches to overcome the major drawbacks associated with Pt(II)-based chemotherapy focused on the development of kinetically inert Pt(IV)-based prodrugs, as well as Ru-based compounds.[79,95-98] Recently, Keppler et al. introduced maleimide-functionalised Pt(IV) complexes targeted to bind to human serum albumin and thus to enhance selective accumulation in tumor tissue [99]. SEC-ICP-MS was employed to monitor the Pt and S trace simultaneously upon incubation of the complexes in calf serum, proving significant and rapid binding to the fraction containing HSA [99].

Aleksenko et al. studied indazolium trans-[tetrachloridobis(1H-indazole)ruthenate(III)] (KP1019), a HSA [79]. Bytzek et al. investigated the sodium salt of the Ru drug (KP1339) in an animal model using CE-ICP-MS and SEC-IC-ICP-MS for cross validation. Again the interaction of the drug with HSA and transferrin was addressed [80]. In addition, two other Ru compounds were studied by the previously described monolithic column approach upon incubation in serum [81].

Dyson et al. studied RAPTA-T, an organometallic ruthenium (II)-arene complex using elemental speciation analysis as assisting approach for proteomics [82]. Multidimensional protein identification technology (MudPIT) was implemented as proteomics measurement platform [100]. In the past, the use of biphasic chromatographic columns showed to be beneficial for studying metallodrug-protein adducts. The first application of MudPIT concerned a study on cisplatin-HSA adduct formation [101]. Wolters et al. combined SEC-ICP-MS determination with proteomics addressing cancer cell models. SEC-ICP-MS of different cellular fractions revealed the fractions with the highest abundance of metals. Subsequently, MudPIT analysis revealed several hundred interesting protein targets in the relevant fractions [82].

Table 3. Figures of merit in speciation analysis carried out in the last five years with different mass spectrometry techniques and different separation tools

Reference	**Compound**	**Sample**	**Method**	**Figures of Merit**
[68]	Cisplatin	In vivo studies in Drosophila melanogaster	LC-ICP-MS, IDA, Comet assay, SMART assay	Analysis of DNA-adducts. Quantification by species-unspecific IDA. Digestion Recovery: 85 ± 10%. LOD: 0.5 pmol for GG-cisplatin. Precision: 6-12%. Column: Agilent Zorbax XDB-C18 narrow-bore. Column Recovery: 68%.
[69]	Oxaliplatin	Human colorectal cancer cells. In vitro studies.	LC-ESI-MS, LC-SF-ICP-MS, UV detection.	Analysis of DNA-adducts. Columns: Waters Xterra C_{18} and C_8 and Phenomenex. Synergi ether linked phenyl bonded silica. LOD: 0.14 ppb Pt.
[70]	Cisplatin, oxaliplatin, carboplatin	Human serum incubations.	Monolithic discs affinity-anion exchange ICP-MS. UV detection.	Analysis of protein-adducts. Quantification by species unspecific IDA on-line. Column: CIM Protein G and CIM DEAE disks. Recovery of the column: 95%. Repeatability: 3%. Highest LOD: 0.710 ng mL^{-1} of Pt in for Pt-HSA. Lowest LOD: 0.195 ng mL^{-1} of Pt fo unbound Pt.
[71]	Cisplatin	Ex vivo incubations (protein standards in physiological buffers).	SEC-IC-ICP-MS	Analysis of protein adducts. Columns: BioSuite 125 4 µm UHR SEC column and CIM mini DEAE disks. LOD: 8 pmol based on SO measurement Column Recovery: >95%. Number of theoretical plates (Tf/Alb): 450/1080.
[72]	Oxaliplatin, (in liposomes).	Liposome samples.	CE-ICP-MS	Analysis of liposome formulations. Precision: 2.9%. LOD: 29 ng mL^{-1} Pt. Recovery: 100%.
[73]	Cisplatin (in liposomes)	Liposomes samples in Human Plasma. In vitro study.	CE-ICP-MS	Analysis of liposome formulations and protein-adducts. LOD: 41 ng mL^{-1} Pt (in 20% v/v of plasma). Precision: 2.1% (in 20% v/v of plasma). Recovery: 100% (in 20% v/v of plasma).

Table 3. Figures of merit in speciation analysis carried out in the last five years with different mass spectrometry techniques and different separation tools

Reference	**Compound**	**Sample**	**Method**	**Figures of Merit**
[74]	Cisplatin	Water	LC-ICP-MS	Analysis of hydrolysis products. Quantification by species-unspecific IDA on-line. Lowest LOD and LOQ: 0.0273 ng Pt/mL and 0.0909 ng Pt/mL for monoaquahydroxycisplatin. Highest LOD and LOQ: 0.1726 ng Pt/mL and 0.5753 ng Pt/mL for cisplatin. Column: HILIC. Column Recovery: 96% for cisplatin and 99% for monoaquacisplatin. Repeatability: <2.3%.
[75]	Oxaliplatin	Patient Urine	Ultra-fast HPLC-ICP-MS	Analysis of hydrolysis products. Column: zorbax stable bond c18, particle size 1.8 µm. LOD: 0.05 µg L^{-1} oxaliplatin. LOQ: 0.17 µg L^{-1} oxaliplatin. Repeatability retention time: 0.24%. Repeatability peak area: 2.2%. Column Recovery: 101.7±2.2%. Peak asymmetry: 1.01. Capacity factor k': 3.9.
[76]	Cisplatin	Cancer cell	LC-ICP-MS	Analysis of adduct formation with small molecular weight proteins. Column: Discovery HSF5 and Hypercarb. LOD for Pt: 0.013 µg L^{-1} with Discovery HSF5 and 0.11 µg L^{-1} with hypercarb. Recovery Hypercarb: 11% for total cytosolic Pt species and 92.4 ± 4.6% for cisplatin standard. Recovery Discovery HSF5: >50% for total cytosolic Pt species and 100.2±1.4% for cisplatin standard. Quantification by species- specific IDA and comparison to external calibration.
[77]	Cisplatin	Cancer Cells	LC-ICP-QMS, (FI)-ICP-MS, ICP-SFMS	Analysis of adduct formation with small molecular weight proteins. LOD in LC-ICP-QMS: 60 ng L^{-1} Pt.. Repeatability in LC-ICP-QMS: 5%. LOD in ICP-SFMS: 0.007 µg L^{-1} Pt. Column: Discovery HSF5. Column Recovery: >50% for total cytosolic Pt species. 100.2±1.4% for cisplatin standard.

Table 3. Figures of merit in speciation analysis carried out in the last five years with different mass spectrometry techniques and different separation tools

Reference	**Compound**	**Sample**	**Method**	**Figures of Merit**
[78]	Oxaliplatin (in liposomes)	Liposome samples.	SEC-DRC-ICP-MS	Analysis of liposomes formulations. Column: Shodex Asahipak GS-520 HQ 7.5x 300 mm, 7 µm particle size, maximum pore size of 2000 Å. Repeatability: 2.9%. LOD: 0.3 ng mL^{-1} P and 0.05 ng mL^{-1} Pt.
[79]	Ru-based drug KP1019	In vitro studies in intracellular conditions.	CE-ICP-MS	Analysis of protein-adducts LOD: $1x10^{-7}$ M Fe.
[80]	Ru-based drug NKP-1339	In vivo mouse plasma.	CZE-ICP-MS, SEC-IC-ICP-MS	Analysis of protein-adducts. LOD in SEC-IC-ICP-MS: 4.5 µM and 0.05 µM for SO signal and Ru respectively. LOD in CZE-ICP-MS: 29.7 µM and 0.35 µM for HSA and Ru respectively. Column recovery: 70% for Ru.
[81]	Ru-based drug KP418	In vitro study in Human Serum	Monolithic discs affinity-anion exchange ICP-MS. UV detection	Analysis of protein-adducts. Quantification by species unspecific IDA on-line. Column: CIM Protein G and CIM DEAE disks. Highest LOD and LOQ: 0.027 µg mL^{-1} and 0.090 µg mL^{-1} respectively for unbound Ru. Lowest LOD and LOQ: 0.0041 µg mL^{-1} and 0.0137 µg mL^{-1} respectively for Ru bound to IgG. RSD: 3.5%. Recovery column: 97±2%.
[82]	Ru-based drug RAPTA-T	Human cancer cells. In vitro study.	SEC-ICP-MS, MudPIT	Analysis of protein-adducts. LOQ: 3.8 µg L^{-1} of Ru in SEC-ICP-MS. SEC-Column: GE Superdex 200 10/300 GL.

References

1 J. Sabine Becker, *J Mass Spectrom*, 2013, **48**, 255-268.

2 C. J. Fahrni, *Curr Opin Chem Biol*, 2007, **11**, 121-127.

3 J. S. Becker, M. Zoriy, A. Matusch, B. Wu, D. Salber, C. Palm and J. S. Becker, *Mass Spectrom Rev*, 2010, **29**, 156-175.

4 J. S. Becker, A. Matusch and B. Wu, *Anal Chim Acta*, 2014, **835**, 1-18.

5 D. Pozebon, G. L. Scheffler, V. L. Dressler and M. A. G. Nunes, *J Anal At Spectrom*, 2014, **29**, 2204-2228.

6 V. Trunova, A. Sidorina, V. Zvereva and B. Churin, *J Trace Elem Med Biol*, 2013, **27**, 76-77.

7 D. Hare, C. Austin and P. Doble, *Analyst*, 2012, **137**, 1527-1537.

8 I. Konz, B. Fernández, M. Fernández, R. Pereiro and A. Sanz-Medel, *Anal. Bioanal. Chem.*, 2012, **403**, 2113-2125.

9 A. E. Egger, S. Theiner, C. Kornauth, P. Heffeter, W. Berger, B. K. Keppler and C. Hartinger, *Metallomics*, 2014, **6**, 1616-1625.

10 A. Matusch, C. Depboylu, C. Palm, B. Wu, G. U. Höglinger, M. K. H. Schäfer and J. S. Becker, *J. Am. Mass Spectrom.*, 2010, **21**, 161-171.

11 J. A. T. Pugh, A. G. Cox, C. W. McLeod, J. Bunch, B. Whitby, B. Gordon, T. Kalber and E. White, *J. Anal. At. Spectrom.*, 2011, **26**, 1667-1673.

12 D. Hare, B. Reedy, R. Grimm, S. Wilkins, I. Volitakis, J. L. George, R. A. Cherny, A. I. Bush, D. I. Finkelstein and P. Doble, *Metallomics*, 2009, **1**, 53-58.

13 C. Austin, D. Hare, T. Rawling, A. M. McDonagh and P. Doble, *J Anal At Spectrom*, 2010, **25**, 722-725.

14 A. Izmer, D. Gholap, K. De Houwer, F. Cuyckens and F. Vanhaecke, *J Anal At Spectrom*, 2012, **27**, 413-418.

15 D. Gholap, J. Verhulst, W. Ceelen and F. Vanhaecke, *Anal. Bioanal. Chem.*, 2012, **402**, 2121-2129.

16 D. Pozebon, V. L. Dressler, M. F. Mesko, A. Matusch and J. S. Becker, *J. Anal. At. Spectrom.*, 2010, **25**, 1739-1744.

17 J. S. Becker, M. V. Zoriy, C. Pickhardt, N. Palomero-Gallagher and K. Zilles, *Anal Chem*, 2005, **77**, 3208-3216.

18 M.-M. Pornwilard, R. Weiskirchen, N. Gassler, A. K. Bosserhoff and S. J. Becker, *PLoS One*, 2013, **8**, e58702.

19 C. Austin, F. Fryer, J. Lear, D. Bishop, D. Hare, T. Rawling, L. Kirkup, A. McDonagh and P. Doble, *J Anal At Spectrom*, 2011, **26**, 1494-1501.

20 I. Konz, B. Fernández, M. L. Fernández, R. Pereiro, H. González, L. Álvarez, M. Coca-Prados and A. Sanz-Medel, *Anal Bioanal Chem*, 2013, **405**, 3091-3096.

21 M. Bonta, H. Lohninger, M. Marchetti-Deschmann and A. Limbeck, *Analyst*, 2014, **139**, 1521-1531.

22 C. Giesen, L. Waentig, T. Mairinger, D. Drescher, J. Kneipp, P. H. Roos, U. Panne and N. Jakubowski, *J Anal At Spectrom*, 2011, **26**, 2160-2165.

23 C. S. Allardyce, P. J. Dyson, F. R. Abou-Shakra, H. Birtwistle and J. Coffey, *Chem Comm*, 2001, 2708-2709.

24 I. Khalaila, A. Bergamo, F. Bussy, G. Sava and P. J. Dyson, *Int. J. Oncol.*, 2006, **29**, 261-268.

25 E. Moreno-Gordaliza, C. Giesen, A. Lázaro, D. Esteban-Fernández, B. Humanes, B. Cañas, U. Panne, A. Tejedor, N. Jakubowski and M. M. Gómez-Gómez, *Anal. Chem.*, 2011, **83**, 7933-7940.

26 M. Zoriy, A. Matusch, T. Spruss and J. S. Becker, *Int. J. Mass Spectrom.*, 2007, **260**, 102-106.

27 O. Reifschneider, C. A. Wehe, I. Raj, j. Ehmcke, G. Ciarimboli, M. Sperling and U. Karst, *Metallomics*, 2013, **5**, 1440-1447.

28 S. Theiner, C. Kornauth, H. P. Varbanov, M. Galanski, S. Van Schoonhoven, P. Heffeter, W. Berger, A. E. Egger and B. K. Keppler, *Metallomics*, 2015, **7**, 1256-1264.

29 A. E. Egger, C. Kornauth, W. Haslik, S. Hann, S. Theiner, G. Bayer, C. G. Hartinger, B. K. Keppler, U. Pluschnig and R. M. Mader, *Metallomics*, 2015, **7**, 508-515.

30 J. Bianga, A. Bouslimani, N. Bec, F. Quenet, S. Mounicou, J. Szpunar, B. Bouyssiere, R. Lobinski and C. Larroque, *Metallomics*, 2014, **6**, 1382-1386.

31 M. Tanner and D. Günther, *Anal Chim Acta*, 2009, **633**, 19-28.

32 H. A. O. Wang, D. Grolimund, C. Giesen, C. N. Borca, J. R. H. Shaw-Stewart, B. Bodenmiller and D. Günther, *Anal Chem*, 2013, **85**, 10107-10116.

33 S. J. M. Van Malderen, J. T. van Elteren and F. Vanhaecke, *J Anal At Spectrom*, 2015, **30**, 119-125.

34 M. Tanner and D. Günther, *Anal Bioanal Chem*, 2008, **391**, 1211-1220.

35 O. Borovinskaya, S. Gschwind, B. Hattendorf, M. Tanner and D. Günther, *Anal Chem*, 2014, **86**, 8142-8148.

36 O. Borovinskaya, B. Hattendorf, M. Tanner, S. Gschwind and D. Gunther, *J Anal At Spectrom*, 2013, **28**, 226-233.

37 A. Gundlach-Graham, M. Burger, S. Allner, G. Schwarz, H. A. O. Wang, L. Gyr, D. Grolimund, B. Hattendorf and D. Günther, *Anal Chem*, 2015.

38 L. Mueller, H. Traub, N. Jakubowski, D. Drescher, V. Baranov and J. Kneipp, *Anal Bioanal Chem*, 2014, **406**, 6963-6977.

39 D. Drescher, C. Giesen, H. Traub, U. Panne, J. Kneipp and N. Jakubowski, *Anal. Chem.*, 2012, **84**, 9684-9688.

40 L. Wedlock and S. J. Berners-Price, *Austral J Chem*, 2011, **64**, 692-704.

41 C. R. M. Grovenor, K. E. Smart, M. Kilburn, J. R. Dilworth, B. Martin, C. Hawes and R. E. M. Rickaby, *Appl Surf Sci*, 2006, **252**, 6917-6924.

42 A. V. Klein and T. W. Hambley, *Chem Rev*, 2009, **109**, 4911-4920.

43 Z. Qin, J. A. Caruso, B. Lai, A. Matusch and J. S. Becker, *Metallomics*, 2011, **3**, 28-37.

44 P. Hoppe, S. Cohen and A. Meibom, *Geostand Geoanal Res*, 2013, **37**, 111-154.

45 N. Usami, Y. Furusawa, K. Kobayashi, S. Lacombe, A. Reynaud-Angelin, E. Sage, T.-D. Wu, A. Croisy, J.-L. Guerquin-Kern and C. Le Sech, *Int J Radiat Biol*, 2008, **84**, 603-611.

46 L. E. Wedlock, M. R. Kilburn, R. Liu, J. A. Shaw, S. J. Berners-Price and N. P. Farrell, *Chem Comm*, 2013, **49**, 6944-6946.

47 A. A. Legin, A. Schintlmeister, M. A. Jakupec, M. Galanski, I. Lichtscheidl, M. Wagner and B. K. Keppler, *Chem Sci*, 2014, **5**, 3135-3143.

48 M. D. Hall, G. J. Foran, M. Zhang, P. J. Beale and T. W. Hambley, *J Am Chem Soc*, 2003, **125**, 7524-7525.

49 E. Wexselblatt and D. Gibson, *J. Inorg. Biochem.*, 2012, **117**, 220-229.

50 M. D. Hall, H. L. Daly, J. Z. Zhang, M. Zhang, R. A. Alderden, D. Pursche, G. J. Foran and T. W. Hambley, *Metallomics*, 2012, **4**, 568-575.

51 M. Hall, C. Dillon, M. Zhang, P. Beale, Z. Cai, B. Lai, A. J. Stampfl and T. Hambley, *J Biol Inorg Chem*, 2003, **8**, 726-732.

52 M. D. Hall, R. A. Alderden, M. Zhang, P. J. Beale, Z. Cai, B. Lai, A. P. J. Stampfl and T. W. Hambley, *J Struct Biol*, 2006, **155**, 38-44.

53 A. A. Hummer, P. Heffeter, W. Berger, M. Filipits, D. Batchelor, G. E. Büchel, M. A. Jakupec, B. K. Keppler and A. Rompel, *J Med Chem*, 2013, **56**, 1182-1196.

54 G. Mehta, A. Y. Hsiao, M. Ingram, G. D. Luker and S. Takayama, *J. Control. Rel.*, 2012, **164**, 192-204.

55 R. A. Alderden, H. R. Mellor, S. Modok, M. D. Hall, S. R. Sutton, M. G. Newville, R. Callaghan and T. W. Hambley, *J. Am. Chem. Soc.*, 2007, **129**, 13400-13401.

56 L. R. Kelland, *Nat. Rev. Cancer*, 2007, **7**, 573-584.

57 M. Galanski, V. B. Arion, M. A. Jakupec and B. K. Keppler, *Curr. Pharm. Des.*, 2003, **9**, 2078-2089.

58 A. R. Timerbaev, *J Anal At Spectrom*, 2014, **29**, 1058-1072.

59 K. D. Mjos and C. Orvig, *Chemical Reviews*, 2014, **114**, 4540-4563.

60 E. E. M. Brouwers, M. Tibben, H. Rosing, J. H. M. Schellen and J. H. Beijnen, *Mass Spectrom. Rev.*, 2008, **27**, 67-100.
61 B. Meermann and M. Sperling, *Anal Bioanal Chem*, 2012, **403**, 1501-1522.
62 A. R. Timerbaev, K. Pawlak, S. S. Aleksenko, L. S. Foteeva, M. Matczuk and M. Jarosz, *Talanta*, 2012, **102**, 164-170.
63 C. G. Vogiatzis and G. A. Zachariadis, *Anal Chim Acta*, 2014, **819**, 1-14.
64 M. Groessl and C. Hartinger, *Anal Bioanal Chem*, 2013, **405**, 1791-1808.
65 T. T. Morris, Y. Ruan, V. A. Lewis, A. Narendran and J. Gailer, *Metallomics*, 2014, **6**, 2034-2041.
66 C. Moller, H. S. Tastesen, B. Gammelgaard, I. H. Lambert and S. Sturup, *Metallomics*, 2010, **2**, 811-818.
67 C. Brauckmann, C. Wehe, M. Kieshauer, C. Lanvers-Kaminsky, M. Sperling and U. Karst, *Anal Bioanal Chem*, 2012, 1-10.
68 G. D. Sar, L. Aguado, M. Montes Bayón, M. A. Comendador, E. Blanco González, A. Sanz-Medel and L. M. Sierra, *Mutat Res Toxicol Environ*, 2012, **741**, 81-88.
69 A. Zayed, G. D. D. Jones, H. J. Reid, T. Shoeib, S. E. Taylor, A. L. Thomas, J. P. Wood and B. L. Sharp, *Metallomics*, 2011, **3**, 991-1000.
70 A. Martinčič, M. Cemazar, G. Sersa, V. Kovač, R. Milačič and J. Ščančar, *Talanta*, 2013, **116**, 141-148.
71 S. Hann, T. Falta, K. Boeck, M. Sulyok and G. Koellensperger, *J Anal At Spectrom*, 2010, **25**, 861-866.
72 T. T. N. Nguyen, J. Østergaard, S. Stürup and B. Gammelgaard, *Anal Bioanal Chem*, 2012, **402**, 2131-2139.
73 T. T. N. Nguyen, J. Østergaard, S. Stürup and B. Gammelgaard, *Anal Bioanal Chem*, 2013, **405**, 1845-1854.
74 J. Vidmar, A. Martinčič, R. Milačič and J. Ščančar, *Talanta*, 2015, **138**, 1-7.
75 G. Koellensperger and S. Hann, *Anal Bioanal Chem*, 2010, **397**, 401-406.
76 T. Falta, P. Heffeter, A. Mohamed, W. Berger, S. Hann and G. Koellensperger, *J Anal At Spectrom*, 2011, **26**, 109-115.
77 G. Hermann, P. Heffeter, T. Falta, W. Berger, S. Hann and G. Koellensperger, *Metallomics*, 2013, **5**, 636-647.
78 T. T. T. N. Nguyen, S. Sturup, J. Ostergaard, U. Franzen and B. Gammelgaard, *J Anal At Spectrom*, 2011, **26**, 1466-1473.
79 S. S. Aleksenko, M. Matczuk, X. Lu, L. S. Foteeva, K. Pawlak, A. R. Timerbaev and M. Jarosz, *Metallomics*, 2013, **5**, 955-963.
80 A. K. Bytzek, K. Boeck, G. Hermann, S. Hann, B. K. Keppler, C. G. Hartinger and G. Koellensperger, *Metallomics*, 2011, **3**, 1049-1055.
81 A. Martinčič, R. Milačič, J. Vidmar, I. Turel, B. K. Keppler and J. Ščančar, *J Chromatogr A*, 2014, **1371**, 168-176.
82 D. A. Wolters, M. Stefanopoulou, P. J. Dyson and M. Groessl, *Metallomics*, 2012, **4**, 1185-1196.
83 M. Sulyok, S. Hann, C. G. Hartinger, B. K. Keppler, G. Stingeder and G. Koellensperger, *J Anal At Spectrom*, 2005, **20**, 856-863.
84 M. Groessl, M. Terenghi, A. Casini, L. Elviri, R. Lobinski and P. J. Dyson, *J. Anal. At. Spectrom.*, 2010, **25**, 305-313.
85 E. G. Vlakh and T. B. Tennikova, *J Chromatograph A*, 2009, **1216**, 2637-2650.
86 T. T. T. N. Nguyen, J. Østergaard, S. Stürup and B. Gammelgaard, *Int J Pharm*, 2013, **449**, 95-102.
87 P. B. Farmer, K. Brown, E. Tompkins, V. L. Emms, D. J. L. Jones, R. Singh and D. H. Phillips, *Toxicol Appl Pharm*, 2005, **207**, 293-301.
88 B. Liedert, D. Pluim, J. Schellens and J. Thomale, *Nucleic Acids Research*, 2006, **34**, e47-e47.

89 F. J. P. Hoebers, D. Pluim, A. A. M. Hart, M. Verheij, A. J. M. Balm, G. Fons, C. R. N. Rasch, J. H. M. Schellens, L. J. A. Stalpers, H. Bartelink and A. C. Begg, *Cancer Chemother Pharmacol*, 2008, **61**, 1075-1081.

90 D. G. Sar, M. Montes-Bayón, E. Blanco-González and A. Sanz-Medel, *Trends in Analytical Chemistry*, 2010, **29**, 1390–1398.

91 G. D. Sar, M. Montes-Bayón, E. Blanco González, L. M. Sierra, L. Aguado, M. A. Comendador, G. Koellensperger, S. Hann and A. Sanz-Medel, *Anal. Chem.*, 2009, **81**, 9553-9560.

92 S. Hann, G. Koellensperger, Z. Stefanka, G. Stingeder, M. Furhacker, W. Buchberger and R. M. Mader, *J Anal Atom Spectrom*, 2003, **18**, 1391-1395.

93 S. Hann, Z. Stefánka, K. Lenz and G. Stingeder, *Anal Bioanal Chem*, 2005, **381**, 405-412.

94 K. Lenz, G. Koellensperger, S. Hann, N. Weissenbacher, S. N. Mahnik and M. Fuerhacker, *Chemosphere*, 2007, **69**, 1765-1774.

95 R. Trondl, P. Heffeter, C. R. Kowol, M. A. Jakupec, W. Berger and B. K. Keppler, *Chemical Science*, 2014, **5**, 2925-2932.

96 V. Novohradsky, L. Zerzankova, J. Stepankova, O. Vrana, R. Raveendran, D. Gibson, J. Kasparkova and V. Brabec, *J Inorg Biochem*, 2014, **140**, 72-79.

97 P. Heffeter, K. Böck, B. Atil, M. Reza Hoda, W. Körner, C. Bartel, U. Jungwirth, B. Keppler, M. Micksche, W. Berger and G. Koellensperger, *J Biol Inorg Chem*, 2010, **15**, 737-748.

98 P. J. Dyson and G. Sava, *Dalton Trans.*, 2006, 1929-1933.

99 V. Pichler, J. Mayr, P. Heffeter, O. Domotor, E. A. Enyedy, G. Hermann, D. Groza, G. Kollensperger, M. Galanksi, W. Berger, B. K. Keppler and C. R. Kowol, *Chem Comm*, 2013, **49**, 2249-2251.

100 B. Fränzel and D. A. Wolters, *Proteomics*, 2011, **11**, 3651-3656.

101 J. Will, D. A. Wolters and W. S. Sheldrick, *ChemMedChem*, 2008, **3**, 1696-1707.

III. CONCLUSIONS AND OUTLOOK

The murine colon cancer CT-26 model was used to evaluate the anticancer activity and pharmacokinetic behavior of novel platinum(IV) drug candidates (after i.p. and p.o. administration) in comparison to satraplatin and the clinically applied platinum(II) drug oxaliplatin. Subsequently, we determined the average platinum content by means of ICP-MS in different organs (kidney, liver, lung and muscle), serum and tumor of CT-26-bearing mice upon treatment with the respective platinum compounds. Metabolisation of the platinum(IV) compounds was studied by SEC-ICP-MS in mice serum samples, indicating that already 2 h after oral treatment the parent drug has been completely metabolized and/or bound to plasma proteins. Oral and intraperitoneal treatment with one of the compounds ((OC-6-33)-dichloridobis((4-ethoxy)-4-oxobutanoato) bis(ethylamine)platinum(IV)) resulted in high tissue and platinum tumor levels and tumor growth delay to some extent. These results together with the high *in vitro* cytotoxicity and cell accumulation led us to select this compound for NanoSIMS experiments as well as to perform further LA-ICP-MS investigations.

We have developed and validated a quantitative LA-ICP-MS method based on matrix-matched calibration standards, spiked with the analytes of interest (Pt and Ru). The concentrations were verified by microwave-assisted acid digestion of the homogenized liver standard and metal quantification by ICP-MS. Subsequently, the established LA-ICP-MS bioimaging approach allowed us to obtain quantitative, spatially-resolved information on metal distribution in substructures of different tissue types (including renal tissue, spleen, liver and tumor tissue). LA-ICP-MS proved to be advantageous to assess the extent of metal uptake into histologically heterogeneous tissue compared to the average metal concentration determination by ICP-MS. Considering the complex tumor microenvironment, we have demonstrated that LA-ICP-MS is capable to discern the metal accumulation specifically located in tumor. Comparison of the metal distribution pattern with the underlying histology revealed elevated platinum levels in loose, soft tissue compared to the more solid areas of the tumor. In addition, the platinum levels were studied for oxaliplatin and satraplatin in renal structures by LA-ICP-MS, revealing increased platinum accumulation in the cortex compared to the medulla, which is in accordance to results for the nephrotoxic drug cisplatin. However, oxaliplatin and satraplatin have not exhibited signs of nephrotoxicity in clinical trials and therefore, we could show that solely the platinum pattern determined by LA-ICP-MS is not indicative for the nephrotoxic potential of platinum-based drugs.

The elucidation of the anticancer activity and penetration depth of platinum-based compounds into tumor tissue could help in the rational design of new classes of selective and effective chemotherapeutics with improved selectivity and therapeutic index. We have demonstrated the value of LA-ICP-MS as imaging tool in preclinical metal-based anticancer drug development. However, in the field of metal-based anticancer drug research, the potential of LA-ICP-MS using recent developments in laser technology is still far from being fully exploited in terms of single cell imaging, high spatial resolution, fast acquisition times and internal standardization.

Publications in scientific journals

- ‘Tumor microenvironment in focus: LA-ICP-MS bioimaging of a preclinical tumor model upon treatment with platinum(IV)-based anticancer agents’
  Sarah Theiner, Christoph Kornauth, Hristo P. Varbanov, Markus Galanski, Sushilla Van Schoonhoven, Petra Heffeter, Walter Berger, Alexander E. Egger, Bernhard K. Keppler, *Metallomics*, **2015**, 7, 1256-1264

- ‘Comparative *in vitro* and *in vivo* pharmacological investigation of platinum(IV) complexes as novel anticancer drug candidates for oral application’
  Sarah Theiner, Hristo P. Varbanov, Markus Galanski, Alexander E. Egger, Walter Berger, Petra Heffeter, Bernhard K. Keppler, *J. Biol. Inorg. Chem.*, **2015**, 20(1): 89-99

- ‘Extravasation of Pt-based chemotherapeutics – Bioimaging of their distribution in resectates by Laser Ablation-Inductively Coupled Plasma-Mass Spectrometry (LA-ICP-MS)’
  Alexander E. Egger, Christoph Kornauth, Werner Haslik, Stephan Hann, **Sarah Theiner**, Günther Bayer, Christian G. Hartinger, Bernhard K. Keppler, Ursula Pluschnig, Robert M. Mader, *Metallomics*, **2015**, 7, 508-515

- ‘A novel class of bis- and tris-chelate diam(m)inebis(dicarboxylato)platinum(IV) complexes as potential anticancer prodrugs’
  Hristo P. Varbanov, Simone Göschl, Petra Heffeter, **Sarah Theiner**, Alexander Roller, Frank Jensen, Michael A. Jakupec, Walter Berger, Markus Galanski, Bernhard K. Keppler, *J. Med. Chem.*, **2014**, 57(15): 6751-6764

- ‘Quantitative bioimaging by LA-ICP-MS: a methodological study on the distribution of Pt and Ru in viscera originating from cisplatin- and KP1339-treated mice’
  Alexander E. Egger, **Sarah Theiner**, Christoph Kornauth, Petra Heffeter, Walter Berger, Bernhard K. Keppler, Christian G. Hartinger*, Metallomics*, **2014**, 6(9): 1616-1625

- Contribution to a book chapter: **‘Analysis of Pt- and Ru-based anticancer drugs – new developments’** in Metallomics: Analytical Techniques and Speciation Methods published by Wiley-VCH (Weinheim, Germany), **Sarah Theiner**, Luis Galvanez-Montano, Gunda Köllensperger, Bernhard K. Keppler, submitted

Participation in conferences and scientific sessions

- XVIIth International Conference on BioInorganic Chemistry (ICBIC), Beijing, China, July 2015
  Poster presentation, 'Investigating tumor response and therapy-related side-effects of platinum-based drug treatment in a preclinical tumor model by (LA-)ICP-MS'

- 20th International Mass Spectrometry Conference (IMSC), Geneva, Switzerland, August 2014
  Oral presentation, 'Investigation of the pharmacological behavior of novel platinum(IV)-based anticancer agents by means of ICP-MS and LA-ICP-MS'

- 7th International Symposium on Bioorganometallic Chemistry (ISBOMC), Vienna, Austria, July 2014
  Poster Presentation, 'Tracking of platinum(IV)-based anticancer drugs in mice tissues by ICP-MS and LA-ICP-MS'

- MassSpec-Forum-Vienna-2014, Vienna, Austria, February 2014
  Oral presentation, '*In vivo* evaluation of novel platinum(IV) anticancer drug candidates using ICP-MS and LA-ICP-MS'

- XVIth International Conference on BioInorganic Chemistry (ICBIC), Grenoble, France, July 2013
  Poster presentation, 'Bioimaging and quantification of metal-based anticancer drugs using LA-ICP-MS'

- 9. ASAC JunganalytikerInnen Forum, Vienna, Austria, June 2013
  Oral presentation, 'LA-ICP-MS: Quantification approaches'

- XIth International Symposium on Platinum Coordination Compounds in Cancer Chemotherapy, Verona, Italy, October 2012, Participant

- 23. ICP-MS Anwendertreffen, Tulln, Austria, September 2012
  Oral presentation, '*In vivo* Tracking metallbasierender Zytostatika mittels ICP-MS und LA-ICP-MS für pharmakokinetische Studien'

- Conference on Imaging Mass Spectrometry, Ourense, Spain, September 2012
  Poster presentation, 'Quantification strategy including internal standardization for elemental imaging of biological tissues using LA-ICP-MS'

IV. CURRICULUM VITAE

Personal Information

Name	Sarah Theiner
Academic Title	Mag. rer. nat.
E - Mail	sarah.theiner@univie.ac.at
Date and location of birth	1987-06-07, Vienna (Austria)
Nationality	Austria

Work experience

Dates	From March 2012 till now
Occupation or position held	PhD student/Researcher
Main activities and responsibilities	Scientific work and research
Name and address of employer	Institute of Inorganic Chemistry, University of Vienna, Währinger Strasse 42, Vienna 1090, Austria
Dates	From September 2012 till now
Occupation or position held	University assistant
Main activities and responsibilities	Attending student practise exercises and supervising students
Name and address of employer	Institute of Inorganic Chemistry, University of Vienna, Währinger Strasse 42, Vienna 1090, Austria

Education and training

Dates	May 2012 till now
PhD thesis	‘Pharmacokinetic studies of metal-based anticancer drugs using ICP-MS, LA-ICP-MS and HPLC-ICP-MS’ in the frame of the ‘Translational Cancer Therapy Research Platform’ Supervisor: o. Univ.-Prof. DDr. Bernhard K. Keppler
Principal subjects/Occupational skills covered	Bioanalytical Chemistry, Analytical Method Validation, Medicinal Inorganic Chemistry, Drug Development
Name and type of organisation providing education	Bioinorganic Chemistry Group (B. K. Keppler), Institute of Inorganic Chemistry, University of Vienna, Währinger Strasse 42, Vienna 1090, Austria

Dates	September 2005 – November 2011
Title of qualification awarded	Mag. rer. naturalis (Chemistry), summa cum laude
Diploma thesis	‘The use of strontium isotope ratio measurements by MC-ICP-MS or fundamental studies on diagenesis and for the reconstruction of animal migration at the Celtic excavation site Roseldorf’ Supervisor: Ao. Univ. Prof. DI Dr. Thomas Prohaska, University of Natural Resources and Life Sciences, Vienna
Principal subjects/Occupational skills covered	Analytical Chemistry, Chemistry of Food Analysis, Inorganic Chemistry, Organic Chemistry, Physical Chemistry, Biochemistry, Theoretical Chemistry and Spectroscopy
Name and type of organization providing education	University of Vienna, Vienna, Austria Währinger Strasse 42, Vienna 1090, Austria

Dates	October 2012 till now
Study	Bachelor Study Ancient History
Name and type of organization providing education	University of Vienna, Vienna, Austria

Dates	September 1997 – June 2005
Maturity examination	2005-06-05, summa cum laude
Name and type of organisation providing education	Grammar school, Purkersdorf, Austria

Scientific exchange

Dates	April 2015 – July 2015
Principal subjects/Occupational skills covered	Bioanalytical Chemistry, Medicinal Inorganic Chemistry Drug Development, Mass Spectrometry
Name and type of organization providing education	Prof. Paul J. Dyson Laboratory of Organometallic and Medicinal Chemistry (LCOM), École polytechnique fédérale de Lausanne (EPFL), Lausanne, Switzerland

Granted Projects and Awards

- 'Kurzwissenschaftliches Auslandsstipendium' (KWA) from the University of Vienna for the scientific stay in the group of Prof. Paul Dyson at the EPFL in Lausanne, Switzerland from April 2015 until July 2015.
- Winner of the poster award on ICBIC 17 in Beijing, China, 2015 for the poster presentation 'Investigating tumor response and therapy-related side effects of platinum-based drug treatment in a preclinical tumor model by (LA-)ICP-MS'

Personal Skills and Competences

Mother tongue	German
Other languages	English (C1), French (B2) Swedish (A1), Bulgarian (A1) Greek (A2), Latin, Ancient Greek
Social skills and competences	Experience in teaching/supervising students: I have been an assistant in basic inorganic and analytical chemistry practical courses, as well as in the basic course 'Chemisches Rechnen' for chemistry and biology students. In addition, I was supervising several students in practical courses in ICP-MS and was co-supervisor of a master work
Technical skills and competences	ICP-MS (including ICP-QQQ-MS, ICP-MC-MS) Laser ablation-ICP-MS, HPLC-ICP-MS HPLC, ESI-MS
Computer skills and competences	Operational systems – Windows XP, Windows 7, MAC OSX MS Office applications, Chem Draw, EndNote, etc.
Other skills and competences	Ability for problem solving, hard-working, creative, well-organized, patient, well-developed presentation skills due to several participations in scientific sessions/conferences, able to face up the deadlines related to my projects and manuscripts